

The Alpha Foundation for the Improvement of Mine Safety and Health, Inc

Final Technical Report

Cover Page

AFC719FO-100 – Research and Refinement of a Methane Watchdog System to Improve Longwall Mine Safety

Organization: West Virginia University Research Corporation

Principal Investigator: Derek Johnson, PhD, PE
Office: 304-293-5725, **Cell:** 304-216-6592, **Fax:** 304-293-6689
Email: derek.johnson@mail.wvu.edu
Co-Principal Investigator: Nigel Clark, PhD

Period of Performance: August 1st, 2020 – December 31st, 2022

Acknowledgement/Disclaimer

“This Study was sponsored by the Alpha Foundation for the Improvement of Mine Safety and Health, Inc. (ALPHA FOUNDATION). The views, opinions and recommendations expressed herein are solely those of the authors and do not imply any endorsement by the ALPHA FOUNDATION, its Directors and staff.”

Contents

Cover Page	1
Abbreviations	3
1.0 Executive Summary	5
2.0 Problem Statement and Objective.....	7
2.1 Problem Statement	7
2.2 Project Objectives	7
3.0 Research Approach	9
3.1 Ejector Improvements	9
Methane Sampling	9
Initial Design	9
Improved Design	12
3.2 Methane Sensor Improvements	25
3.3 Signal Processing Improvements	28
3.4 Mine Like Environment Evaluations	36
3.5 System Integration for Deployment	54
3.6 Modeling and Demonstration of Capabilities	59
4.0 Summary of Accomplishments.....	72
4.1 Key Design Findings.....	72
5.0 Dissemination Efforts and Highlights.....	75
5.1 Intellectual Property	75
5.2 Theses.....	75
5.3 Public Dissemination.....	75
6.0 Conclusions and Impact Assessment	77
7.0 Recommendations for Future Work.....	79
8.0 References.....	80
9.0 Appendices.....	82
9.1 Appendix A: Final Ejector Drawings.....	82
9.2 Appendix B: Additional Test Details	84
9.3 Appendix C: Additional Information for MWS Certification.....	90
9.4 Appendix D: 1-D Modeling Code.....	116

Abbreviations

AI	Artificial Intelligence
ARPA-E	Advanced Research Projects Administration - Energy
ASME	American Society of Mechanical Engineering
°C	Degrees Celsius
CAD	Computer Aided Draft
CFD	Computation Fluid Dynamics
CFL	Courant-Friedrich-Lewy
cfm	Cubic Feet per Minute
CFR	Code of Federal Regulations
CH ₄	methane
CNG	Compressed Natural Gas
CO	Carbon Monoxide
CPH	Central Processing Hub
DAQ	Data Acquisition
dc/dt	change in concentration over time
DCM	Differential Coefficients Method
FFS	Full Flow Sampler System
ft/s	feet per second
HG	headgate
IRS	Infrared Sensor (Dynament)
kg/m ² s	kilograms per square meter second
kg/m ³	kilograms per cubic meter
kPa	kilo Pascals
LEL	Lower Explosive Limit
lpm	liters per minute
m	meter
m/s	meters per second
mA	milli Amp
mm	millimeter
MOS	Metal Oxide Sensors (MQ-4)
MSHA	Mine Safety and Health Administration
MWS	Methane Watchdog System
NDIR	New Dual-wavelength Infrared (Gasmitter)
OD	Outer Diameter
ODE	Ordinary Differential Equation
OTT	Office of Technology Transfer
ppm	parts per million
psia	pound-force per square inch - absolute
psig	pound-force per square inch - gage
PTFE	Teflon

RH	Relative Humidity
RPM	Revolutions Per Minute
SCFM	Standard Cubic Feet per Minute
SDF	Scaling Design Factor
SIT	Sequential Inversion Technique
SLPM	Standard Liters Per Minute
TG	tailgate
VDC	Volts Direct Current
VOD	Ventilation On Demand
WVU	West Virginia University

1.0 Executive Summary

Excessive methane emissions associated with longwall mining can create dangerous conditions during operations. Our research team at West Virginia University (WVU) has completed additional research and demonstration of a second-generation of the Methane Watchdog System (MWS). The ultimate goal of the research is to build upon our previous work to improve the MWS. The MWS is cost-effective, multi-nodal network of methane sensors that can be deployed across an entire longwall system and to enable intelligent monitoring of localized zones of high methane concentration.

In the first program, we proposed that active sampling be used to enable monitoring of shield tips and gob areas of the shields. We first proposed that systems utilize water ejectors as a low-cost method to create suction flow with no moving parts. In order to improve ejector performance (i.e., maximize the gas sample to water consumption), we completed computational fluid dynamics (CFD) modeling and experimental tests to create a new and improve multi-nozzle ejector capable of providing 2 standard liters per mine (SLPM) of sampling with only 1 SLPM of water, with a peak flow ratio of 2.61.

Previously we examined we examined a cheap metal oxide sensor (MOS – 10s of dollars) and an infrared sensor deployed in mines (IRS – 100s of dollars). We noted each sensor had strengths and weaknesses. In this program we evaluated a new infrared sensor (NDIR - \$800) and demonstrated that it retained the best characteristics of both first generation sensors. When included in the MWS the T90 of the system was only 17 – 20 seconds, which included a transport delay of ~4 seconds. Therefore, this active MWS nodal approach met or exceeded the response characteristics of currently deployed methane sensors. The NDIR was accurate of a wide range from methane concentration from 100s of ppm to 2% or more. In addition, we noted that and demonstrated it could easily be zeroed and calibrated while installed in a mock mine.

All active sampling systems will include transport delay and sampling diffusion when deployed for real time monitoring as we identified at the end of the first research project. In our current work we completed extensive characterization of the system response focused on the second generation NDIR. We developed a method to reconstruct sharpened sensor values and reduced error over six cases from 19% to only 4%. We demonstrated that such a sharpening method would ensure that short peak methane concentrations could be identified if the in-situ method were applied.

In this research, we also conducted additional evaluations similar to the first program. However, this time we utilized the WVU Mine Training Academy to create a mock longwall face. This demonstration improved the velocity and geometry over previous wind tunnel experiments. The overall length was increased from 100 to 300' and we were able to produce controlled and repeatable ventilation velocities from 1 to 2 m/s. We used a custom full flow sampling system provide methane to the mock mine facility in the forms of both stationary and mobile tests. While concentrations were still limited due to safety, we demonstrated that the MWS could detect methane concentrations from 100s to ppm to 1%. Even with limited concentrations, we showed that the MWS was capable of measuring methane enhancements in areas where ventilation decreased, and recirculation occurred – common issues in tailgate (TG) regions of longwalls. We demonstrated that the system methane response was able to track a mobile plume and that observed data matched well with supplied injection locations. We also demonstrated that the system response shape could be used to infer direction of the methane plume (with or against

ventilation velocity direction). While demonstration tested the low concentration capabilities of the system, we recreated emissions in a 2-D model of the facility and showed that peak methane and concentration decay profiles that were measured matched well with those produced from CFD models.

In this program, we also discussed the MWS with MSHA and industry officials. As such, we identified additional key regulations that such a system would be required to meet to undergo a successful MSHA approval process. We developed documentation necessary to submit with the system for an evaluation. We also identified currently approved components and explosion proof enclosures that could replace our prototype components on the pathway to transition the MWS to real world deployment in mines.

Finally, we also used our findings and literature to create a 1-D model to assess the benefits and capabilities of the MWS over a range of longwall mining scenarios. Our modeling findings demonstrate that a multi-nodal MWS system could be used to reduce or avoid dangerous methane scenarios. Our work matched well with literature (and our demonstrations at the mine facility) in that ventilation velocity reductions across the face yield higher methane concentrations that should be monitored at the TG. These particular scenarios could be avoided by deployment of a single MWS node or conventional sensor in these locations. However, modeling suggests that dangerous methane plumes can occur across the entire longwall face, which demonstrates the key strength of a multi-nodal approach. We use the model to demonstrate a deployed MWS could be used in real-time to adjust shearer speed to avoid costly shutdowns and enable continuous cuts across the entire face.

Overall, our research was successful in completing the key research tasks in the development of a second generation MWS prototype. The results presented herein, lay the foundation necessary for an MWS system to be commercialized, certified, and deployed in an active mining environment. As the world continues to see coal consumption increase, mines must continue to improve safety. Our second generation MWS has been demonstrated as a possible technology to ensure the safety of continued longwall mining operations.

2.0 Problem Statement and Objective

2.1 Problem Statement

While there has been focus on alternative energy sources, global coal use was set to rise by 1.2% in 2022, which eclipsed the previous production record set in 2013 [1]. Longwall mining in underground coal mines is considered the safest and most productive mining method. Due to its high productivity, methane emissions from the large, newly exposed coal face and from the gob area are often high. Mine explosions may be initiated by these high methane concentrations. Longwall mine safety continues to remain an area of ongoing research worldwide.

A review of recently literature finds that most research has recently focused on deploying various machine learning or artificial intelligence (AI) methods to predict methane from coal mining operations [2, 3, 4]. For example, Demirkan et al., utilized computational fluid dynamics (CFD) coupled with AI. Their study referenced the Upper Big Branch Accident but also noted current monitoring systems are lacking as they do not provide coverage across the entire face. Their solution of AI and CFD modeling requires extensive computational and time requirements. For this very reason it is crucial that multi-nodal monitoring networks such as the Methane Watchdog System (MWS) be developed and deployed in mines. Such deployment targets improved safety but would also serve to gather valuable data necessary to inform modelling work developed by others. These issues were further highlighted Juganda in his 2020 thesis research [5]. Their CFD modeling suggested that monitoring of methane at the shearer body and the tailgate region along was insufficient to ensure safety. They noted that methane sensors should be deployed at the upper front shield tip as our work as suggested to ensure that the highest methane concentrations are monitored. In fact, their proposed locations on 3-D drawings match those we have presented.

2.2 Project Objectives

Therefore, our goal to build upon the findings from our previous research project to further develop and refine the MWS and increase its ability to predict hazardous conditions. The MWS is a cost-effective, multi-nodal network of methane sensors that is distributed across the entire longwall system and serves as an intelligent method to detect localized zones of high methane concentration. The system will not only detect these scenarios but will also provide the ability to automatically de-energize or control equipment to avoid potential explosive scenarios. We developed a second generation system and focused on improving the performance of the system through additional experimental research, modeling, and simulated mine research. Key performance metrics included continued focus on improvements of nodal accuracy and response time, as well as capabilities to pre-emptively detecting hazardous conditions based on continuously monitoring methane across the face and gob areas.

Our goal was to advance the knowledge-base and experimental data necessary to ensure that the MWS can be deployed in mines affordably in the interests of enhancing mine worker safety and maintaining productivity. To achieve this overall goal, we conducted further research on the following areas:

- 1.) Ejector Improvements - reducing water consumption of ejectors through redesign for compressed liquid streams at higher pressures,
- 2.) Methane Sensor Improvements - evaluation of state-of-the-art dual wavelength, infrared sensors to improve response time and accuracy,
- 3.) Signal Processing Improvements - development of signal sharpening techniques to enhance predictive capabilities,
- 4.) Mine Environment Evaluations - develop new data sets for system performance in an established simulated mine facility,
- 5.) System Integration for Deployment - examine MSHA and shield integration requirements to enable future deployments in active mines, and
- 6.) Modeling and Demonstration of Capabilities - build upon previous modeling to assess additional benefits of shearer or ventilation control.

3.0 Research Approach

In this section, we summarize the approach and results for the six aforementioned research areas.

3.1 Ejector Improvements

Methane Sampling

Current methane monitoring is typically achieved by fixed methane sensors on the shearer itself. As such the sensor represents passive sampling in that a sample pump is not used to transport the sample from a given location to the sampling sensor itself. Passive methane monitoring is required at the shearer but some industry has mounted sensors near the tail gate and similar detectors are worn by mine workers. The goal of the MWS is to provide additional sensor locations across the entire longwall from headgate (HG) to tailgate (TG). Further, the system samples from difficult to reach locations such as near the shield tips and near the gob areas. As such, an active sampling approach was required to transport the samples to a central sensor location at each sampling node. There are a variety of methods for active sampling and our research focused on a water powered ejector system to eliminate the need for an electro-mechanical sampling pump at each node location. Pressurized water is available throughout the longwall for dust suppression and for fire protection systems. However, water consumption should be minimal to reduce waste. In this research, we utilized additional CFD modeling combined with novel 3-D printed ejectors to reduce water consumption, while maintaining sample flow rate and sample pressure requirements.

Initial Design

We previously reported on the results of a conventional single nozzle ejector and highlight summary results here. Table 3.1.1 presents a summary of the geometry of the of the initial ejector and Figure 3.1.1 presents an image of the 3-D printed ejector.

Table 3.1.1: Initial ejector design dimensions.

Nozzle Diameter	$D_n = 1.1 \text{ mm}$
Nozzle Angle	$\theta_n = 18^\circ$
Mixing Chamber Diameter	$D_m = 2.2 \text{ mm}$
Mixing Chamber Length	$L_m = 22.1 \text{ mm}$
Included Diffuser Angle	$\theta_d = 6^\circ$
Diffuser Length	$L_d = 22.6 \text{ mm}$
Diffuser Outlet Diameter	$D_d = 4.6 \text{ mm}$
Distance between nozzle outlet and mixing chamber inlet	$NXP = 1.1 \text{ mm}$
Water Inlet Diameter	$D_w = 3.2 \text{ mm}$
Air inlet Diameter	$D_a = 3.2 \text{ mm}$



Figure 3.1.1: 3-D printed ejector.

The ejector was tested in the laboratory over eight operational points. Figure 3.1.2 and Table 3.1.2 show results where the water pressure remained constant, and the suction pressure was controlled via a valve. The ejector had two distinct operational curves. As the suction pressure was decreased with the valve, the ejector transitioned from the “High” pressure curve to the “Low” pressure curve around 93.8 kPa (13.6 psia). The transition between performance of the “High” and “Low” pressure curves was likely due to a flow regime change as both audible and visual changes were noted. Dirix and Wiele investigated the mass transfer in a jet loop reactor, which consisted of a liquid-gas ejector. Their experiments showed that at higher gas flowrates, around a flow ratio of 1.3, a transition from bubble flow to jet flow occurred [6]. Otake et al. similarly concluded that the same transition occurred when the flow ratio was between 1 and 2 [7]. Dirix and Wiele also noted that in bubble flow, the interfacial area between the dispersed bubbles and the continuous liquid stream was directly proportional to the gas holdup, unlike in jet flow. They showed that the mass transfer rate in jet flow was independent of the gas holdup for flow ratios less than 3 [6]. In an ejector, a liquid jet forms as the liquid exits the nozzle and travels axially through the ejector. At some axial location, the jet breaks up and the gas disperses into the liquid, creating bubbly flow. According to Cunningham and Dopkin, an ejectors performance depends on the location of the jet break-up [8]. If this breakup occurs too soon (at an “early” location), like in the mixing chamber, the energy dissipation rate from the liquid inhibits the entrainment of the suction fluid (the gas sample in this case). It was therefore concluded that the optimum location of jet breakup was at the end of the mixing chamber [8].

Based these findings, it was believed that jet breakup was likely occurring before the end of the mixing chamber when operating on the “High” pressure curve, before the transition. The ejector performance increased after the transition (on the “Low” pressure curve) since the air flowrate decreased at a lower rate with decrease in suction pressure than before the transition. Therefore, in order to keep the flowrate as consistent as possible with minor fluctuations in pressure that may occur, operation on the “Low” pressure curve was ideal. While all points on the “Low” pressure curve satisfied the capability to overcome pressure losses through the sampling unit,

there were no points on the “Low” pressure curve which satisfied the requirement of sampling at an air flowrate of at least 2 SLPM (0.071 SCFM). Table 3.1.2 presents only the points on the “Low” pressure curve. Note that the water pressure and flowrate for all points were 482.6 kPa (70 psig) and 1.7 LPM (0.06 CFM), respectively.

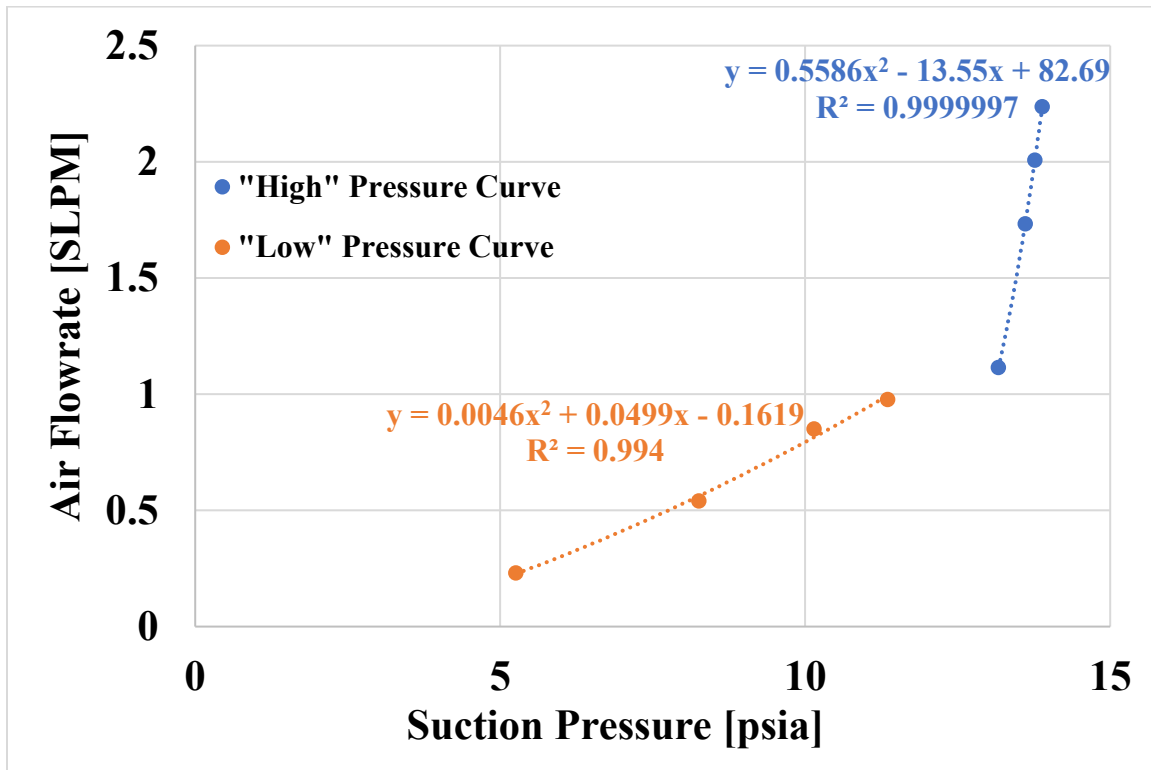


Figure 3.1.2: Ejector performance curves.

Table 3.1.2: Points of "Low" pressure curve.

Air Suction Pressure [kPa (psia)]	Air Flowrate [SLPM]	Air Flowrate [LPM]
78.6 (11.4)	0.98	1.17
69.6 (10.1)	0.85	1.14
57.2 (8.3)	0.54	0.89
36.5 (5.3)	0.23	0.60

Table 3.1.3 presents the experimental results for the test where suction pressure remained constant, and the water pressure was varied.

Table 3.1.3: Initial design ejector test with constant air suction pressure.

Water Pressure [psig]	Air Mass Flowrate [SLPM]	Air Volumetric Flowrate [LPM]	Water Flowrate [LPM]	Outlet Pressure [psia]	Flow Ratio
40	0.50	0.70	0.69	13.47	1.01
50	0.68	0.95	0.76	13.55	1.24
60	0.91	1.27	0.83	13.65	1.52
70	1.04	1.44	0.89	13.69	1.63
Constants: *Air Suction Pressure ≈ 11 psia *Air Temperature $\approx 24^{\circ}\text{C}$ *Water Temperature $\approx 24^{\circ}\text{C}$					

Improved Design

To improve the performance of the ejectors, a multi-nozzle geometry was examined experimentally and with CFD studies. Table 3.1.4 presents a summary of the multi-nozzle ejector designed dimensions. Figures 3.1.3 and 3.1.4 show the CAD model of the multi-nozzle ejector disassembled and assembled, respectively. Figures 3.1.5 and 3.1.6 show the 3D printed multi-nozzle ejector de-assembled and assembled for testing, respectively. Appendix A includes the CAD drawings of the final multi-nozzle ejector.

Table 3.1.4: Multi-Nozzle ejector design dimensions

Nozzle Diameter	$D_n = 0.45 \text{ mm}$
Nozzle Angle	$\theta_n = 16^{\circ}$
Mixing Chamber Diameter	$D_m = 4 \text{ mm}$
Mixing Chamber Length	$L_m = 24 \text{ mm}$
Included Diffuser Angle	$\theta_d = 10^{\circ}$
Diffuser Length	$L_d = 24 \text{ mm}$
Diffuser Outlet Diameter	$D_d = 8.2 \text{ mm}$
Distance between nozzle outlet and mixing chamber inlet	$NXP = 4 \text{ mm}$
Water Inlet Diameter	$D_w = 6.35 \text{ mm}$
Air inlet Diameter	$D_a = 6.35 \text{ mm}$

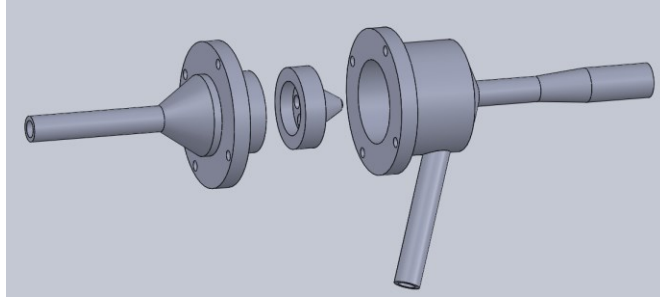


Figure 3.1.3: Disassembled multi-nozzle ejector CAD model.

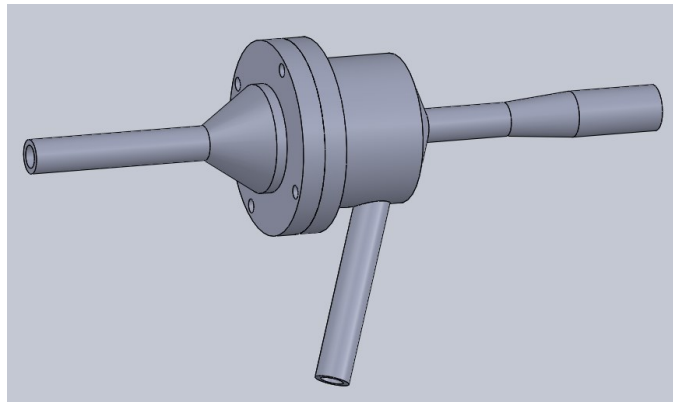


Figure 3.1.4: Assembled multi-nozzle ejector CAD model.



Figure 3.1.5: Disassembled multi-nozzle ejector.

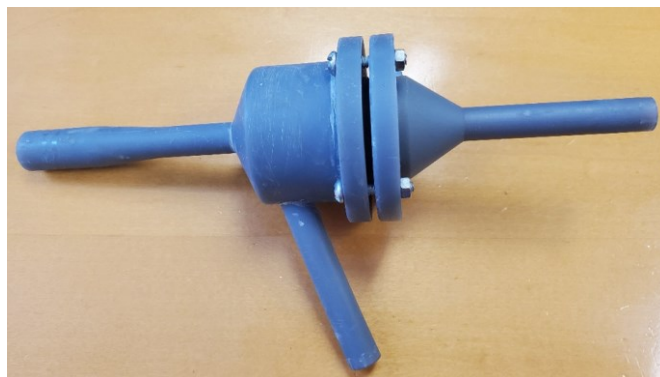


Figure 3.1.6: Assembled multi-nozzle ejector.

Figures 3.1.7 through 3.1.11 show the results of the five tests conducted with the multi-nozzle ejector where the water pressure was around 207, 276, 310, 379, and 448 kPa (30, 40, 45, 55, and 65 psig), respectively. All tests two distinct performance curves. The performance for the multi-nozzle ejector also increased when operating at lower pressures, which provides for broader applicability based on pressures available in the mines. Operation on the “Low” pressure curve was ideal to utilize the increased performance and allow for more consistent flowrates with minor fluctuations in pressure that can occur. Note that to utilize the “Low” pressure curve, a throttling valve needs to be integrated with each ejector to control the suction pressure. Such a valve within the node box would enable periodic adjustment based on the installed flow sensor on the sample exit stream.

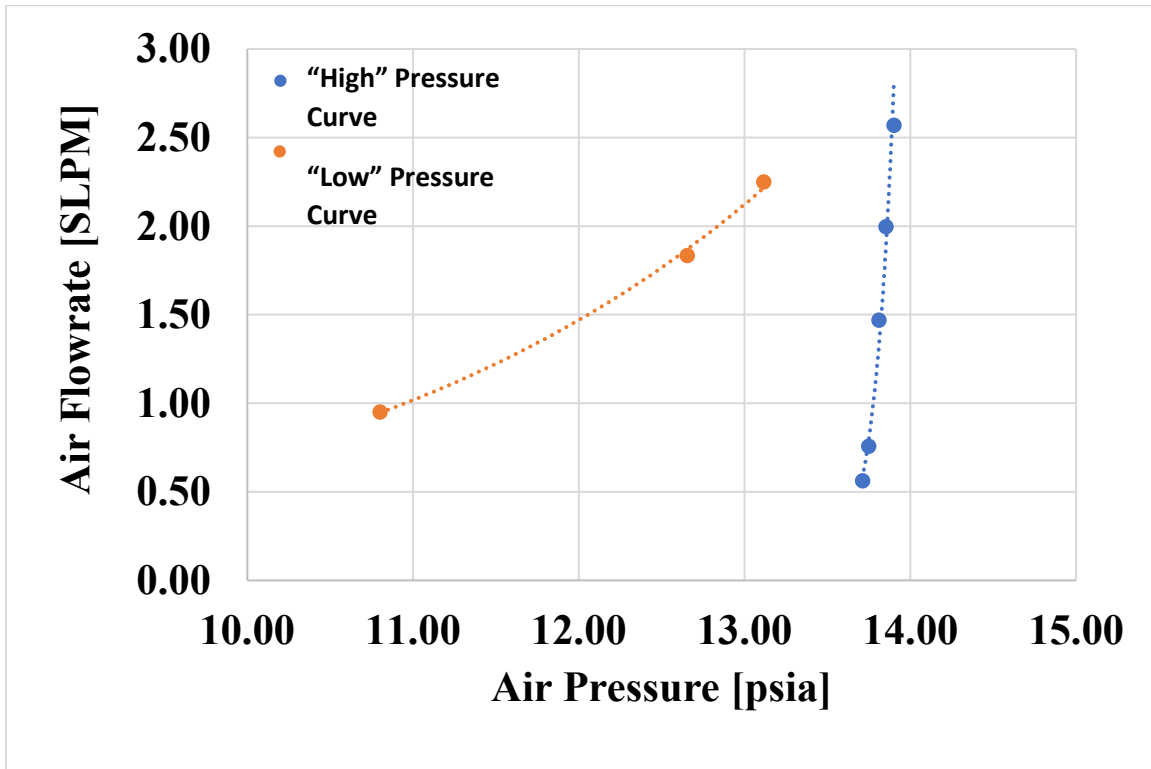


Figure 3.1.7: Multi-nozzle ejector test (water pressure \approx 30 psig).

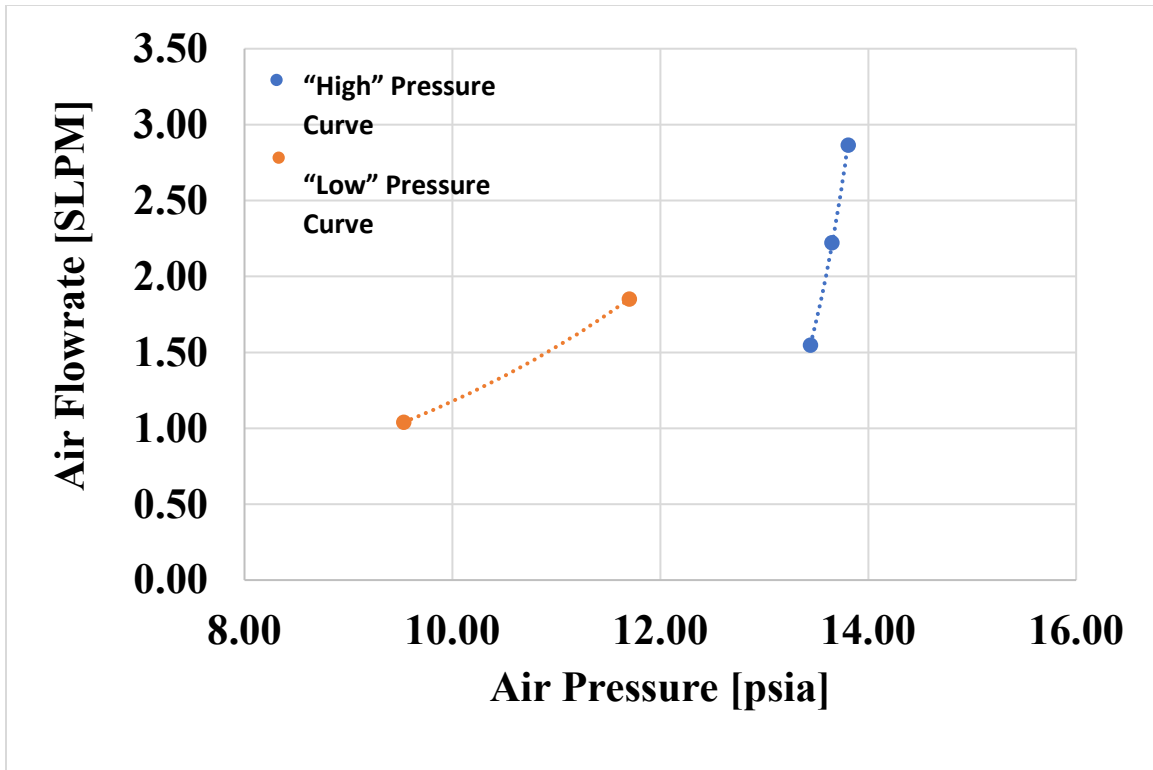


Figure 3.1.8: Multi-nozzle ejector test (water pressure \approx 40 psig).

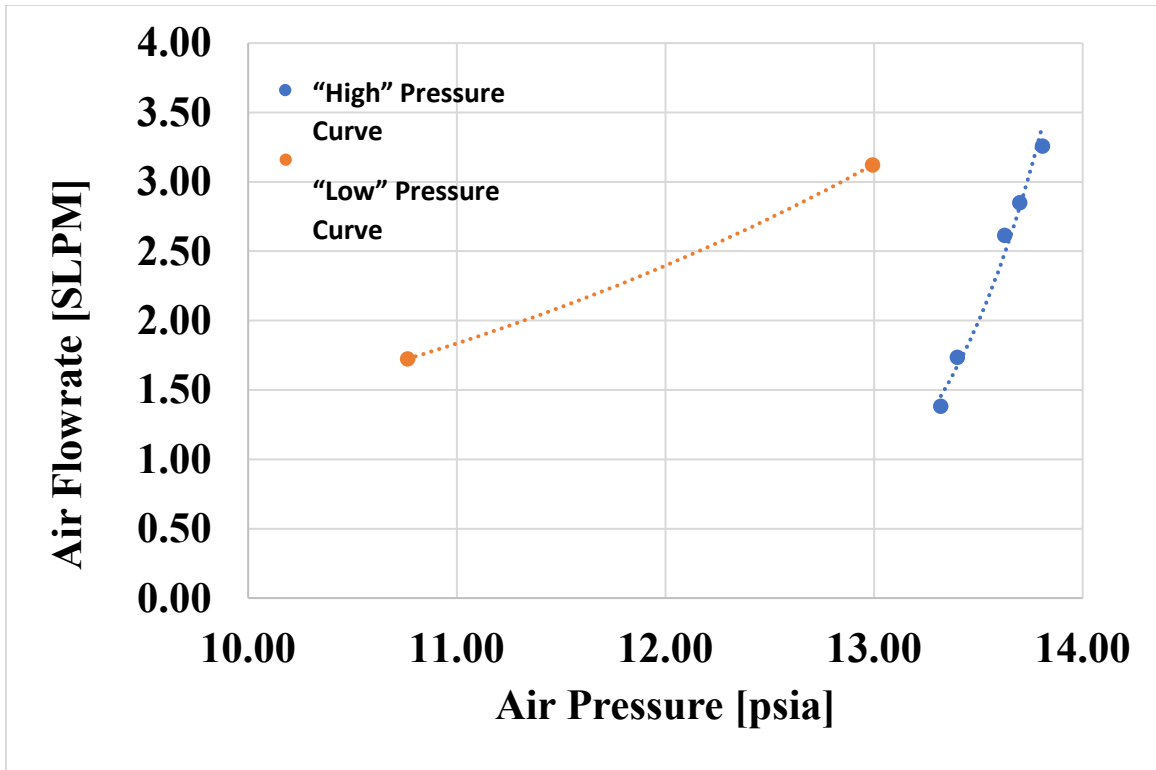


Figure 3.1.9: Multi-nozzle ejector test (water pressure ≈ 45 psig).

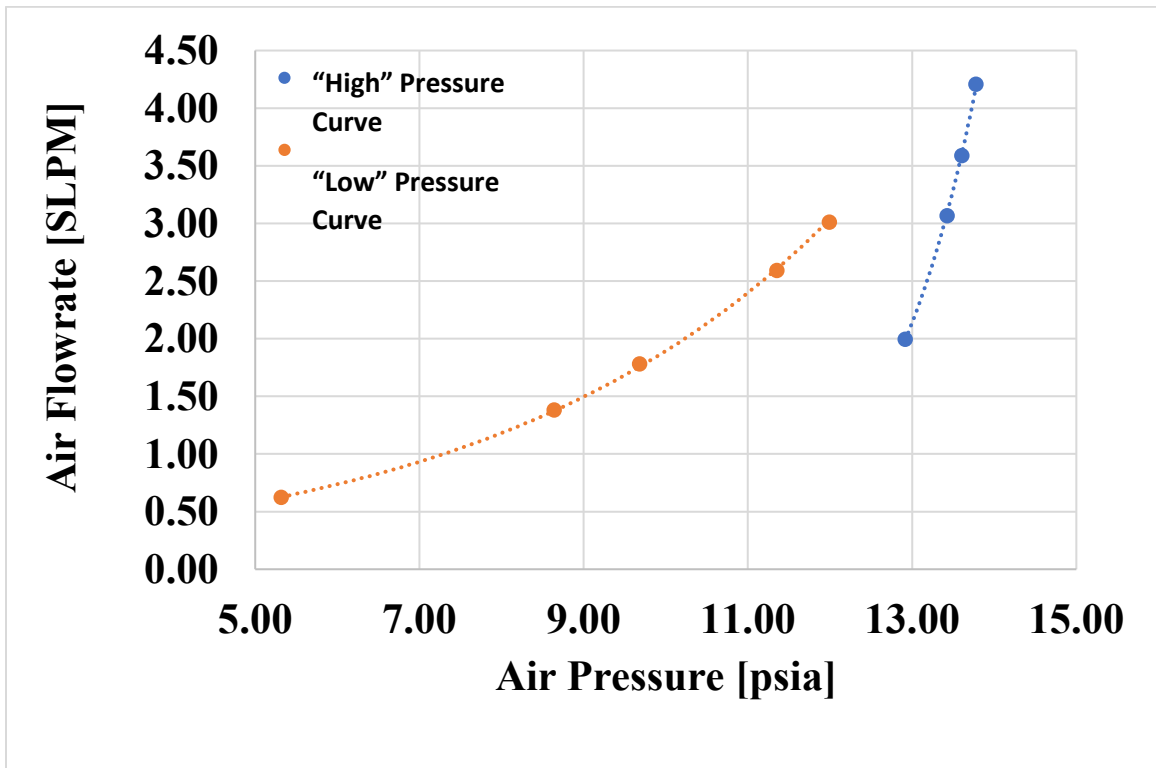


Figure 3.1.10: Multi-nozzle ejector test (water pressure ≈ 55 psig).

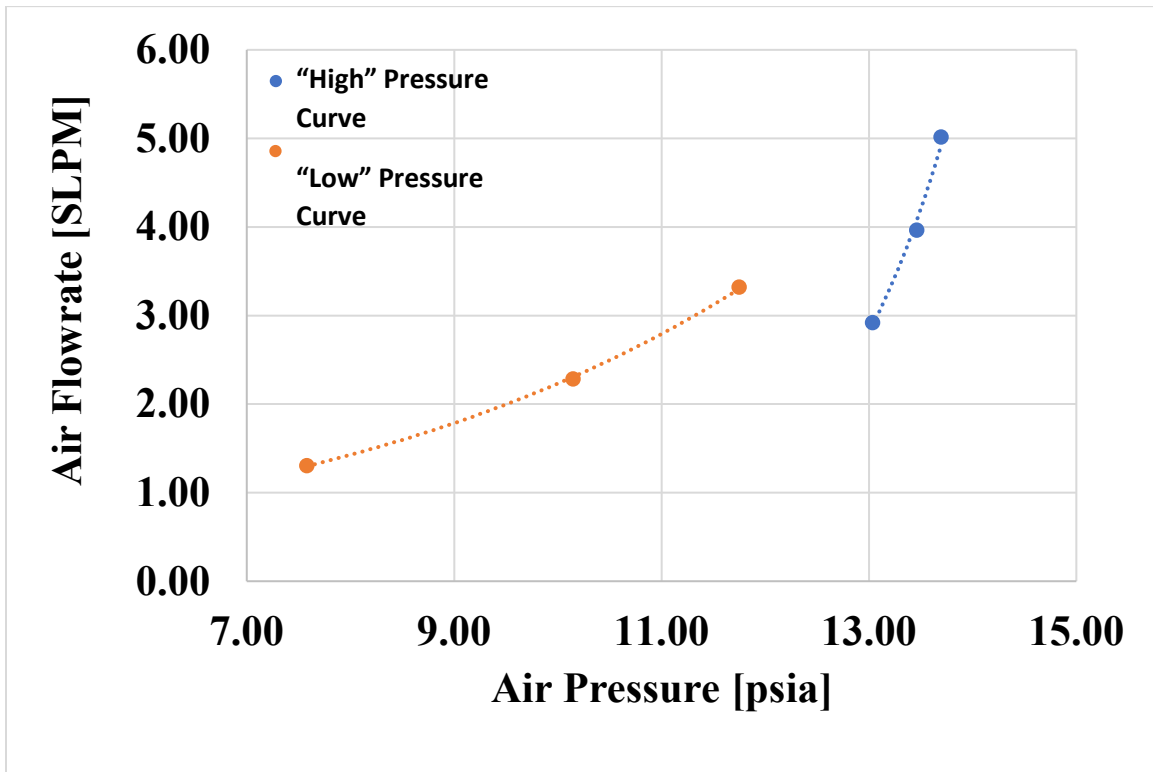


Figure 3.1.11: Multi-nozzle ejector test (water pressure \approx 65 psig).

Table 3.1.5 presents the results from the test where the absolute air suction pressure remained constant at 76 kPa (11 psia) and the water pressure was increased in 69 kPa (10 psig) increments. Figure 3.1.12 shows the relationship between the air flowrate and the water pressure. Figure 3.1.13 shows the relationship between the flow ratio and water pressure. Based on the later, the maximum flow ratio had nearly been achieved and that increasing the water pressure further would not significantly improve the flow ratio.

Table 3.1.5: Multi-nozzle ejector test with constant air suction pressure.

	Water Pressure [psig]	Air Mass Flowrate [SLPM]	Air Volumetric Flowrate [LPM]	Water Flowrate [LPM]	Outlet Pressure [psia]	Flow Ratio
Point 1	10	0.04	0.06	0.56	13.81	0.11
Point 2	20	0.71	0.98	0.77	13.90	1.28
Point 3	30	1.20	1.65	0.91	13.91	1.81
Point 4	40	1.70	2.34	1.04	13.99	2.25
Point 5	50	2.13	2.94	1.15	14.11	2.56
Point 6	60	2.60	3.58	1.26	14.28	2.85
Point 7	70	2.89	3.98	1.33	14.50	3.00
Constants: *Air Suction Pressure ≈ 11 psia *Air Temperature $\approx 30^{\circ}\text{C}$ *Water Temperature $\approx 24^{\circ}\text{C}$						

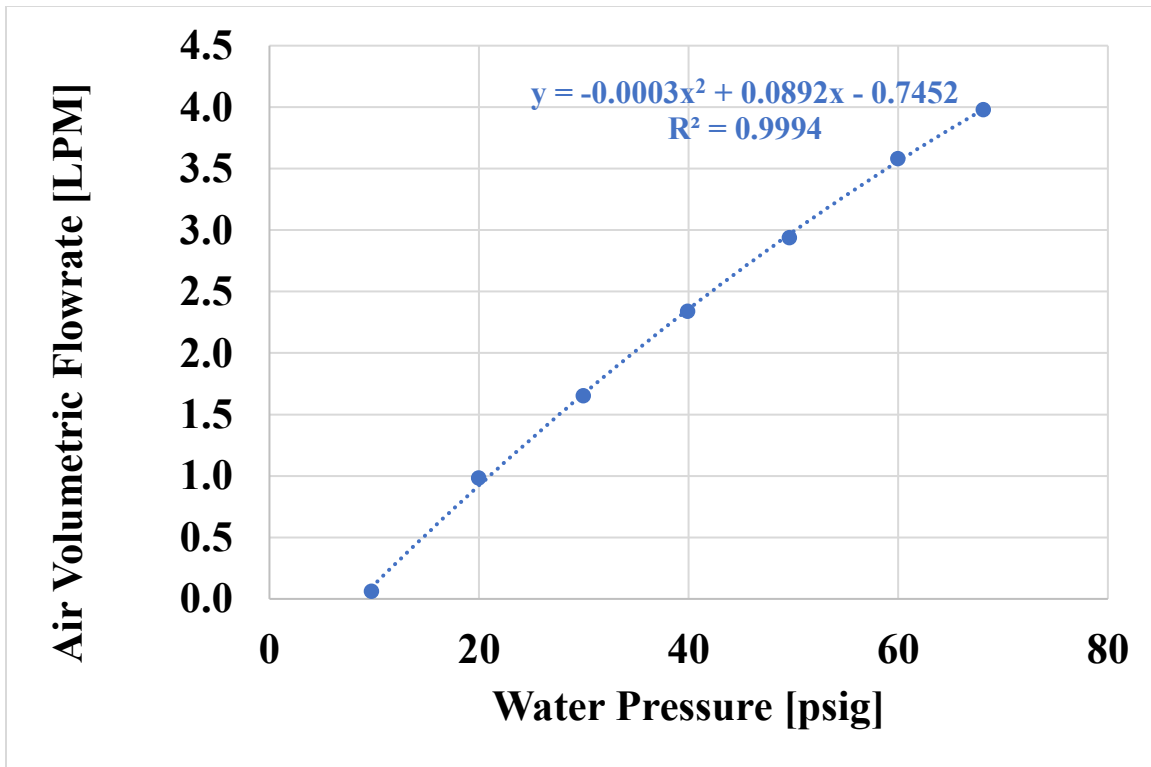


Figure 3.1.12: Relationship between air flowrate and water pressure.

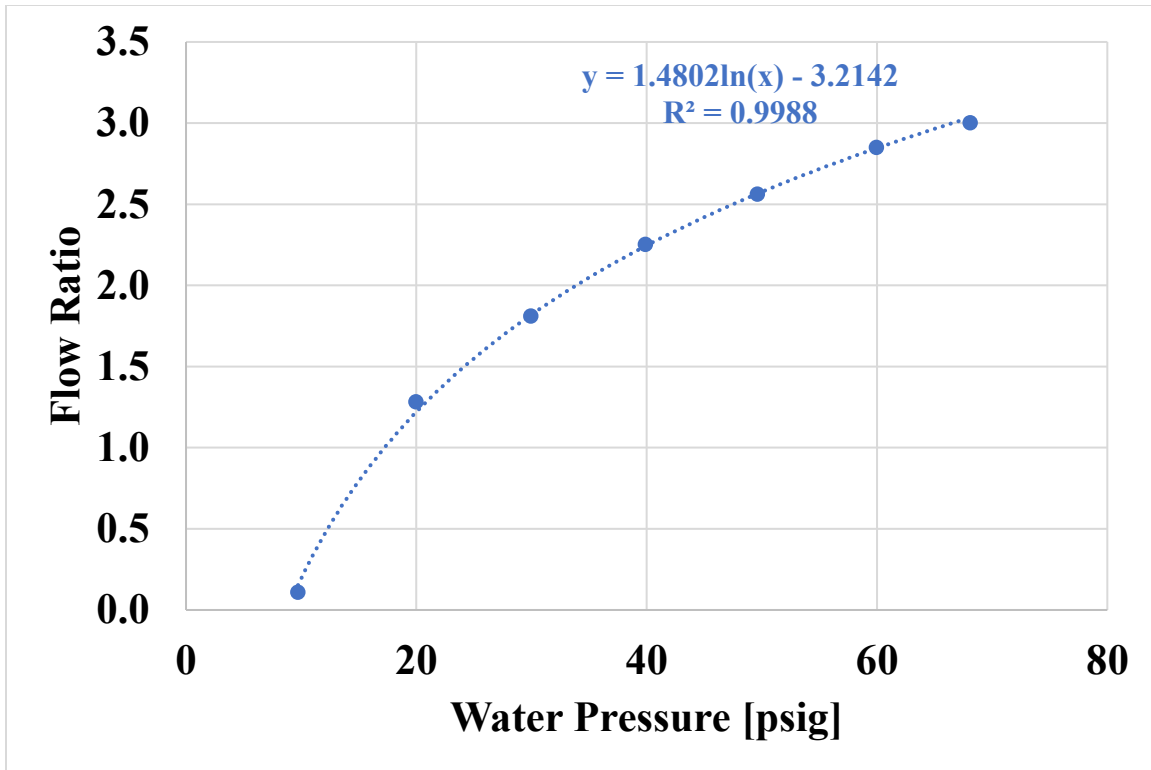


Figure 3.1.13: Relationship between flow ratio and water pressure.

CFD Modelling

Table 3.1.6 provides the results from the CFD model of experimental Points 3 through 7 of the and Table 3.1.7 presents a summary of the comparison between experimental and modeled results. Points 1 and 2 are not shown since the model did not perform properly for these two lowest pressures. Percent difference values were calculated to compare the air flowrates (mass and volumetric) and the flow ratios. The modelled results showed good agreement with the experimental results where all percent difference values were less than 31% and all the percent difference values calculated to compare the flow ratios were less than 17%. Based on these results, it was recommended that the model be used only for water pressures of 276 kPa (40 psig) (Point 4) and greater. With Point 3 eliminated, all percent difference values were less than 20%.

Table 3.1.6: CFD model results for Points 3 through 7.

	Standardized Air Volumetric Flowrate [SLPM]	Air Volumetric Flowrate [LPM]	Water Flowrate [LPM]	Flow Ratio
Point 3	1.64	2.19	1.03	2.13
Point 4	2.04	2.72	1.17	2.32
Point 5	2.40	3.19	1.29	2.47
Point 6	2.71	3.62	1.42	2.56
Point 7	2.92	3.90	1.50	2.59

Table 3.1.7: Comparison of experimental to modeled results.

	Standardized Air Volumetric Flowrate [% difference]	Air Vol. Flowrate [% difference]	Flow Ratio [% difference]
Point 3	30.90	27.80	16.24
Point 4	18.08	14.87	3.13
Point 5	11.55	8.38	-3.79
Point 6	4.18	1.01	-10.94
Point 7	1.15	-2.02	-14.64

Figure 3.1.14 shows the modelled flow ratios overlapping the plot of the experimental flow ratios (Figure 3.1.13). The modelled flow ratio trend was “flatter” than that of the experimental results, meaning the water pressure had lesser effect on the flow ratio in the model than experimentally. However, both experimental and modelled flow ratio trends seem to have nearly reached a maximum value since there was only about a 5% increase of the flow ratios from Point 6 to Point 7 of the experimental data. Therefore, it was predicted that increasing the water pressure further would not significantly improve the flow ratio.

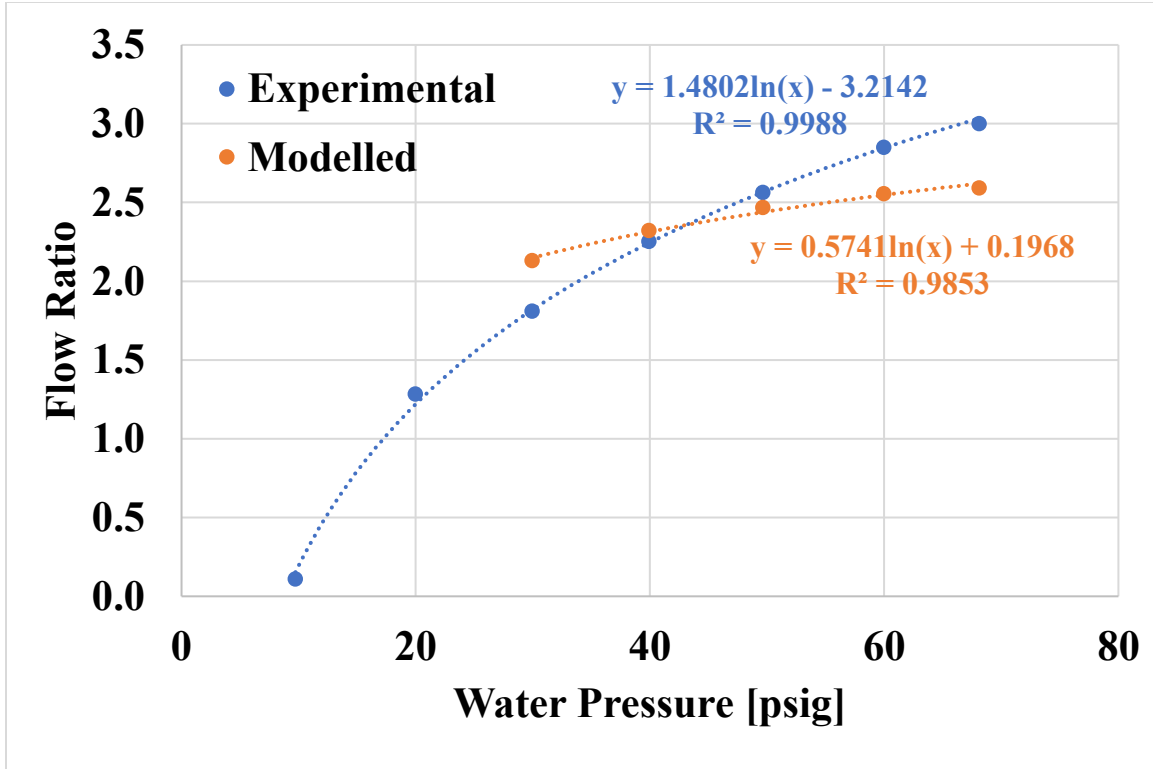


Figure 3.1.14: Modelled flow ratios compared to experimental.

The CFD model was used to estimate the flowrates and flow ratio when the water pressure was increased to 689 kPa and 1034 kPa (100 psig and 150 psig). The models' outlet pressure input was estimated from the trendline of the outlet pressures in preceding experimental tests. Figure 3.1.15 shows the plot of outlet pressures, including the trendline and equation used for the input estimation. Table 3.1.8 presents the results from the two models. The results show that the flow ratio is nearly unchanged from that of Point 7 (see Table 3.1.6), as expected.

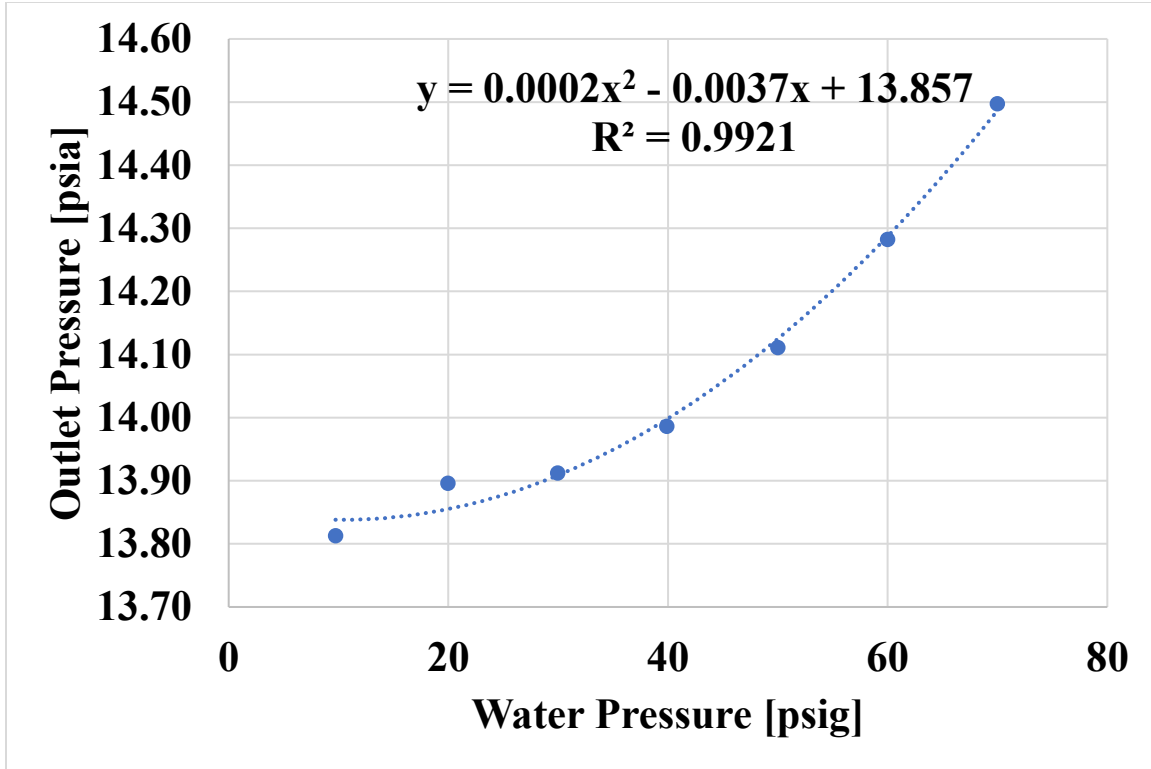


Figure 3.1.15: Outlet pressure trend from experimental data.

Table 3.1.8: Modelled results for water pressures of 100 and 150 psig.

Water Pressure [psig]	Air Mass Flowrate [SLPM]	Air Volumetric Flowrate [LPM]	Water Volumetric Flowrate [LPM]	Flow Ratio
100	3.53	4.71	1.81	2.60
150	4.24	5.65	2.20	2.56

Since it seemed the flow ratio was nearly maximized and the modelled results showed that the ejector was capable of sampling at a flowrate above the requirement, a scaling design factor (SDF) of 0.75 was calculated and applied to the geometry. The CFD model was then used to calculate the resulting flowrates of the scaled-down ejector with a water pressure of 689 kPa (100 psig). Table 3.1.9 presents the modelled results of the scaled-down ejector which verified that the application of the SDF resulted in a sampling flowrate of around 2 SLPM (0.071 SCFM) with less water consumption. There was around a 44% percent decrease in water consumption from the model of the original multi-nozzle design (1.81 LPM (0.06 CFM)) to the scaled-down design (1.01 LPM (0.04 CFM)). Therefore, for a 10-node system, the total water consumption would be around 10.1 LPM (0.36 CFM). Table 3.1.10 presents the dimensions of the scaled-down multi-nozzle ejector design. Figures 3.1.16, 3.1.17, and 3.1.18 shows the contours for the air volume fraction, velocity, and pressure from the CFD model, respectively.

Table 3.1.9: CFD model results of the scaled-down design.

Air Mass Flowrate [SLPM]	Air Volumetric Flowrate [LPM]	Water Volumetric Flowrate [LPM]	Flow Ratio
1.98	2.64	1.01	2.61

Table 3.1.10: Scaled-down design dimensions.

Nozzle Diameter	$D_n = 0.34 \text{ mm}$
Nozzle Angle	$\theta_n = 16^\circ$
Mixing Chamber Diameter	$D_m = 3 \text{ mm}$
Mixing Chamber Length	$L_m = 18 \text{ mm}$
Included Diffuser Angle	$\theta_d = 10^\circ$
Diffuser Length	$L_d = 18 \text{ mm}$
Diffuser Outlet Diameter	$D_d = 6.2 \text{ mm}$
Distance between nozzle outlet and mixing chamber inlet	$NXP = 3 \text{ mm}$

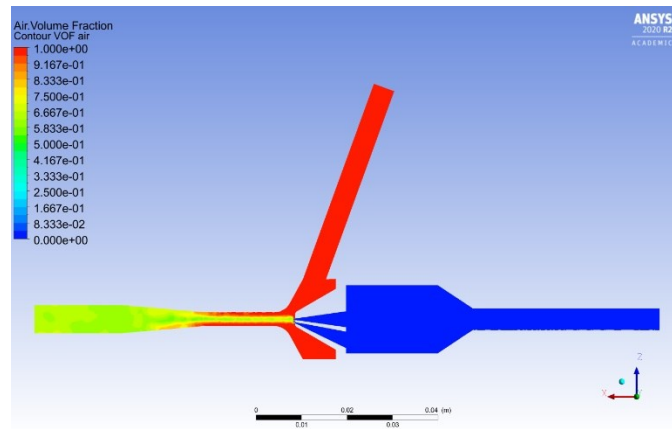


Figure 3.1.16: Air volume fraction contour.

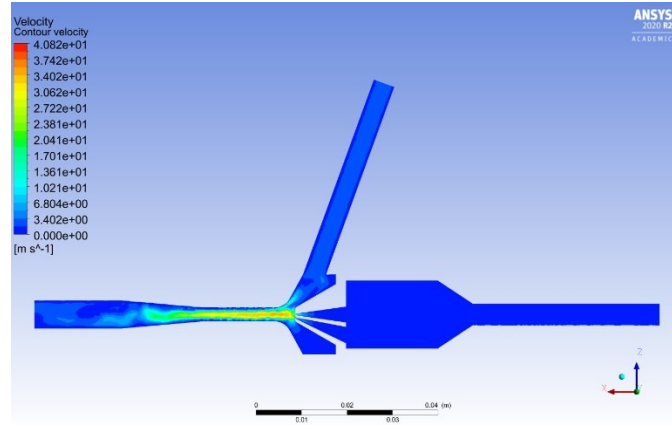


Figure 3.1.17: Velocity contour.

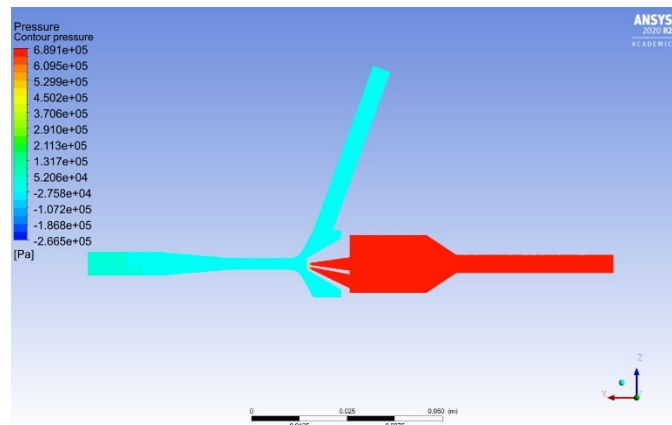


Figure 3.1.18: Pressure contour.

Ejector Improvement Results Summary

We used experimental research, 3-D printing, and CFD to create an improved ejector design. The overall goal was to efficiently sample 2 SLPM at operating pressure drops of the system at various water supply pressures. To achieve this, a multi-nozzle ejector provided increased performance. We showed that sample flow rates of at least 2 SLPM could be achieved with the new design over a broad range of pressures. The maximum experimental flow ratio (gas/water) was around 3 and the corresponding modelled flow ratio was around 2.6. These flow ratios were 58% and 37% greater than the average flow ratio calculated from values found in the literature review, which were around 1.9, respectively. The flow rate ratio of the new design was also 62.5% higher than the original designs. Water consumption was reduced by around 33-50% compared to the initial designs.

According to KOMATSU's PRS Water Spray Summary, the longwall shields' sprayers used approximately 227 LPM (8.02 CFM) of water while in operation [9]. Therefore, with the integration of the MWS, shield water consumption would increase by only around 4.4%. Based on water supply information provided by Murray Energy, total water consumption while in operation is around 1080 LPM (38.1 CFM), which includes water consumption for the shearer,

belt drives, and leaks [10]. This means total water consumption would only increase by approximately 0.94% with the integration of the MWS. In either case, the new multi-nozzle design would provide a cost effective method to provide active sampling over a wide range of available water pressures without the need for electrotechnical pumps.

3.2 Methane Sensor Improvements

Prior Sensor Evaluation Results

The first generation MWS examined the Dynamet Infrared Sensor (IRS) and the MQ-4 Metal-Oxide Sensor (MOS). When calibrated on known methane concentrations, both sensors were accurate around the 1-2% methane region which is important due to the requirements to alarm and shut down at 1 or 1.5% methane by volume. It is noted that the MOS responded non-linearly while the IRS responded linearly. When tested across various atmospheric conditions it was noted that the MOS sensor required extensive correction factors to account for sample temperature, pressure and most importantly relative humidity. The IRS was less impacted by environmental changes. Response time and decay time was also evaluated as they are important parameters to ensure the MWS can quickly respond to dangerous conditions. The MOS generally had a faster response than the IRS but a far longer decay time. Finally, the MQ-4 showed higher sensitivity at lower concentrations (~100s of ppm), while the IRS had higher error at low concentrations. Therefore, in the second generation MWS, we examined a different sensor in hopes that it would retain the best attributes of both previously examined sensors.

New Sensor Evaluation

The new sensor evaluated was the Gasmittor new dual-wavelength infrared sensors (NDIR), similar in operating principle to the IRS. As such the NDIR provided a linear calibration from 0-2% methane on the output of 4-20 mA. The smaller detection range over the output of 4-20mA provides the Gasmittor with a lower detection limit of 0.01% CH₄ (100 ppm). A marked improvement over the Dynamet's poor performance under 0.2% CH₄. At the highest price point (\$800) the sensor provided superior accuracy and response characteristics. Figure 3.2.1 displays the linear calibration profile as well as the performance at lower methane concentrations (< 0.1% or 1000 ppm). Figure 3.2.2 shows both the rise and decay responses to the presence of methane embody the speedy rise time of the MOS while possessing the decay characteristics of the IRS.

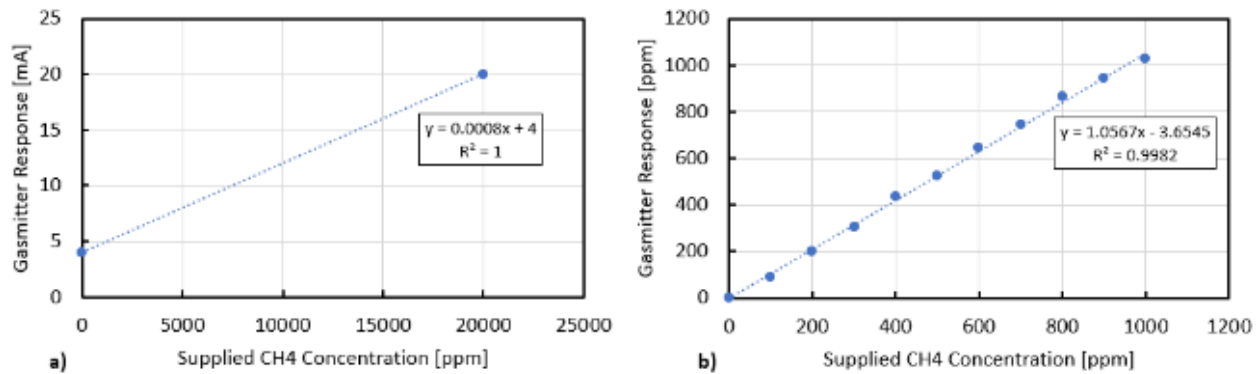


Figure 3.2.1: a) Linear span calibration for NDIR sensor. b) Performance at lower detection limit.

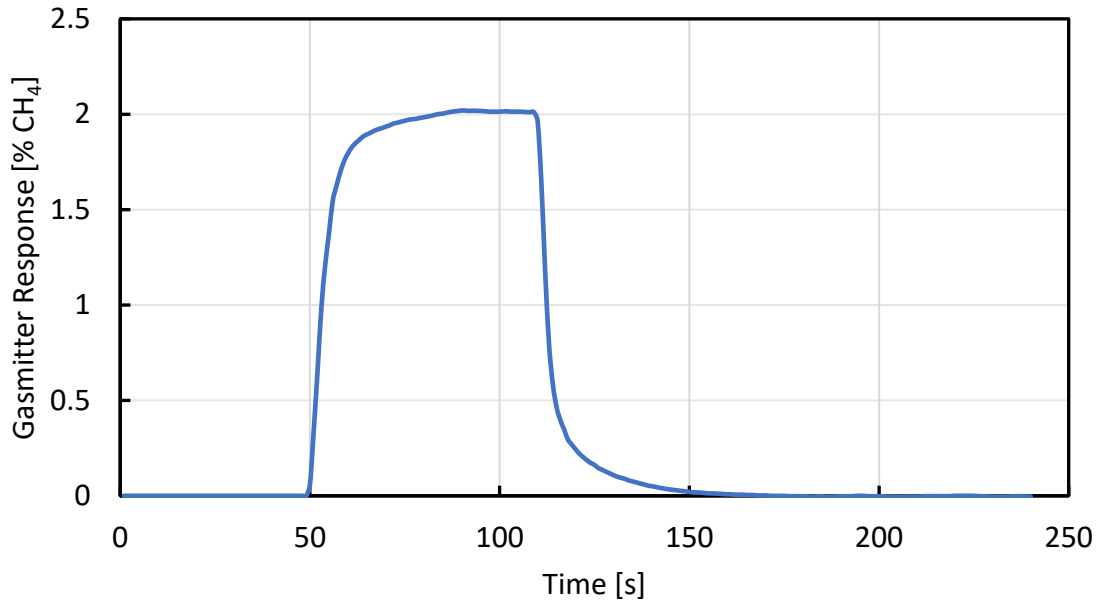


Figure 3.2.2: NDIR response to 2% methane.

Table 3.2.1 presents the response characteristic results for the three sensors under the definitions mentioned above. Two magnitudes of step inputs (1.01% and 2.01% CH₄) were evaluated for the rise and decay times analysis; both of which presented similar results. These characteristic times of the individual sensors are further validated by the following analysis, where the step input to the system is reduced and periodic to access response limitations in a transient environment.

Table 3.2.1: Rise and Decay times for the MOS, IRS, and NDIR sensors.

Sensor	Step Input of 1.01% CH ₄			Step Input of 2.01% CH ₄		
	T90 [s]	T-50 [s]	Ts [s]	T90 [s]	T-50 [s]	Ts [s]
MOS	6	12	>120	5	14	>120
IRS	22	17	28	24	14	31
NDIR	17	5	59	20	5	72

Note: Sampling rate was 2 SLPM. Sample transport delay was ~4 s.

Unlike the MOS and IRS, the NDIR is equipped with its own data acquisition software GasVision [11]. In this software, sensor calibrations are performed, and factory settings are available for modification. The factory settings consist of sensor filter adjustments which control a sample averaging method to limit the noise or sensitivity of the sensor when jumps in concentration are detected. These settings provide an additional layer of tuning by which the sensor response can be optimized for the application and reduction of response times.

Provided these capabilities, factory settings were adjusted to sharpen response times. As a result, the T90 response time of the NDIR sensor was reduced from 17 seconds to 10 seconds. Note this response time is for the entire MWS sampling at 2 SLPM, which included the transport delay

time of ~ 4 seconds. Therefore, the tuned settings in GasVision produced a sensor response time of around 6 seconds. The operation manual provided from Sensors Inc. reports an expected sensor response time (T90) to be within 3 to 45 seconds. Table 3.2.2 presents the re-evaluated rise and decay times for the criteria presented previously for the optimized NDIR sensor.

Table 3.2.2: Rise and Decay times for tuned NDIR sensor.

Sensor	Step Input of 1.01% CH ₄			Step Input of 2.01% CH ₄		
	T90 [s]	T-50 [s]	Ts [s]	T90 [s]	T-50 [s]	Ts [s]
Gasmitter (optimized)	10	6	17	10	5	16

Note: Sampling rate was 2 SLPM. Sample transport delay was ~ 4 s.

Though response times were significantly reduced without any additional postprocessing or reconstruction techniques, the subsequent results were consistent with the factory tuned settings. As a result of sharpening the response with the filter settings, the response became more characteristic of a second-order system. This second-order behavior created a more complex system to model and over defined the characteristic response. As a result, signal reconstruction techniques developed in the following sections are not consistent with the first-order system present with the factory settings.

New Sensor Summary

We tested the new NDIR sensor under the same controlled laboratory tests as the original sensors and results did confirm that the NDIR retained the better attributes of both previous sensors. Therefore, it was the focus of continued research. However, the sensor was integrated within the first generation sampling system to enable continued evaluation of all three sensor. The NDIR was installed ahead of the sampling block to retain its improved response characteristics. Figure 3.2.3 provides an overview of the NDIR (Gasmitter) integrated into the sample node box.

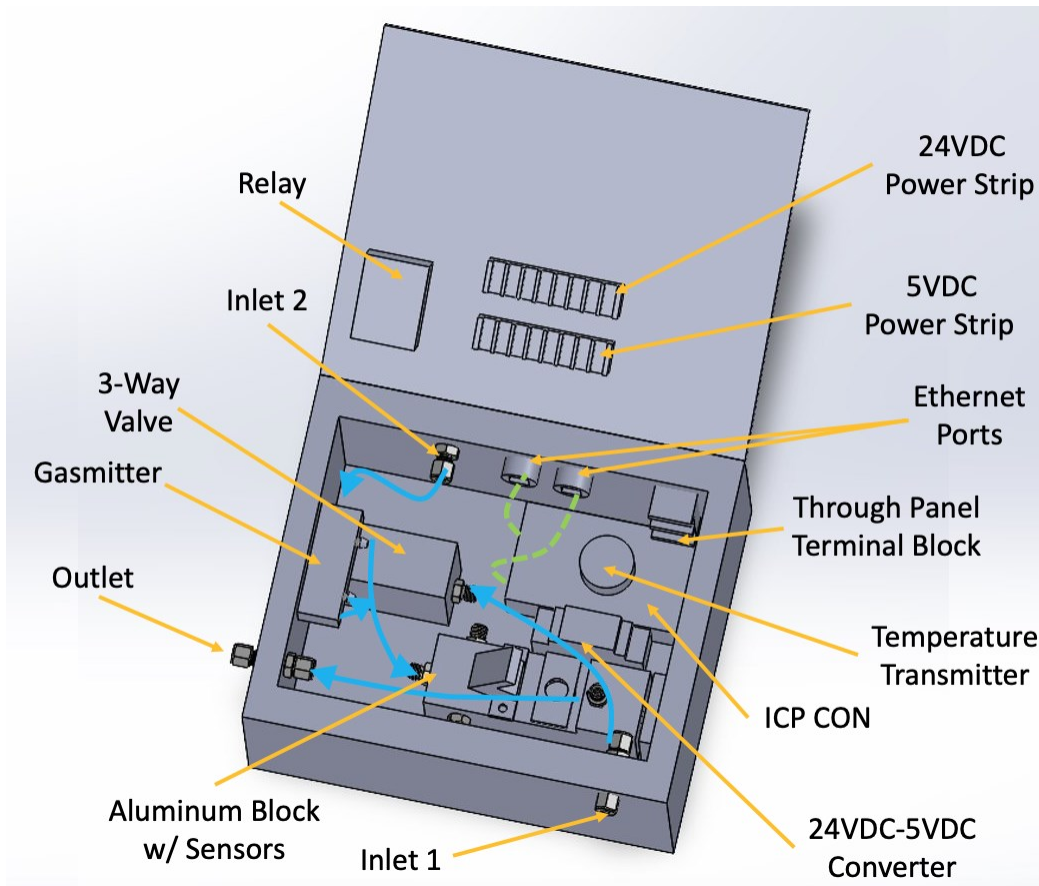


Figure 3.2.3: 2nd Generation MWS Nodal Sample Box with NDIR Integrated.

3.3 Signal Processing Improvements

Delay and Diffusion

At the end of the first generation project, we identified the key issues of delay and diffusion that should be addressed to ensure accurate temporal monitoring of high methane concentrations that should trigger corrective action. Such effects are often overlooked as time-invariant systems will eventually reach the desired response for steady-state operation. It is imperative that detection of a dangerous concentration of methane in the sampling area should be both reliable and rapid. For the response due to dead volumes, it is possible to infer a step rise in concentration from the time-varying sensor response. More broadly, the sensor response can be transformed to yield a prediction of the concentration history at the sampling point, yielding a faster decision on setting an alarm. The decision to set an alarm relies on confidence in the time-varying accuracy of the signal and a measure of the variability of the system due to fouling, sensor deterioration, and flow variation. As noted before, the NDIR had a baseline response time of 17 seconds (10 seconds tuned) and the ability to decay to 50% within 5 seconds. For this reason, the signal processing focused on the NDIR.

Response Characterizations

The first sensor response tests were periodic burst tests that consisted of successive step inputs of 1% CH₄. Input bursts were of fixed and equal duration of time spent “on” and “off”. For example, a test where methane was released for 20 seconds would wait 20 seconds before

releasing another event. Laboratory air containing no methane was sampled in between events. These tests differ from the previous set of experiments because the sensor was not allowed to return to its baseline output before a successive event was released. Figure 3.3.1 presents the response of the NDIR sensor where the duration of the successive burst is reduced from 40 to 5 seconds. As the bursts become shorter in duration (continuous) the effects of delay and diffusion became more prominent.

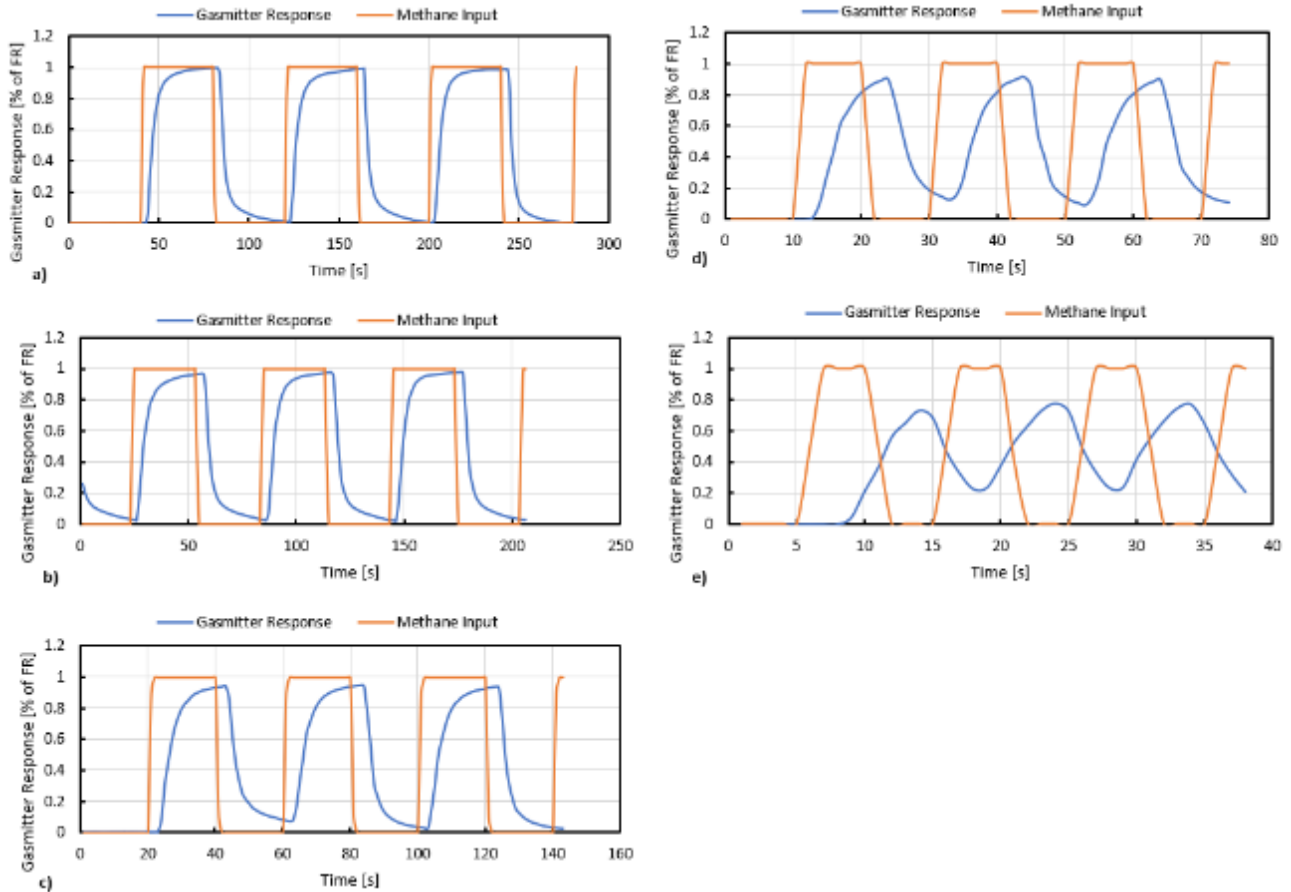


Figure 3.3.1: Dynamic response of NDIR sensor to periodic step inputs at durations (frequencies) of: a) 40, b) 30, c) 20, d) 10, and e) 5 seconds

The results from the periodic inputs were then compiled to form a trend that was associated with the frequency. Figure 3.3.2 presents the projected error or expected response of the NDIR sensor to a periodic input of any duration. The periodicity of the input function mimicked the transient nature of the expected methane profiles within the longwall mine. From here, the sensors' ability to rise to an input and return is challenged, which resulted in a diffused output of the MWS system. In reality, methane would diffuse quickly in the longwall section and present a more continuous function. Therefore, ramp inputs and simulated data were also created to further understand the expected performance of the MWS in the longwall domain.

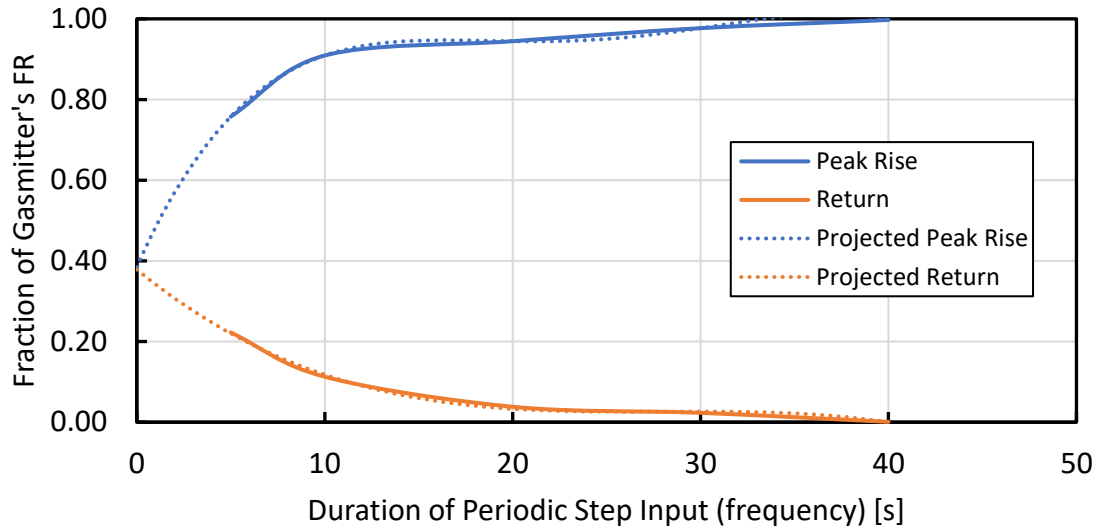


Figure 3.3.2: Projected NDIR dynamic response characteristics to periodic step inputs of 1% CH₄. Equivalent to the amplitude ratio and dynamic error.

A ramp input was then introduced to the MWS for further evaluation of the response characteristics. The ramp input provided an additional method for measuring the systems response time, which was previously found to be around 17 seconds with the NDIR sensor. Figure 3.3.3 presents the criteria used for evaluating the systems response to the ramp input. Equation 3.3.1 was used to calculate the system response time from the two resulting functions, where *error* is the deviation to the true value at a given instance and the *slope* is the ramp rate.

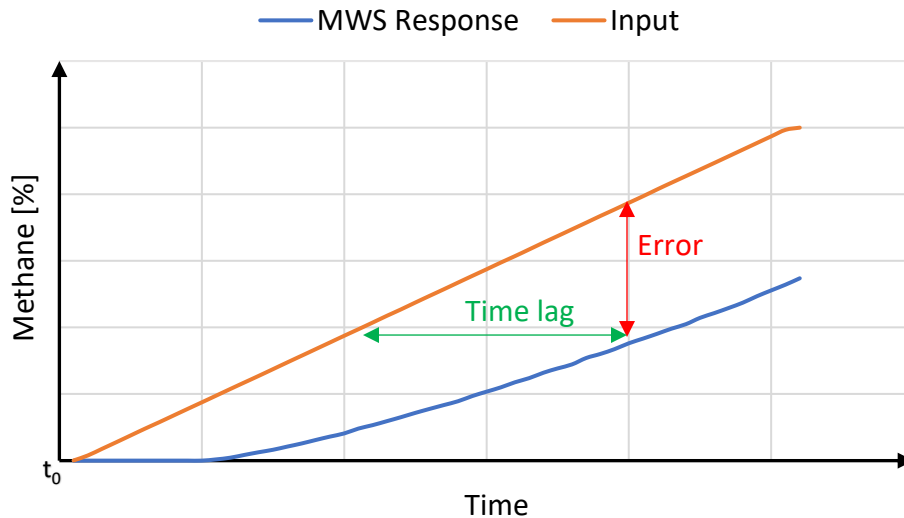


Figure 3.3.3: Definitions used to evaluate ramp input results.

$$Response\ Time = \frac{error}{slope} \quad (3.3.1)$$

Unlike the sudden change in concentration provided by the step input tests, the ramp input creates two unique linear response characteristics. The determined response time was a function

of both the real time error and the shift in signal as a result of transport and sensor response delay. Figure 3.3.4 presents the resulting response to the ramp input. The input and output data were reduced to include only the range of data where the two curves are near parallel.

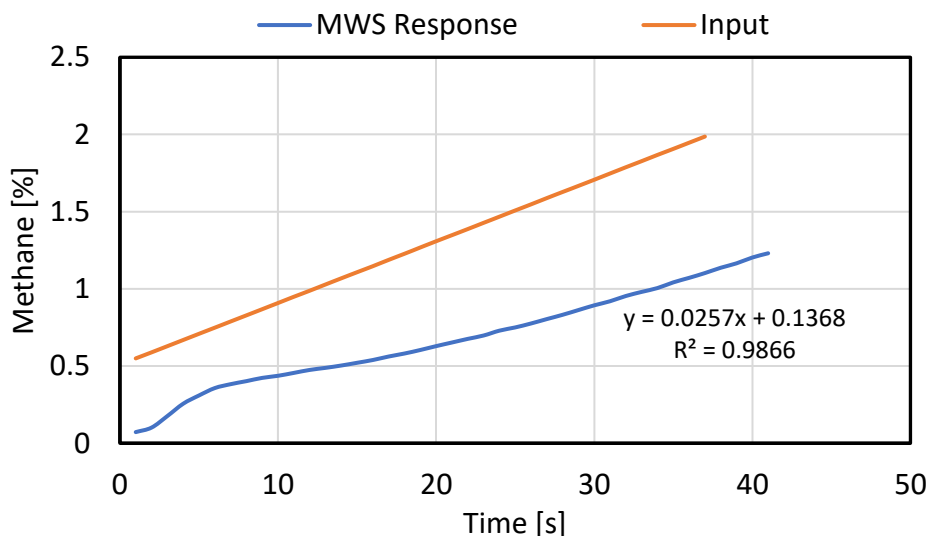


Figure 3.3.4: MWS Response to the ramp input.

A response time was found to be 16.5 seconds from the ramp input test, which validated the 17 seconds determined from the step input test. Due to limitations in sensing range and flow control in the laboratory, the MWS output data that made up the slope was averaged. With a ramp rate of 0.04 (% CH₄ per second), the resolution was quite low and would need to be lower to achieve a longer set of data before the maximum concentration is reached.

We then created time varying methane concentration profiles based on 1-D models. This enabled us to assess the impacts of delay and diffusion on more realistic data. Figure 3.3.5 shows the results of these tests. The regulatory limit of 1% is presented in all plots. The supplied concentration is presented as the dashed line while the NDIR response is a solid line. Of key concern was when the MWS did not detect 1% methane even though it had been supplied, which could lead to in-situ safety issues.

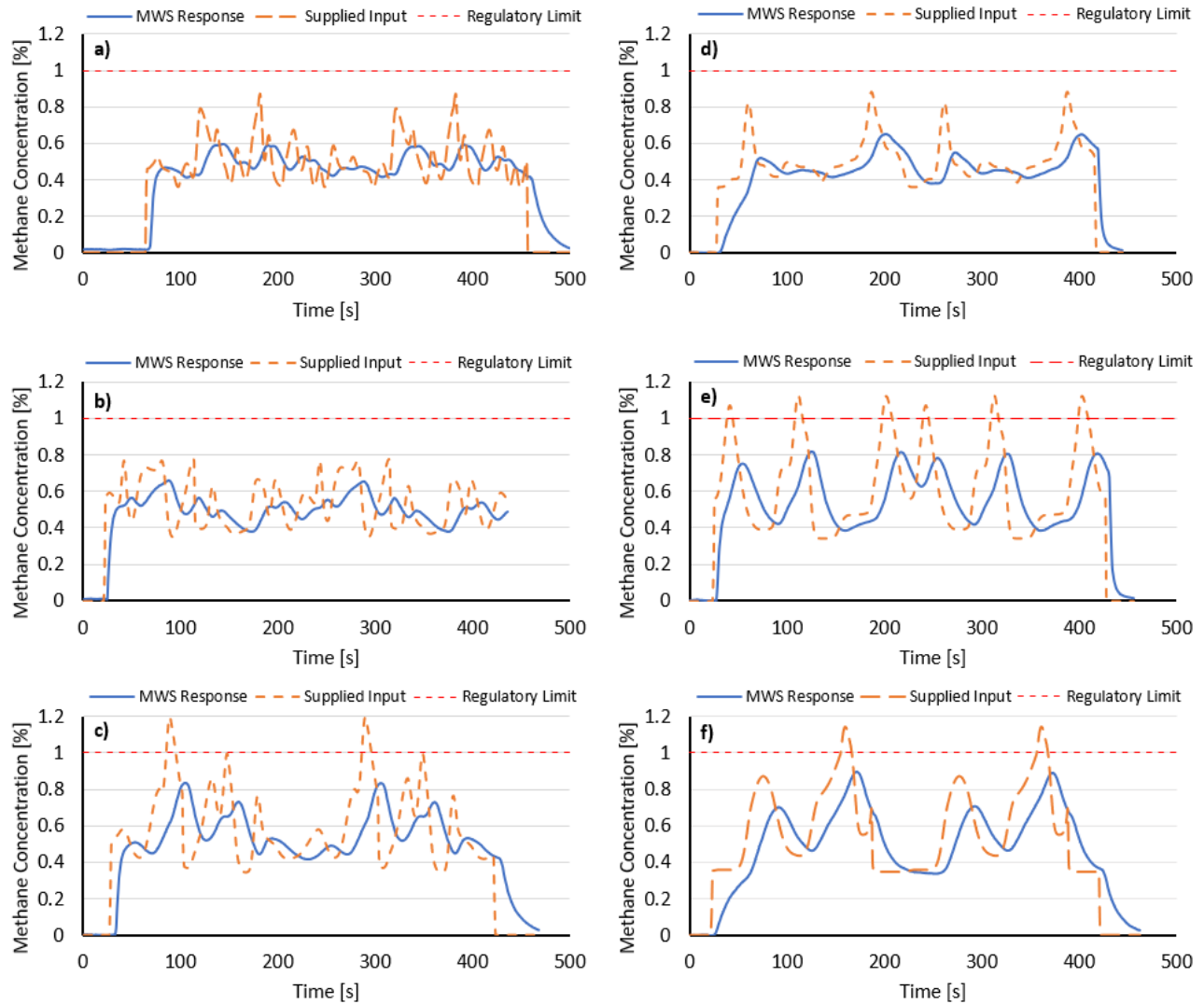


Figure 3.3.5: Laboratory evaluation of MWS performance using ‘Node 5’ simulation data. Fluctuation in ventilation rates at increments of: a) 6, b) 9, c) 12, d) 15, e) 18, and f) 21 seconds.

Sharpening Technique

Previous work had addressed the common issue that concerns the dampened and delayed output from analyzer measurements. Clark and Madireddy discussed two methods for reconstructing transient automotive emission measurements collected from a dilution tunnel within the laboratory setting [12, 13]. Similarly, the collected data was delayed and diffused due to the transport of sample and the analyzers response. The Sequential Inversion Technique (SIT) and Differential Coefficients Method (DCM) [14] were compared against a “fast responding” analyzer. Reconstructed data were then shifted back, or time aligned to match the peaks of the input data, since the reconstruction does not correct the delayed time due to the physical transport of the sample. More broadly, dynamic system responses have been well studied among controls and dynamical system modeling fields [15]. Sensor response characteristics can be constructed from simple step and ramp functions applied to the system of interest. The step and

ramp input definitions are consistent with the studies conducted previously here to characterize the Gasmitter and MWS response. More complex structures of a sensor's response exist among second or multi-order responses where overshoot and stabilization periods are present. The response from the MWS was characteristic of a first-order system however, where little to no overshoot or settling period was recognized. A second-order reconstruction was attempted but provided little addition advantage. Instead, an averaging technique was employed.

Consider the first order ODE to be of the form

$$\tau \frac{dy}{dt} + y = Kx \quad (3.3.2)$$

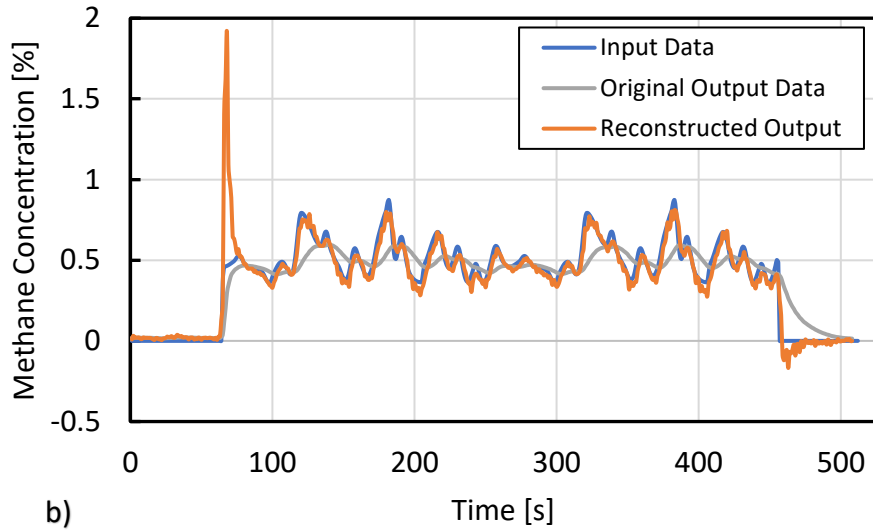
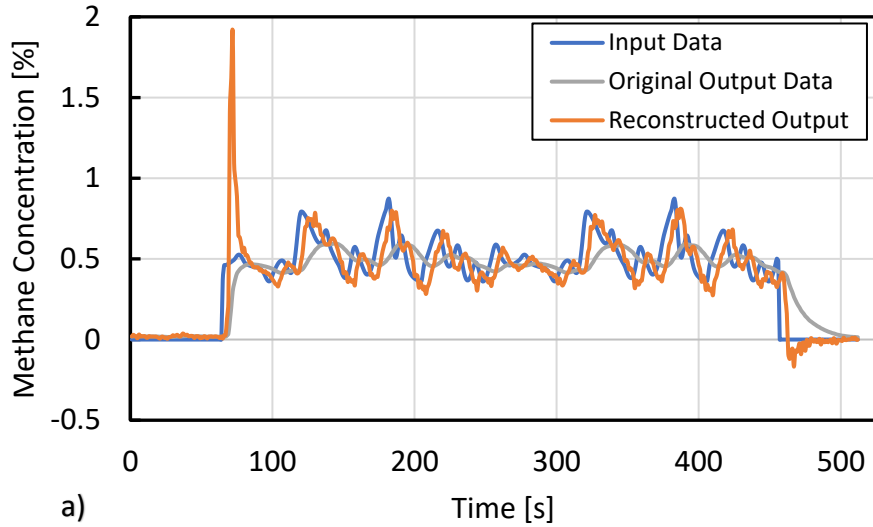
where x is the measured input and y is the systems output. K is the static sensitivity and Tau (τ) is the first-order time constant. The time constant τ is equivalent to the horizontal component of the characteristic ramp input study and was found to be 16.5 seconds. This component being the Time lag which resulted from the MWSs inability to instantaneously respond to the input.

Equation 3.4.1 was then employed to measure the effectiveness and ability to reconstruct the diffused and delayed output data collected from the *Evaluation of System Performance through Simulation Data* studies. These effects were shown above in Figure 3.3-5. The derivative was computed from the backward difference of the 1 Hz data and y consisted of the current uncorrected output value. The reconstructed output can be represented more generally as

$$U(t) = y(t) + \frac{dy}{dt} C_1 \quad (3.3.3)$$

where $U(t)$ is the reconstructed output value and C_1 is the time constant obtained from the ramp response.

At first, Equation 3.3.3 was used to reconstruct the original MWS data collected from the multi-case simulation studies. A time constant (C_1) obtained from the ramp input study of 16.5 was used. An error analyses was conducted with the reconstructed data time aligned to the peaks of the true input data. Therefor the error was defined as the ability of the system to measure the correct magnitude of an event, though it may occur seconds later. The component of delay attributed to only the physical transport of the sample through the system was found to be around 4 seconds. If measurement error can be significantly reduced, then a 4-5 second delay time may be an acceptable tradeoff for the time being. Figure 3.3.6 a) presents the reconstructed output of the MWS in comparison to the true input signal. The original diffused output signal is also included for reference. Figure 3.3.6 b) then presents the time aligned signals which were used to measure the error or correctability of the first-order ODE method.



Figures 3.3.6: First-order reconstructed output of MWS with time constant of 16.5. a) Real-time delayed signal. b) Time aligned to input data.

Though the simple first-order method appears to have significantly improved the diffused output signal, a large spike overshooting the initial input of methane was present. A similar phenomenon occurred at the end of the test by the overshoot noise when returning to zero. This phenomenon was consistent with the Gibbs phenomena commonly encountered in Fourier series of square wave reconstruction [16]. The discontinuity of the function presents noise as the immediate jump was not constructable by the first order ODE and time constant. In other words, the slope of the sensor's response becomes very steep momentarily and is not characteristic to the time constant obtained (16.5). This issue is also what causes the overshoot at the valleys of the signal. Discussed earlier, the NDIR embodies a very quick decay when a methane concentration is removed. This quick decay results in a characteristic response that is not consistent with the rise response, which formed the basis of the reconstruction technique.

With these characteristics now understood, an additional attempt was made to better fit the reconstructed data to the true input data through a conditional program. The program provided the control needed to alter the time constant when the derivative switched from being positive (rise response) to negative (decay response). In addition, a condition was put in place which eliminated the correctional time constant all together when a slope exceeded a threshold of 0.07% CH₄ per second. This would be the result of an immediate step input of methane seen at the beginning and end of the test presented above.

By implementing a conditional program, the time constants were tuned to characterize the rise response and the decay response. The original time constant of 16.5 was increased to 20 to improve the peak responses and a new decay constant of 12 was defined to correct the low or valley concentrations. The discontinuity error was not eliminated at the start of the test; however, it was reduced by nearly 50%. The averaging of two time-steps also noticeably reduced the noise without sacrificing any correctional benefits. Table 3.3.1 presents the results obtained when the reconstruction method is applied to all six simulation cases previously studied. The table contains the average original errors, after time alignment, and the new reduced errors achieved from the reconstruction method. The average error was taken over all continuous relative data in the simulation, omitting the discontinuity error at the beginning.

Table 3.3.1: Error analyses showing improved accuracy with the reconstructed technique.

Case [#]	Original Output [Error]	Reconstructed [Error]	Improved Accuracy [%]
1	15%	4.1%	11%
2	18%	4.4%	14%
3	22%	4.9%	17%
4	12%	3.4%	8.6%
5	26%	3.5%	23%
6	23%	3.6%	19%
Average	19%	4.0%	15%

Signal Processing Improvements Summary

All active sampling systems with sensors will experience delay and diffusion. To minimize this issue, we focused on the NDIR sensor since it had the best balanced characteristics for rise and decay responses. The overall system behaves nearly as a first order system. As such, we were able to use first order reconstruction approach with a time constant of 20 and a decay constant of 12 to reduce error. To overcome slight second order behavior due to rapid changes, we implemented a basic control logic on the rate or rise or decay. With this control implemented, the average error reduced by 15% from 19 to 4%. This sharpening method therefore reduced the error associated with delay and diffusion by 79%. It should be noted that this method cannot eliminate the physical delay of the active sampling system. However, an overall response time of 10-17 seconds meets or exceeds current standards for methane sensors in mining applications.

3.4 Mine Like Environment Evaluations

During the initial program we conducted full systems evaluations in a mock mine that was scaled at about 1/10th the length of current longwalls (100' versus 1000'). Unfortunately, we were not able to produce or maintain ventilation velocities that would be representative of real mines. To produce more realistic evaluations, we repeated these evaluations using the simulated mine facilities with realistic geometry at the WVU Mine Training Academy in Core, WV. This enabled better evaluation at consistent ventilation flow rates since the facility is powered by a diesel fueled blower. In addition, the facility enabled us to extend the scaled length from 100' to over 300' by using the front section of the mock mine (see Figure 3.4.1 and the left most section in the red circle).



Figure 3.4.1: WVU Mine Training Academy proposed for use in system evaluations.

Evaluation Method and Specifications

In addition to tripling the length of the mock longwall, the facility also utilized a diesel powered blower and various flow that's to better simulate long wall ventilation conditions. Figure 3.4.2 presents an overview of the location of the nodes spaced along the “mock” face. Note that the nodes are shown as black circles. These nodes were not evenly spaced due to mounting feasibility due to facility plumbing and equipment. Each node could sample from the face and near to “gob”. Note that the face sampling points were midway down the face wall, which allowed for direct alignment with the injection hose. As such, the “gob” sample points were about center of the cross section at approximately the same elevation. Evaluations primarily focused on sampling from the “mock” face which is denoted by the right most side of the mine and denoted by the blue ovals. Velocity along the general middle center line was measured at nodes 2, 5, and 10 with a sonic anemometer and two cup anemometers respectively. Further,

where doors could be closed, they were as shown by red lines. This ensured that flow was primarily from the left to the right. We note that a section between nodes 8 and 9 could not be closed. This allowed for a reduction in ventilation flow and velocity at nodes 9 and 10. We note that many studies show that flow decreases along the face to leakage into other zones such as the gob area.

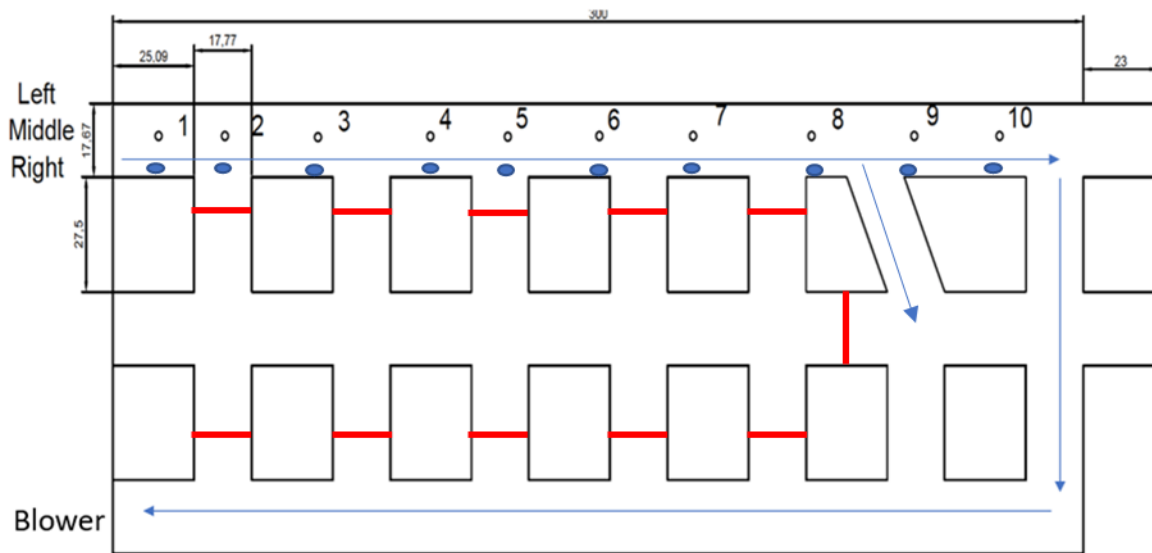


Figure 3.4.2: Overview of Node Placements Along Front Face. The Right Most Side Represents the Longwall Face. Node Locations are Identified with Circles and Blue Ovals Show the Sampling Locations Along the Face. The Left Most Side Represents the Gob. Blue Arrows Indicate the General Ventilation Velocity Flow Paths

Tests included both mobile and stationary injection tests. Methane emissions were created from CNG tanks that were fed through a mass flow controller. These emissions were inducted into the inlet of an explosion proof blower. The blower was part of the WVU FFS system which has been discussed before. The system was capable of varying the flow of the blower and measuring the total flow and methane concentration so create different injection concentration and flow rates. The outlet of the FFS was a wire wound, grounded flexible hose that could be fed back and forth into the mine face. The outlet of the methane injection hose was affixed to a cart with barrels that served as a bluff body. The maximum supplied concentration was about 3.5% by volume or less than 70% of LEL. Handheld methane detectors were utilized and were independent of the MWS to ensure an additional layer of safety. Figure 3.4.3 presents an internal view of the mock facility with the MWS, and methane injection system highlighted. Supplement Video File 1 shows the general setup walking from the rear to the entrance of the mock face.

(https://drive.google.com/file/d/1q40T3Mmhssc1vVRjs4xut5Vd5SLiP_OQ/view?usp=share_link)



Figure 3.4.3: Example of an MWS node and mobile bluff body used to supply methane injection.

Figure 3.4.4 present an example image that shows the injection control FFS system and the separate tent housing the CPH and secondary DAQ recording station. The right of the image shows a view of the CPH during tests. Figure 3.4.5 presents an example of 8 of 18 signals (raw and calculated) logged during evaluations for a single node of the evaluations.

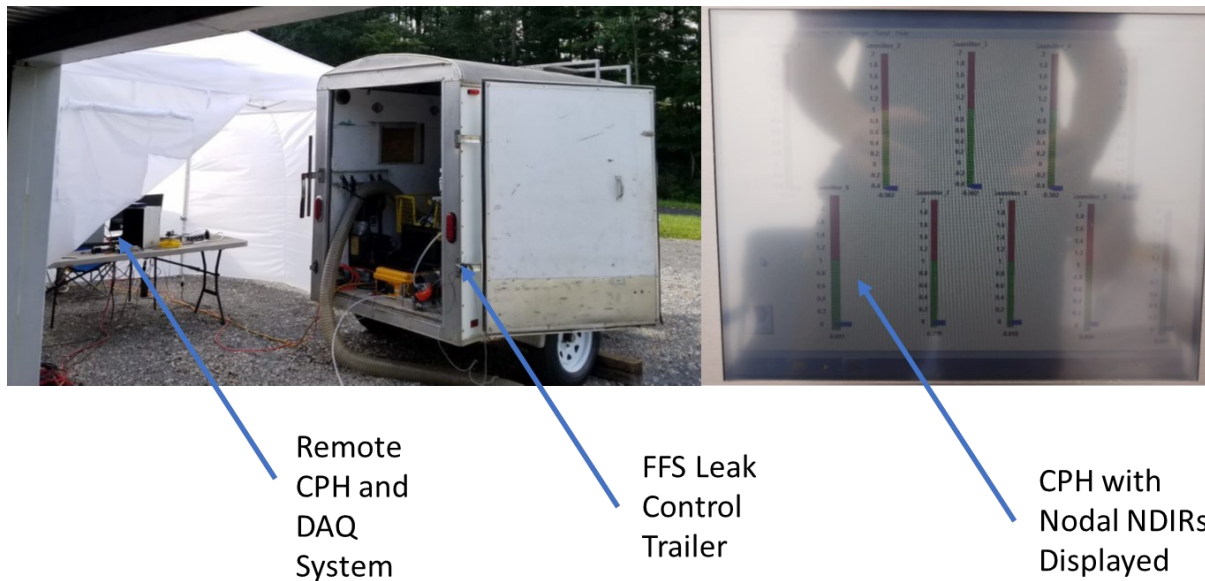


Figure 3.4.4: Images of CPH, FFS, and Secondary DAQ Systems Located Outside of the Tailgate Region.

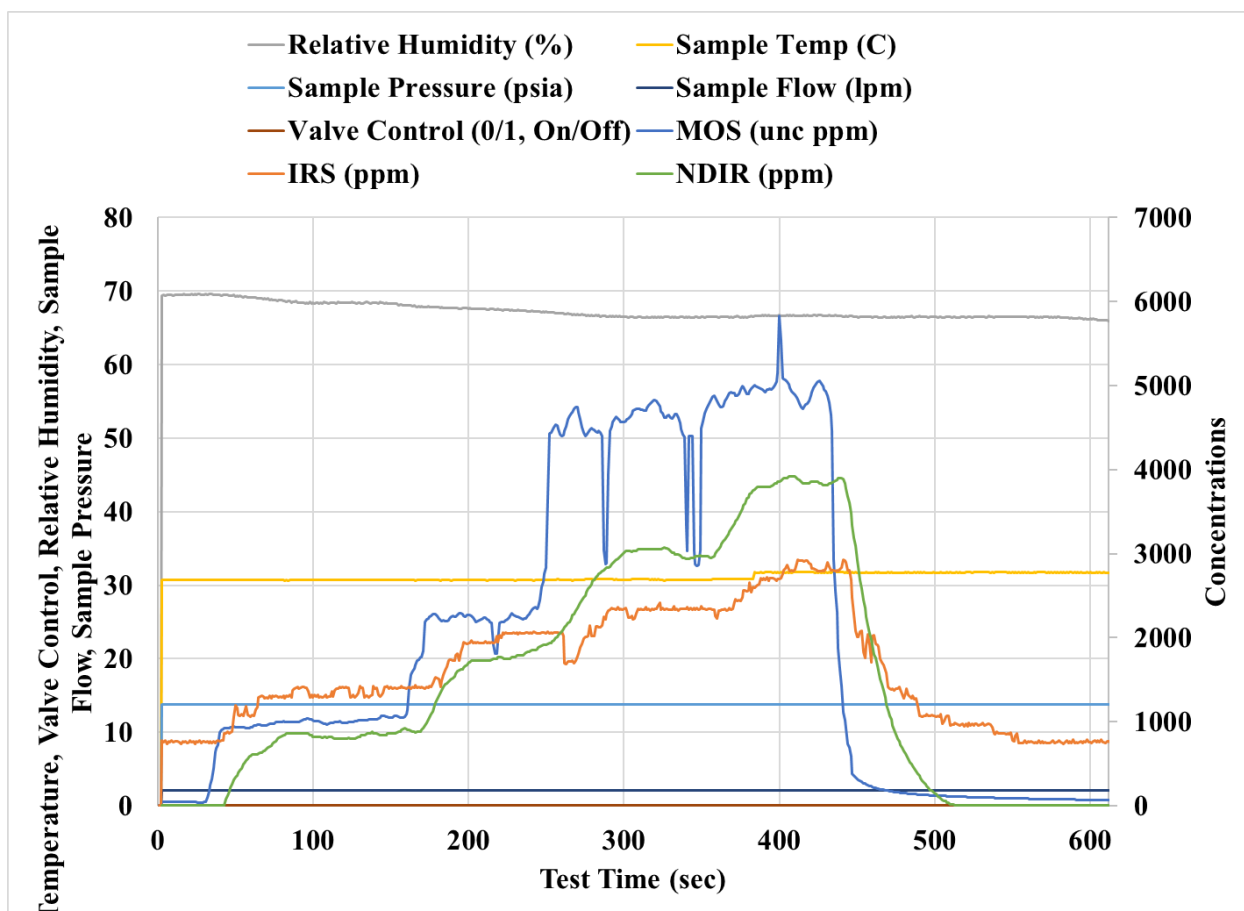


Figure 3.4.5: Example of 8 of the 18 Parameters Monitored and Recorded for Each of the 10 Nodes.

Multiple days of set up and cursory tests were conducted in order to complete system shake downs, understand injection and flow conditions. The mock mine facility was capable of producing ventilation velocities at or above our target of 2 m/s. However, when supplying injections that were lower than the LEL, higher ventilation rates quickly dissipated emission plumes. Note that the mine training facility typically utilizes propane for mock fire and smoke training. As such, we had to utilize compressed natural gas (CNG) tanks external to the building to create injections within the front face. Therefore, we focused on lower flow rates running the fan engine at only around 1000 or 1500 RPM to produce ventilation velocities around 1-1.5 or 1.5-2.0 m/s, respectively.

Table 3.4.1 presents a summary of the tests that occurred after initial shakedown and troubleshooting exercises were completed. Both fan speeds (ventilation velocities) were used in both stationary and mobile tests. For mobile tests, the cart started at the entrance (HG) and proceeding into the mock longwall face until just past Node 10. The injection hose was fed in while the face was traversed and rolled out upon return. Appendix B includes additional details for tests and data collected.

Table 3.4.1: Various Test Conditions During Evaluation of the MWS.

Test	Fan Speed (RPM)	Mobile/ Stationary	Duration (s)	Average Cart Speed (ft/s)	Ventilation Velocity (m/s)				CH ₄ Supplied
					Sonic	Cup Middle	Cup End	Average	
1	1,000	Mobile	900	0.75	0.75	2.99	0.57	1.44	0.75%
2	1,000	Mobile	900	0.75	0.79	2.93	0.48	1.38	1%
3	1,000	Mobile	900	0.75	0.73	2.92	0.57	1.41	1%
4	1,000	Mobile	710	0.90	0.72	2.84	0.44	1.33	1%
5	1,000	Mobile	840	0.99	0.74	2.94	0.49	1.39	1%
6	1,000	Mobile	750	1.02	0.76	2.99	0.53	1.43	1%
7	1,000	Mobile	860	1.00	0.73	2.91	0.49	1.38	2.50%
8	1,500	Mobile	720	1.00	0.91	4.03	0.81	1.92	1%
9	1,500	Mobile	750	1.02	0.96	4.02	0.83	1.94	1%
10	1,500	Mobile	730	1.01	0.99	4.00	0.83	1.94	1%
11	1,500	Mobile	810	1.00	1.01	3.98	0.78	1.92	2.50%
12	1,500	Stationary (3)	620	N/A	0.97	3.77	0.77	1.84	.5-2.5%
13	1,500	Stationary (3)	690	N/A	0.82	2.62	0.49	1.31	.5-2.5%
14	1,000	Stationary (6)	620	N/A	0.81	1.89	0.31	1.00	.5-3.5%
15	1,000	Stationary (6)	500	N/A	0.76	1.79	0.23	0.93	.5-3.5%
16	1,000	Stationary (3)	610	N/A	0.61	1.79	0.54	0.98	.75-2.25%
17	1,000	Stationary (3)	810	N/A	0.61	1.78	0.55	0.98	1-3.5%
18	1,500	Stationary (3)	600	N/A	0.82	3.02	0.86	1.57	1-2%
19	1,500	Stationary (3)	720	N/A	0.85	3.16	0.84	1.62	1-2.5%
20	1,000	Stationary (3)	650	N/A	0.68	2.13	0.58	1.13	1-2.5%
21	1,000	Stationary (3)	580	N/A	0.70	3.32	0.60	1.54	1-2.5%
22	1,000	Stationary (Entrance)	530	N/A	0.91	2.89	0.53	1.44	1-3%

Figure 3.4.6 shows a zoom of Figure 3.4.13 discussed later. To create methane profiles, the FFS controlled methane from CNG tanks into its inlet. The CNG mixed rapidly within the measurement section and long delivery hose. This created methane injection rates of ~100-200 SCFM with delivered concentrations of up to ~3.5% methane by volume. This ensured that a dangerous case of flammable mixtures did not occur within the facility or within the methane injection tube that was housed within the facility. The methane concentration of the FFS was measured with a laser based sensor and represented the maximum concentration delivered at the injection tube outlet located on the mobile bluff body. The red area shows methane near this delivered concentration and that it quickly dissipates to lower concentrations due to the ventilation air. Therefore, accuracy of the MWS sensors cannot be examined directly. However, their diluted responses were verified later on using 2-D CFD to that assessed the rapid dilution. Refer to Figure 3.3.6 and Table 3.3.1 for the overall accuracy of the MWS sensors based on time varying laboratory experiments.

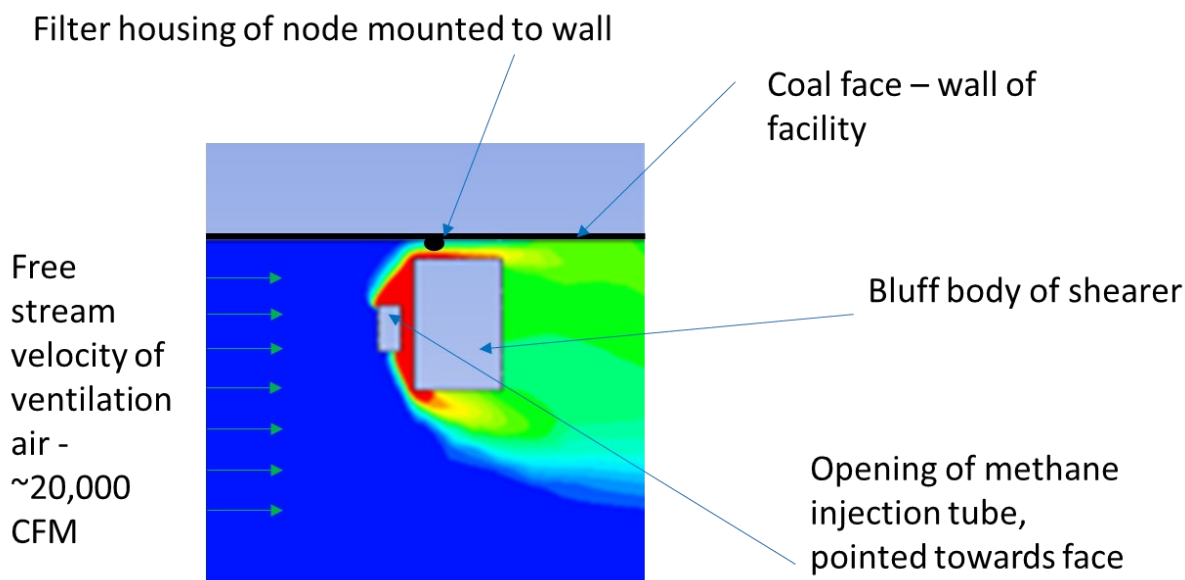


Figure 3.4.6: Example of Methane Injection and Rapid Dilution Due to Ventilation Air. The FFS Concentration Represents an Accurate Concentration Delivered at the Tube Exhaust but was Not the Same Concentration Experienced by the Sampling Points Due to Dilution with Ventilation Air.

Figure 3.4.7 highlights the rapid dilution based on supplied injection concentration at the injection outlet compared to the measured concentrations sampled at the face (wall). The results shown are for Test 16 where, a stationary test where the injection was located at the sampling point of Node 3, similar to geometry highlighted in Figure 3.4.6. Methane was supplied at flow rates from 0 to 4 SCFM in 1 CFM increments until it was turned off at around 420 seconds. A natural dilution ratio 5 to 1 or more occurred between the injection outlet and the sampling inlet. Figure 3.4.8 presents a zoom in view to highlight the nodal sensor behavior. Up to around 150 seconds, we see that the MOS and NDIR are in good agreement, but the IRS reads higher. As the supplied methane flow rates increase further, the MOS sensor tended to diverge with periodic dips in concentration. This test was conducted just after a zero and span of the NDIR and as such represents more accurate data. Note, the MOS and IRS were calibrated before deployment in the

laboratory. The NDIR was capable of being zeroed and span easily after installation of the MWS. The MOS decays rapidly compared to the others while the IRS is the slowest to decay. As mentioned earlier NDIR attains the best response attributes of both other sensors.

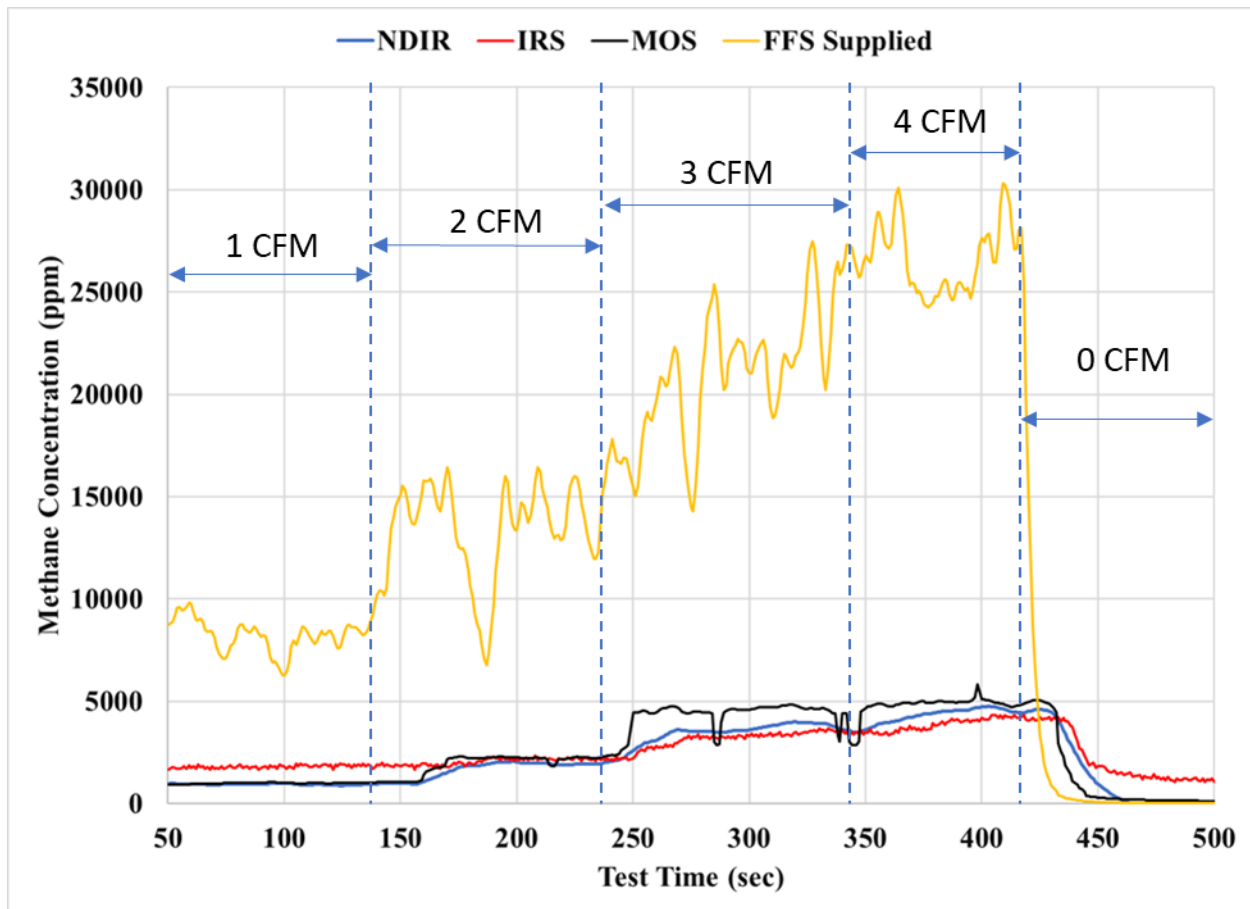


Figure 3.4.7: Example of Rapid Dilution Due to Realistic Ventilation Velocities.

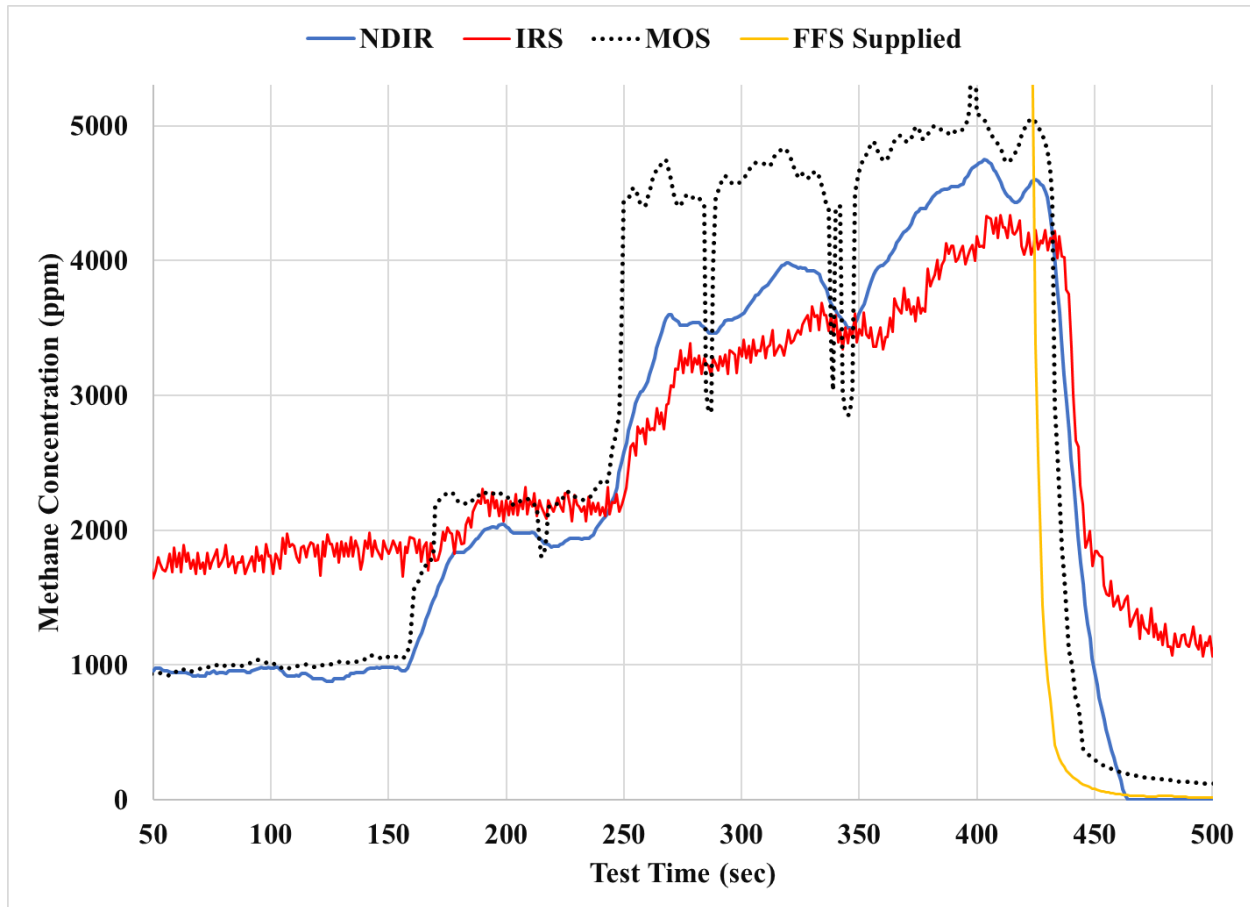


Figure 3.4.8: Example of MWS Methane Sensors Responses During a Stationary Evaluation.

Another important metric to all sensors was ensuring consistent sample flow rates among all nodes. For these evaluations, pumps were used to create the suction pressures from a central location as opposed to running water lines for ejectors. A single mechanical pump was selected solely out of convenience over running separate water lines for each of the 10 nodes or periodically tapping into the facilities fire control plumbing. We previously highlighted that low cost flow measurement sensors could be incorporated into each node. This could allow for the MWS to monitor flows in the case of filter clogging or also be used to inform in-situ sharpening algorithms. Figure 3.4.9 presents the continuous sample flow rate monitoring signals for all ten nodes during Test 16. The average nodal flow rates ranged from 1.95 liters per minute (LPM) to 2.27 LPM or within +13.6 and -3.5% of the setpoints. By incorporating these sensors, the sample flow rates at all locations were monitored by the CPH and these values were utilized during setup to fine tune the flow rates. A similar approach would be used in a real mine where ejector water/gas flow rates could be set using the MWS monitored data.

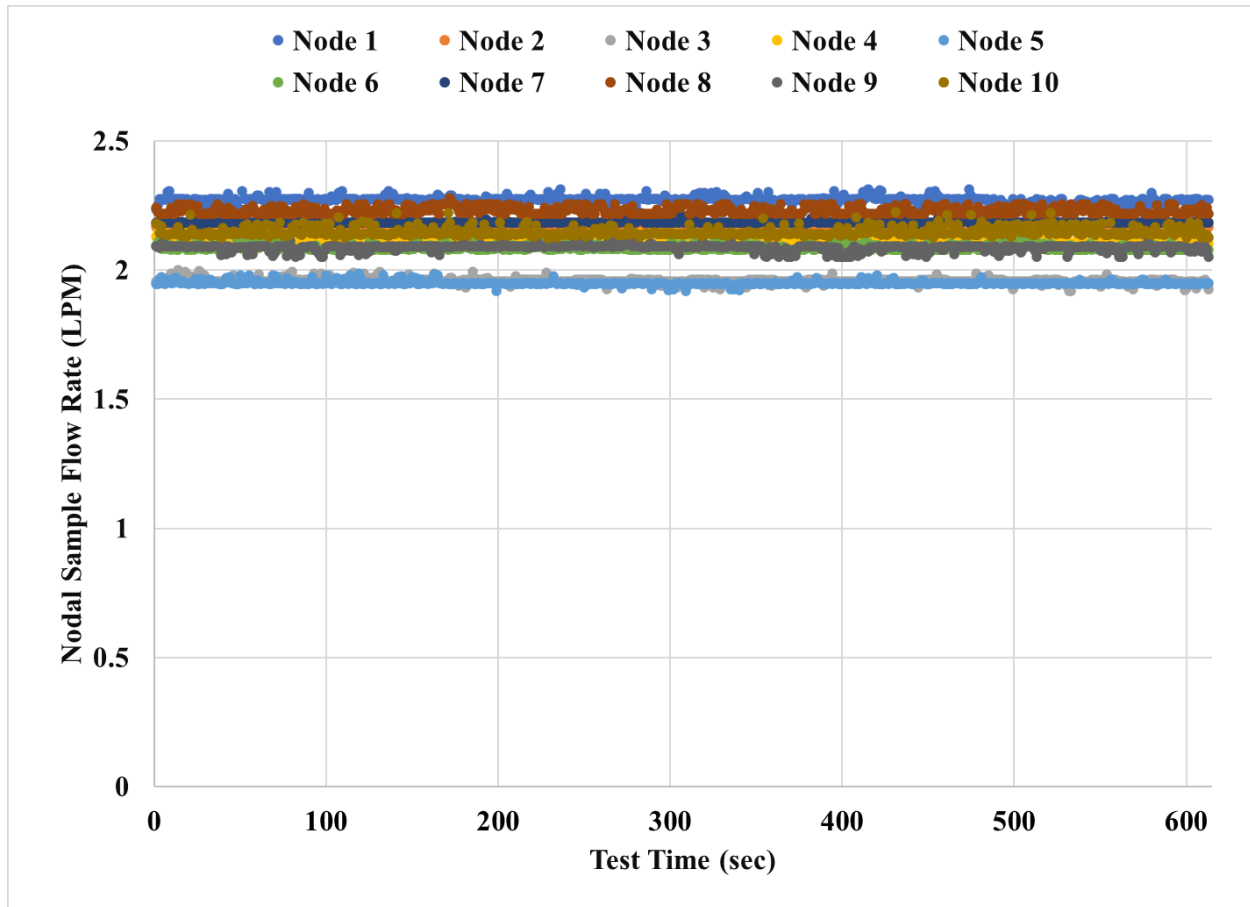


Figure 3.4.9: Example of MWS Nodal Flow Rate Sensors.

Summary of Stationary Tests

A key attribute of the MWS is that it would enable operators to continuously monitor methane emissions across the long wall face. While our evaluations did were not able to demonstrate concentrations at or above 1% due to safety concerns, we were able to demonstrate its capabilities. For the same Test 16 as highlighted in 3.4.7-3.4.9, we can illustrate its monitoring capabilities based on downwind measurements. Figure 3.4.10 shows the response of Node 6, 7, and 8 during this same time period. We see that each nodal concentration tends to increase as a function time due to the increasing methane supplied upwind at Node 3. We see that the concentration rapidly drops from Nodes 3 to 6 due to the rapid dilution in the mock mine. However, we see that dilution effects are lesser between Nodes 7 and 8 as the plume has already become well mixed.

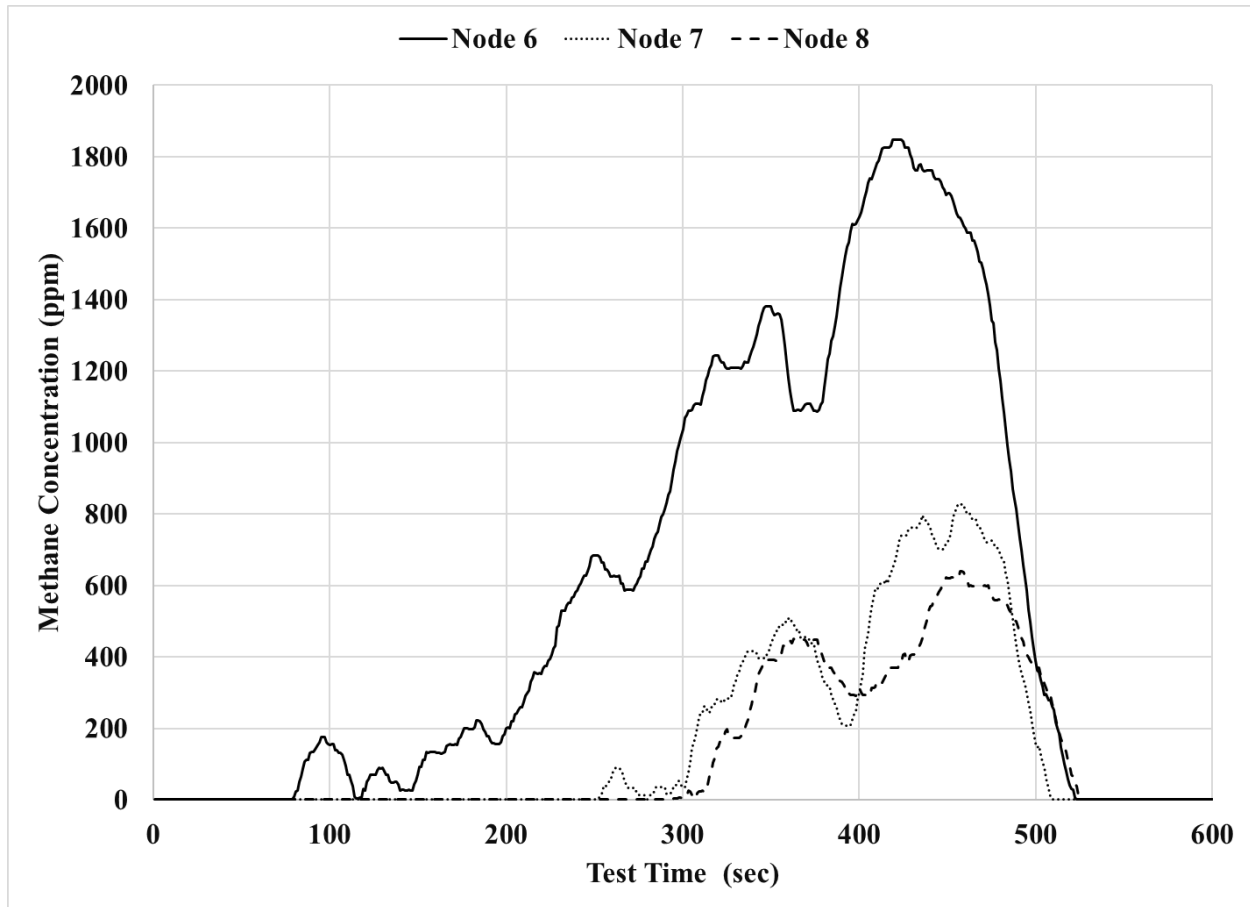


Figure 3.4.10: Example of MWS Capability to Monitor Methane Downwind of Methane Release. Similar Concentration Profiles are Recorded Downwind, but Magnitudes Decrease as Methane Injection is Further Diluted as it Travels Down the Face.

In addition, we note that literature reports of increased methane concentration near tailgates due to ventilation loss and recirculation. Referring to Figure 3.4.2, Nodes 9 and 10 are just past a diverter byway that enabled short circuiting of ventilation air. As such, one would expect that recirculation could be produced in this region. Figure 3.4.11 represents Nodes, 6, 7, and 8 but they have been grayed. Nodes 9 and 10 have been added now as solid and dashed black lines. We see that Node 9 concentrations tend to actually be higher than Node 8, not because of additional methane addition but due to an area of recirculation created by the bypass. Once in this separation region we then see the plume further dilute as the remaining flow travels to Node 10.

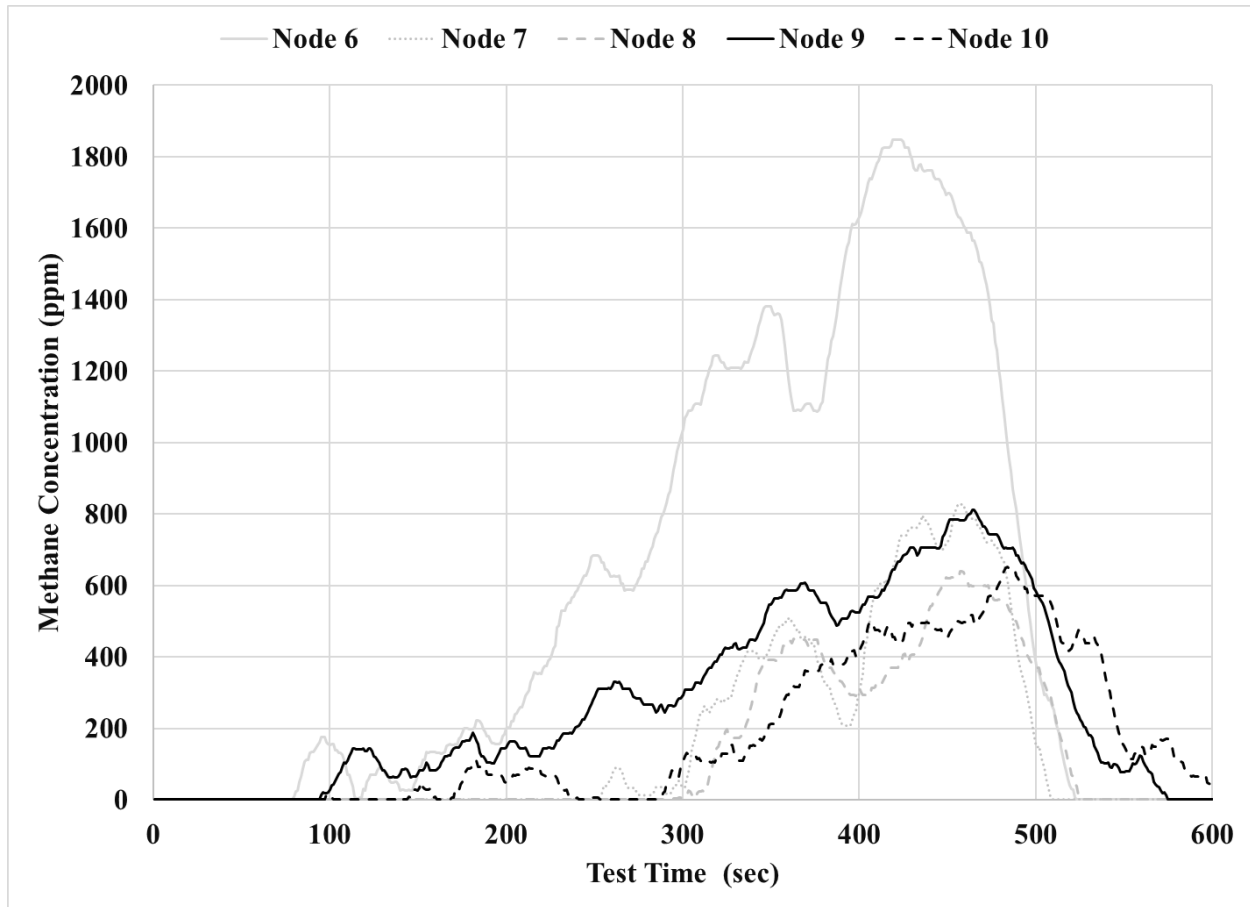


Figure 3.4.10: Nodes 9 and 10 Showing Higher Methane Concentrations than Upwind Node 8 Due to Recirculation.

To verify the operation of the MWS at gas concentrations much lower than 1% we developed a reduced order 2-D model of the mock mine facility. Figure 3.4.12 presents the domain with blocked sections of the facility removed. The inlet flow is fresh air, and the outlet was the resulting mixture at the fan location. Flow rates were adjusted to match well with the average velocities reported in Table 3.4.1. For example, the average velocity of this model was about 1.65 m/s. The average velocity for stationary tests with Node 3 releases with the blower operating at 1,500 RPM was 1.59 m/s – 4% average deviation.

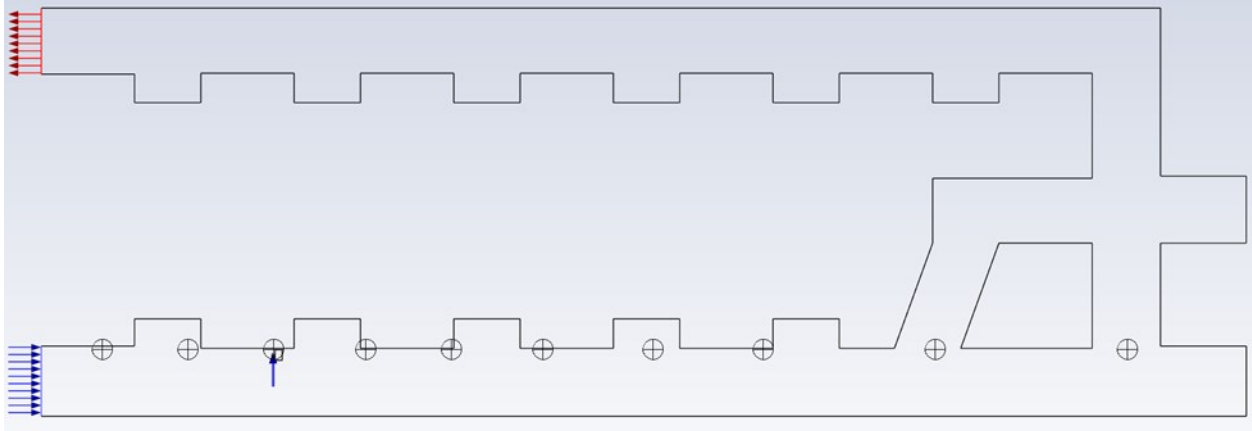


Figure 3.4.12: Reduced Order Flow Domain for 2-D Modeling Verification of Low Concentration Results.

For comparisons with highlighted results above, the following 2-D analysis focuses on stationary test where the methane injection was located an Node 3. Figure 3.4.13 presents a zoomed view of the methane release at the bluff body of the mock shearer. For this analysis, the FFS provided a total flow rate of 160 CFM at an injection concentration of 50% of LEL (2.5% methane by volume). Figure 3.4.14 shows results for the entire domain. It is noted that the as experimental results showed, the majority of the injected methane short circuited after passing Node 8 through the bypass.

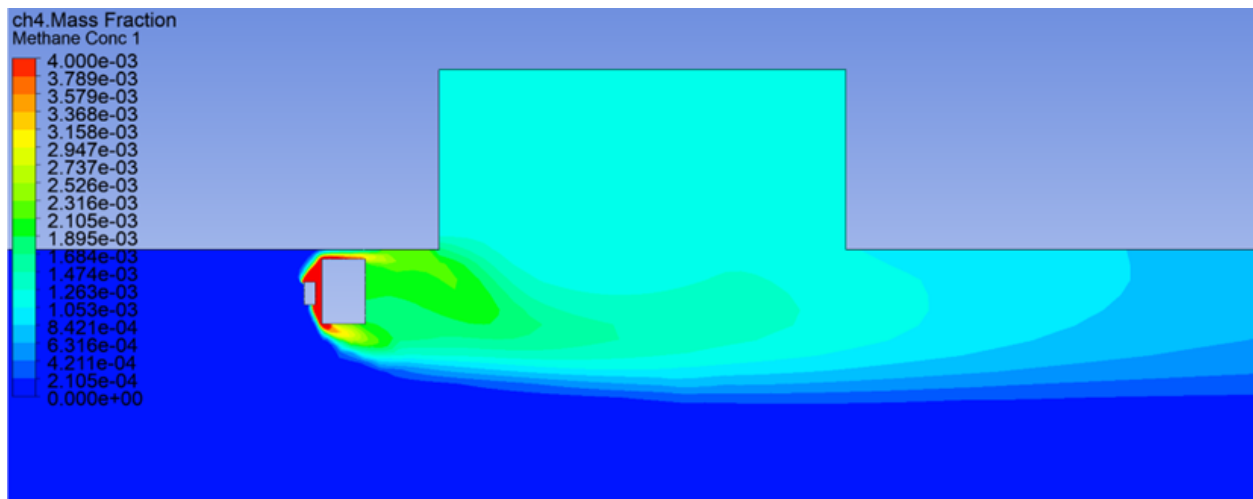


Figure 3.4.13: Stationary Methane Release at Node 3.

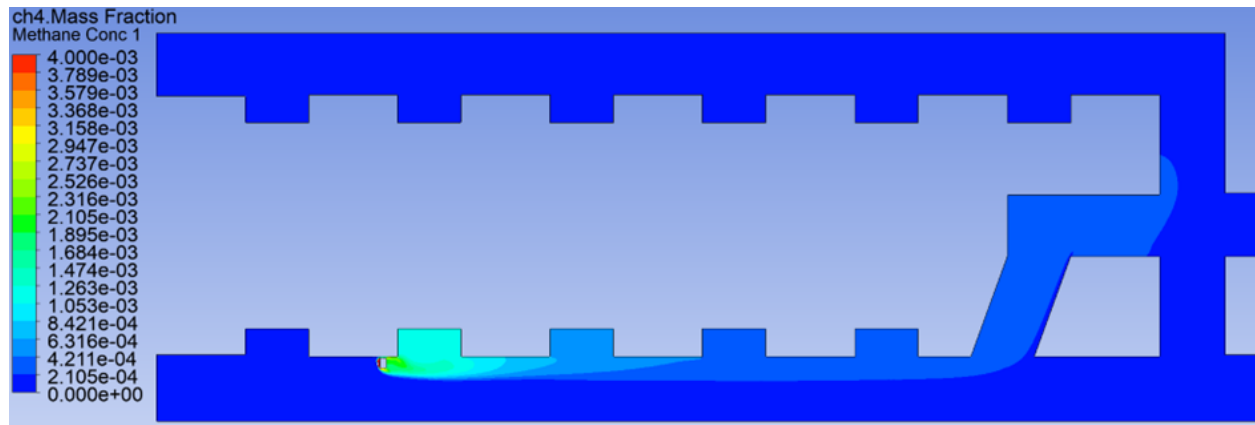


Figure 3.4.14: Dilution of Methane Along the Mock Mine Face and Short Circuiting of Flow at Bypass Between Nodes 8 and 9.

The nodal locations from Figure 3.4.12 were sampled to obtain the average steady concentrations of methane. Figure 3.4.15 shows the nodal data from experiments and 2-D models. The model was verified by comparing the concentration at Node 3 which was within $\pm 10\%$ of the model (measurement uncertainty of the MWS – shown as error bars). The simulated concentration at Node 3 was 1.19% while the average NDIR measured concentration was 1.24% - average deviation of 4.1%. The model predicts the same general behavior as experimental data, a rapid dilution of the injection to concentrations well below 0.2% or less than 2000 ppm. Though difficult to see due to the color coding of Figure 3.4.14, Nodes 9 and 10 of the simulation do show detectable methane concentrations even after the main flow follows the bypass between Nodes 8 and 9. We note that the 2-D modeling was a reduced order model since the various equipment housed within the mock mine facility was not modeled. As such, the model results show the same trend as experimental data but cannot capture smaller recirculation zones that existed within the experimental tests.

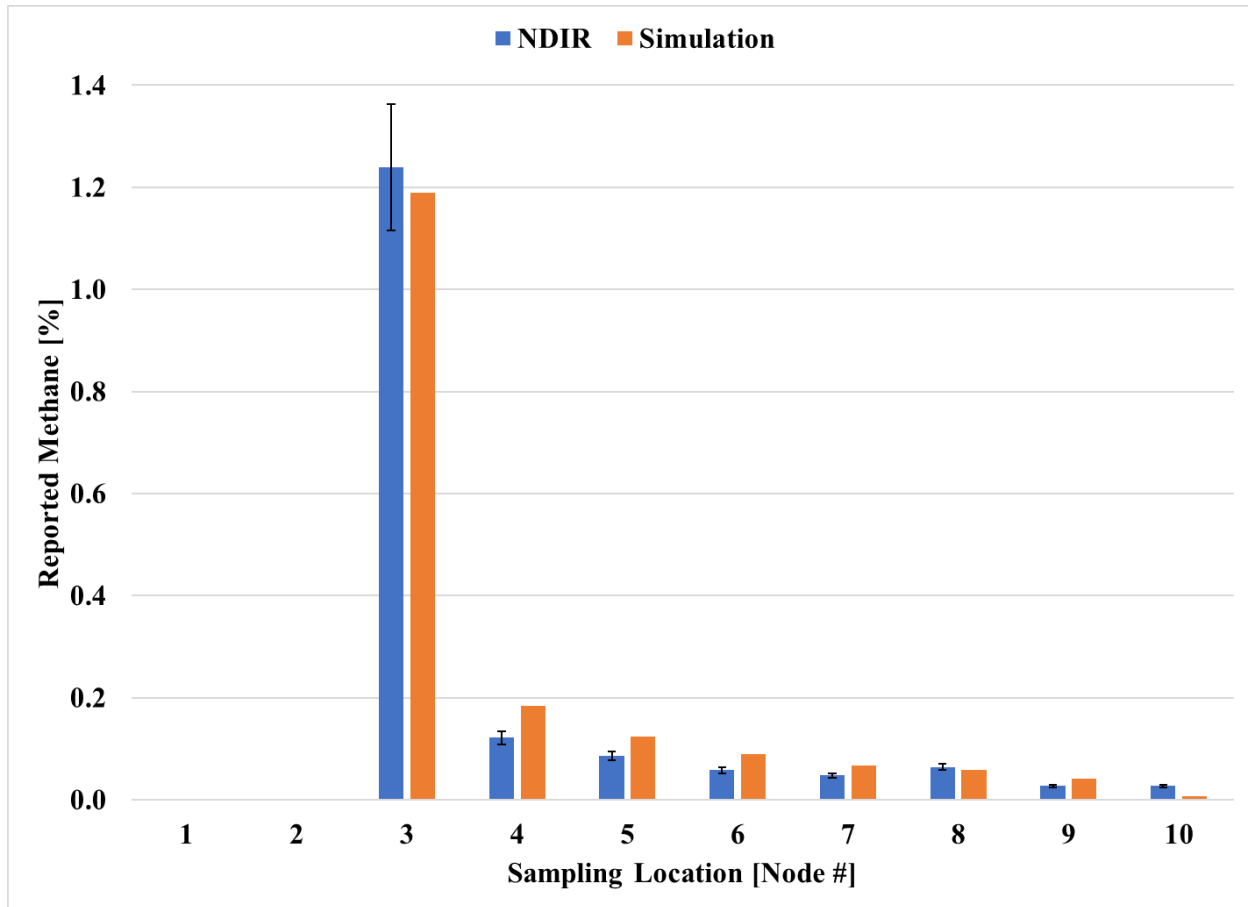


Figure 3.4.15: Comparison of Experimental Measured Nodal Data with Reduced Order 2-D Model Results.

Figure 3.4.16 presents a video plotting the nodal methane concentrations over time for Test 16. For this test, the methane injection was created and focused on Node 3. During this test, the nodal inlets were at approximately the midpoint of the wall representing the face. The fan speed was set at 1000 RPM to reduce ventilation flow and increase downface concentrations. The test was initially started with no methane injection rate, but the injection began at 20 seconds into the test with an initial flow of about 1 CFM. The injection rate was increased by 1 CFM at 150, 235, 340 seconds be back to 0 CFM at 420 seconds. Even with the reduced ventilation flow, we were not able to expose the MWS to concentrations at or above about 0.5%. It is noted that the immediate downwind node responds quickly while other nodes do not detect methane until the injection rate continues to increase. Node 8 had an intermittent connection problem. As discussed before, we do see that Nodes 9 and 10, which are located downwind of the bypass, do register methane emissions ahead of intermediate nodes likely due again to the issue of recirculation. Further, after the injection rate is set to zero Nodes 9 and 10 register methane for longer with Node 10 reporting a higher concentration than Node 9, again due to recirculation beyond the bypass.



Figure 3.4.16: Results of Test 16 – Stationary Test at with Release at Node 3. Node Sample Locations at Middle Height of the Face Wall. Peak Injection Rate of 4 CFM. Animation available here: https://drive.google.com/file/d/1XtYrtl2Pnde-0CcmPILYqiuf63rt5tIX/view?usp=share_link

Figure 3.4.17 presents a video plotting the nodal methane concentrations over time for Test 17. For this test, the methane injection was created and focused on Node 3. However, for this test the nodal sample locations (filters on the mock longwall face) were placed at the top of the face – the general region of the shield tips. The injection rate was then pointed at Node 3 at an approximate angle of 45. Studies and fluid dynamics show that tends to be higher at the shield tips due to buoyancy and the boundary layer effect. The fan speed was set at 1000 RPM just as Test 16. The test was initially started with no methane injection rate, but the injection began at 20 seconds into the test with an initial flow of about 1 CFM. The injection rate was increased by 1 CFM at 155, 280, 445, and 585 seconds and then set be back to 0 CFM at 640 seconds. This enabled a peak injection rate of 5 CFM for a limited duration (injection rate concentration ~3.5%). In this configuration, we see that the methane injection did tend to attach to the boundary layer at the roof/face corner. In fact, this created a measurable concentration at Node 3 of more than 1% which would trigger alarms in real scenarios. Methane was initiated at 20 second and up until about 40 seconds, we see that even with 1 CFM of injection rate the Node detect the 1% threshold. However, this was an artifact of the mass flow controller overshoot when transitioning from 0 to 1 CFM. Shortly after the injection rate increased to 2 CFM Node 3 recorded

concentrations at or above 1.5% which would require automatic de-energization of equipment in real scenarios. The methane injection was turned off at 640 seconds and Node 3 returned to a zero reading in about 38 seconds. This is higher than the decay time in laboratory experiments but due in part to the transport delay of the methane from the FFS as the final methane injected still traveled through just over 300 feet of injection hose before reaching Node 3. Again, we note that Nodes 9 and 10 of the MWS registered methane concentrations at or above Nodes upwind of the bypass, again highlighting the ability to detect high methane concentrations in areas with reduced ventilation flows or zones of high recirculation.



Figure 3.4.17: Results of Test 17 – Stationary Test at with Release at Node 3. Node Sample Locations at Roof/Face Corner – General Shield Tip Location. Peak Injection Rate of 5 CFM. Animation available here:

https://drive.google.com/file/d/12HuEubfYPP9TvROwPOOP1D18MEbcqgiw/view?usp=share_link

Summary of Mobile Tests

We also conducted a variety of various mobile tests. During initial visits, GPS could be intermittently recorded during the HG to TG traverse and its return. However, during the test period, overcast weather conditions further weakened the GPS signal within the metal structure such that it was not capable of being used. As such, we attempted to push the cart at a relatively constant velocity of about 1 ft/s such that the HG to TG pass took about 300 seconds and the return from TG to HG took about 300 seconds.

Figure 3.4.18 presents the results of Test 7. For this test the ventilation fan was set at 1000 RPM with an injection rate of 1 CFM. The upper plot shows the nodal responses over time while the lower plot shows the estimated average location of the cart during the test. A methane injection was initiated at approximately 20 seconds into the test. The cart began the HG to TG pass at about 100 seconds into the test. We see that Node 1 begins to detect diluted methane down wind from the cart at about 80 seconds (60 seconds after release initiated). The pass was completed around 400 seconds (+/-10 seconds). During the HG to TG pass, the concentration at most nodes tends to increase in smaller increments. During the TG to TG pass, the concentration increases tend to be more rapid. This phenomenon was previously reported and is due to the “doppler” effect of the injection source approaching with the ventilation flow direction and against the ventilation flow direction.

We note that Node 2 did not seem to react during the TG to HG pass. This was not due to an MWS error. First, we see that due to the direction of the mock shearer, the return responses are more rapid and short lived since the injection is traveling against the ventilation flow rate. Second, we note that Node 2 fell directly in a cross section door closure area, so that the methane injection did not hit a wall around the node.



Figure 3.4.18: Results of Test 7 – Mobile Test with Injection Rate of 1 CFM and Ventilation Fan Speed of 1000 RPM. Animation available here:

[https://drive.google.com/file/d/1bYRX1Vl_Kb7VYjsNFVd4quVtXRbd3oc7/view?usp=share link](https://drive.google.com/file/d/1bYRX1Vl_Kb7VYjsNFVd4quVtXRbd3oc7/view?usp=share_link)

Figure 3.4.19 presents the results of Test 11. For this test the ventilation fan was set at 1500 RPM. The upper plot shows the nodal responses over time while the lower plot shows the estimated average location of the cart during the test. A methane injection was initiated at approximately 20 seconds into the test. The cart began the HG to TG pass at about 100 seconds into the test. The pass was completed around 400 seconds (+/-10 seconds). In general, the behavior of the MWS was similar to Test 17. The peak concentration detected was higher in this test as compared to Test 7. Even though the fan speed was increased by 50%, the injection rate was double from 1 to 2 CFM, which explains this behavior.



Figure 3.4.19: Results of Test 11 – Mobile Test with Injection Rate of 2 CFM and Ventilation Fan Speed of 1500 RPM. Animation available here:

<https://drive.google.com/file/d/1VXPlJOa8s1HRUAzFqnMzFmlzQn6V4fp8/view?usp=sharing>
e link

Mine Like Evaluation Summary

A variety of MWS evaluations occurred at the WVU Mine Training Academy. This included mobile and stationary tests with varied ventilation flow rates and simulated methane injection rates. We primarily focused on presentation of results from the Gasmittor NDIR sensor though all three sensors were operable during the evaluations. The following are key attributes demonstrated under these more realistic mock mining conditions.

- Methane could be detected and reported across the “face” to the remote CPH located ahead of the entrance (HG region).
- Valves were tested and controlled from the remote CPH location to sample from the “face” and “gob”. Due to high dilution, “gob” sampling locations only yielded measurable concentrations when the injections were direct towards them, as opposed to the “face” (focus of only Test 22).
- The Gasmeter NDIRs were less impacted by temperature and humidity and were easily calibrated with the nodes installed on the “roof” location.
- Nodes could detect methane far below the thresholds of 1 and 1.5% but could also detect cases where those levels were exceeded.
- The MWS was able to detect higher than expected concentrations at Nodes 9 and 10 (compared to upwind nodes). These concentrations were due to the primary flow exiting after Node 8 creating decreased ventilation and increased recirculation in the area of Node 9 and 10. This phenomenon has been highlighted in literature and shows the capability of a single MWS to monitor these areas along with primary nodes across the face.
- The MWS nodal concentrations tended to match well with the location of the bluff body injection cart (mock shearer). In some cases, Node 8 experienced intermittent communication and Node 2 yielded lower concentrations due to its placement in front of an offset.
- The response of the nodes depended on the direction of the moving injection (i.e., with or against the bulk ventilation flow direction). Such response characteristics could be compared with baseline system responses in the laboratory to determine the direction of plumes along the face.
- The rapid decay in downwind concentrations was verified with reduced order 2-D modeling of the mock mine facility. This suggests that the evaluation results of the MWS were likely correct and due to the limited injection rate capabilities due to safety.

3.5 System Integration for Deployment

Any new methane monitoring system must conform to regulatory requirements for safe operation. We reviewed all state and federal requirements and proposed solutions or modification to the current system that would enable a pre-production system to undergo a complete testing and evaluation for permissibility under Part 30 of the Code of Federal Regulations (CFR).

The team initiated conversations with MSHA via former WVU graduate Ms. Sarah Dragonetti that works in the explosion proof division of MSHA. She introduced us to Mr. Terry Garrison (Intrinsic Safety Branch Chief) and Kenneth Darby (ESD Machine Approval and Certification Branch Chief). The MSHA team provided links and to various required certifications and regulations. They also provided a presentation related to Mine-Wide Monitoring Systems which included images of various systems that have deployed throughout mines with electronics installed within explosion proof (X/P) enclosures.

Unfortunately, beyond this information MSHA stated that they would be able to further discuss the process to submit an application but, “Please be advised that we do not discuss your design in detail during this consultation...”.

We also discussed the system with Mr. William Power of CSE Corporation. Mr. Power shared high-level details on their use of X/P enclosures for deployment of their catalytic oxidation sensors on longwall shearers.

We reviewed the following standards and developed the necessary documentation they require or identified already approved items that could be integrated within the MWS. The key changes are summarized below while the complete documentation is presented again as Appendix C.

- ***ASAP 2008: Application Procedures for Evaluation of Mine-Wide Monitoring Systems, Barrier Classifications, and Sensor Classifications***
 - 5.2.4: Create block diagram of system
 - 5.2.5: Manual for Installation and Maintenance
- ***ASAP 2016: Standard Application Procedures for Approval or Evaluation of Intrinsically Safe Apparatus and Associated Apparatus per 30 CFR Part 18***
 - Description of electrical circuits
 - Drawing list adequate to describe all equipment
 - Bill of materials
 - Equipment required to test and inspect devices
- ***ASTP 2232: Spark Ignition Test***
- ***ASTP 2228: Methane Monitor Moisture Test***
 - Assembly must function in environments of relative humidity greater than 85
 - Methane mixture tested at 2.1% and readings recorded
- ***ASTP 2219: Impact Test of Encapsulated Electrical Assemblies***
- ***W.V. Code 36-54-3: Methane Monitors***
- ***W.V. Code 36-54-4: Actions for Excessive Methane***

Based on our original review of standards during the initial project, the review of the above standards, and our discussions with MSHA and industry we propose the nodes of the MWS utilize pre-approved X/P Enclosure 5 - #7015-35223-4. Figure 3.5.1 presents the 3-D CAD drawing of all sensors within the mock node enclosures during both research projects. Figure 3.5.2 present a 3-D CAD drawing of all components within the X/P 5 enclosure. The selected enclosure is slightly larger than the current enclosures. In the prototype, some wiring and connectors were mounted to the seal door. For the X/P enclosure, the face is bolted and removed. The extra space enables all wiring connections to be mounted to the sides of the enclosure to enable removal of the cover for servicing and calibrations.

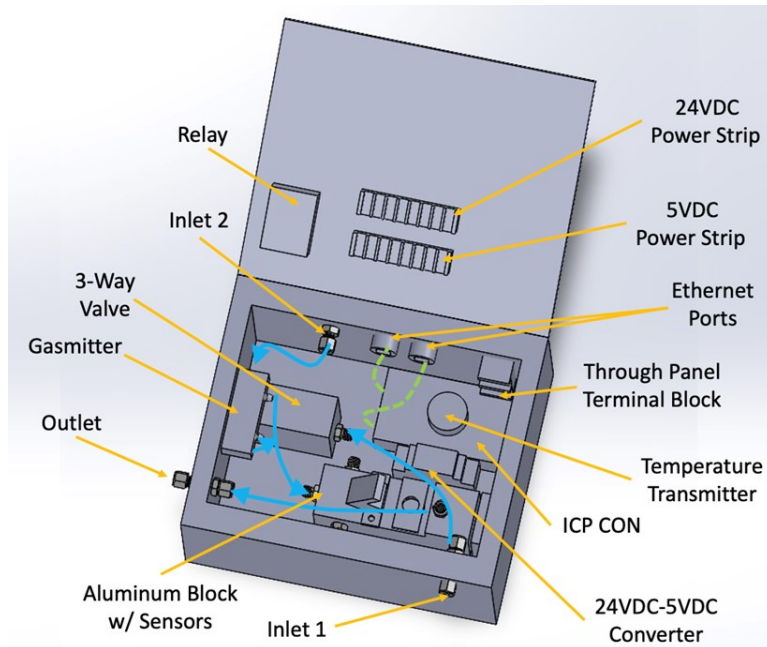


Figure 3.5.1: Prototype with All Sensors and Electronics Mounted within the Enclosure.

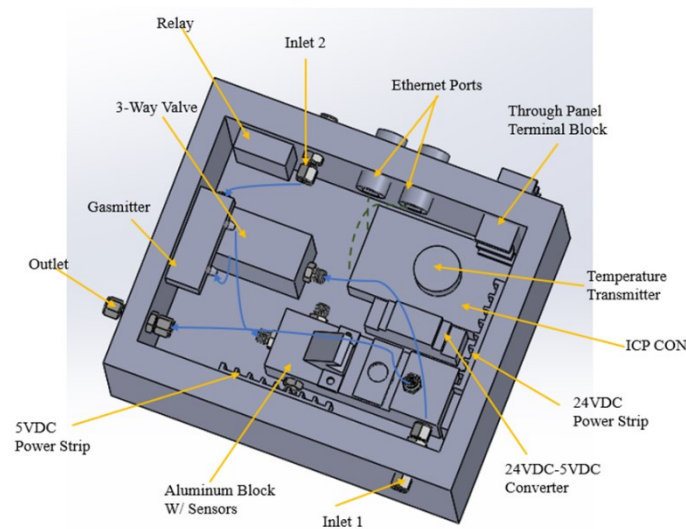


Figure 3.5.2: CAD of X/P 5 Internal Dimensions to Enable Electrical Terminals and Relay to be Mounted with the Enclosure Body.

In discussion with MCI, they are capable of making custom port and glands for the connections necessary for the MWS. We also identified additional MSHA approved items that would be necessary for integration within a shield. Those items include:

- Power Supply
 - Austdac Pty Ltd AC 36W Intrinsically Safe Power Supply
 - <https://www.hubbell.com/austdac/en/Products/Electrical-Electronic/Mining-Products/Power-Supply/AC36W/p/10224587>
- Ethernet Cable
 - Belden 7929A CAT 5e, 4 Pair, Stranded with Foil Shield
 - <https://www.industrialnetworking.com/pdf/Belden-79XXA-Bulk-Cable.pdf>
- Power Cable Connector
 - 400 X/P-TLB 2-pole plug – Model X/P-3309-2
 - https://www.andersonindustrialandmining.com/Mining/xp_tlb400.html
- Ethernet Connector
 - Solexy BXF Explosion-Proof/Intrinsically Safe Ethernet Coupler
 - <https://www.solexy.net/products/explosion-proof-is-ethernet-barrier-coupler-fitting/>

In addition, our system uses relays within boxes and at the CPH. These relays enable the ability to control external mining equipment upon reaching the alarm thresholds. The solid state relays could be replaced with intrinsically safe Start and Stop Relays from Becker SMC which are already approved by MSHA.

- Stop Relay – C4325-001 (Base C4325-002)
- Start Relay – C4325-005 (Base C4325-006)
- <https://beckersmcusa.com/product/intrinsically-safe-relays>

As previously discussed, the system would be integrated within shields as other additional systems have been in industry. Figure 3.5.3 shows a prototype proximity system installed on shield. We note that our selected X/P 5 enclosure is slightly longer than the proximity control unit, but there is ample room to rotate the X/P 5 for similar mounting. Further 3.5.4 shows the previously identified locations for the face and gob sampling point locations. Stainless steel tubing (1/4" OD) could be used with the same ports that we used (PTFE for reduced research cost). As noted in literature [5], the front shield tip location should be exposed to the highest methane concentrations and would be an ideal location for a nodal sampling filter.



Figure 3.5.3: Proposed location of the MWS nodes.

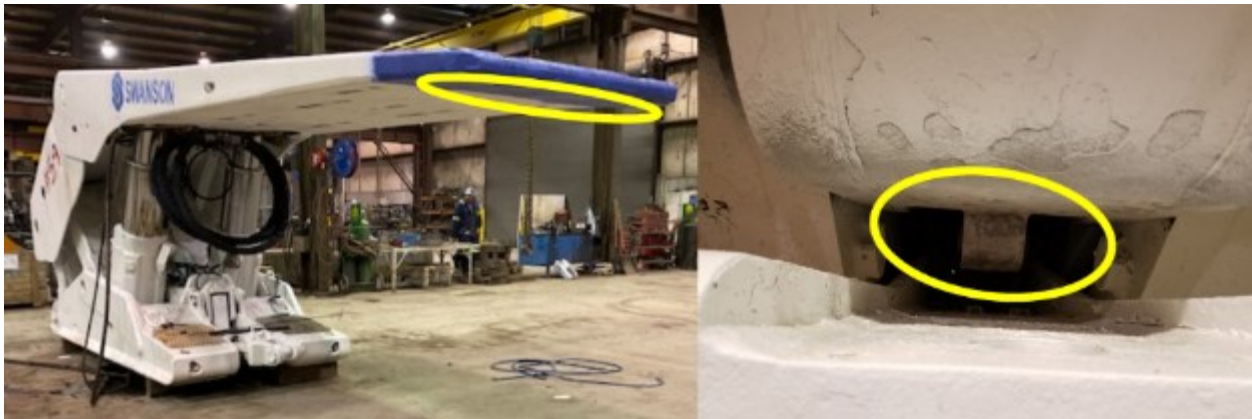


Figure 3.5.4: Proposed locations of the MWS sample locations where filters would be mounted. Left: Near Front Shield Tips (Face Sampling Locations). Right: Near Gob Area at Rear of Shield Pivot Location (View of Left from Rear of Shield Showing Open Area).

System Integration Summary

We attempted to discuss required system modifications that would ensure that an MWS would meet MSHA standards. Although MSHA officials were unable to provide specific review, we gained insight into additional requirements and documentation that should be considered in the design of a certifiable system. For those regulations identified, we have produced the required documentation. Further, informal discussions with industry members were completed. A key

approach for the various electrical components was to utilize an explosion proof enclosure which is common for other electrical and control systems. We selected an already approved enclosure that would be capable of housing all components within the current prototype system. We note that this includes the sampling block that houses the MOS and IRS sensors. We note that even though these sensors were less reliable than the NDIR, they could be deployed within a deployed system to serve as backup sensors to enable continued monitoring in the case of a faulty NDIR sensor. Alternatively, if redundancy were not required the system could deploy other sensors. For example, the MOS (MQ-4) sensor could easily be changed to the MQ-7 or MQ-8 sensors for carbon monoxide (CO) or hydrogen, respectively [17, 18]. Alternatively, an already approved CO sensor from MSA could be incorporated into the same mounting configuration as the IRS [19]. Other sensors could be incorporated to further improve the overall safety of long wall mining systems.

3.6 Modeling and Demonstration of Capabilities

We previously conducted basic modeling to show the initial benefits of implementing the MWS. These scenarios utilized experimentally obtained response times and data gathered from literature to examine a variety of scenarios to highlight the pre-emptive alerts provided by the MWS. The current MWS provides multiple local and global digital outputs that could be used to control isolated, intrinsically safe relays to stop or de-energize equipment. We can configure the system to output signals to modify operational activity such as pre-emptively altering the shearer speed to enable slower, yet continuous production. Studies have shown that gassy mine seams can often experience work stoppage down-times of 50%. Methane can be emitted from the gob area, the floor/ceiling, and the face. In addition, multiple references recognize that the primary source of methane is the mining of coal at the face. With the capability to model the time varying methane concentration across the entire face in near real time, there may exist optimum mining shearer velocity profiles that yield higher production rates compared to conventional fast mining until a stoppage is required. To reduce computational resources, we focused on a 1-D model to create a variety of methane, mining, and ventilation scenarios to assess system capabilities across a more realistic mine geometry.

1-D Modeling Method

Our model included baseline emission due to the natural methane emitted at a constant rate from all possible sources along the long wall. However, it also focused on increased methane emissions due to active mining where the shearer head serves as the primary source of added methane emissions above the baseline emissions. The model included losses along the face for ventilation air and the ability to introduce random elevated emissions due to increasing gassiness in the coal along the face and also with sudden outgassing along the face. An example of the MATLAB code used in the 1-D modeling is found in Appendix D.

In our model the methane is released and mixed with the ventilation air and carried towards the tailgate. As such, it utilized the 1-D advection equation to model the transport and diffusion of methane along the face. This is governed by equation 3.6.1

$$\frac{\partial^2 u}{\partial t^2} = c^2 \frac{\partial^2 u}{\partial x^2} \quad \text{Equation 3.6.1}$$

Equation 3.6.1 can be reduced to its first-order form for the sake of modeling general scenarios in the longwall mine while containing the original properties of the second-order equation. This

form of the wave equation is also commonly referred to as the 1-D linear convection equation and describes a wave propagating in the positive x-direction at some non-zero positive velocity. The first-order linear wave equation is given by Equation 3.6.2.

$$\frac{\partial u}{\partial t} = c \frac{\partial u}{\partial x} \quad \text{Equation 3.6.2}$$

The exact solution to Equation 3.6.1 is shown as Equation 3.6.3. This provided a platform by which discretized algebraic equations can be written that solve the traveling of some function F containing information at velocity c .

$$u(x, t) = F(x - ct) \quad \text{Equation 3.6.3}$$

It was assumed that the ventilation air at the longwall face only travels in the positive x-direction (HG to TG), therefore the associated upwind term will remain constant and the equation for the time step j following the initial condition will be given by Equation 3.6.4.

$$u_i^{j+1} = u_i^j - \frac{c\Delta t}{\Delta x} (u_i^j - u_{i-1}^j) \quad \text{Equation 3.6.4}$$

The stability criterion of the upwind scheme (3.6.4) is consistent with of the Courant-Friedrich-Lewy (CFL) condition. The CFL condition states that the differencing method is conditionally stable if and only if the models transport velocity c is not bigger than the spreading velocity $\Delta x/\Delta t$. This criterion is shown as Equation 3.6.5.

$$\frac{c\Delta t}{\Delta x} \leq 1 \leftrightarrow c \leq \frac{\Delta x}{\Delta t} \quad \text{Equation 3.6.5}$$

Additional Model Details

To match similar studies, the total length of the longwall modeled was 300 m. The width was 6 m, and the height was 3 m – for a total cross sectional area of 18 m². To meet the CFL criteria, the model used a time step dt of 0.2 seconds and a discretized dx of 0.8 m. The assumed air density was 1.229 kg/m³. We note that literature has suggested ventilation velocities of 0.5 to 2 m/s and our mock mine demonstrations focused on velocities over this range with average velocities between 1 and 2 m/s. Noting that ventilation velocity may decrease over the face of the mine due to air losses, we utilized a decaying ventilation profile in the form of Equation 3.6.6.

$$v = Ae^{-200t} \sin(.5\pi ft) + 2.2 - yt$$

Where v is the ventilation velocity at any time t . The peak average velocity was set to 2.2. m/s and allowed to oscillate sinusoidally with both exponential and linear decay across the face. A was fixed at 0.25, f at 10000, and the linear decay factor x was varied from 11 to 44. Figure 3.6.1 presents an example of an oscillating and decaying velocity of model time steps ($y=22$).

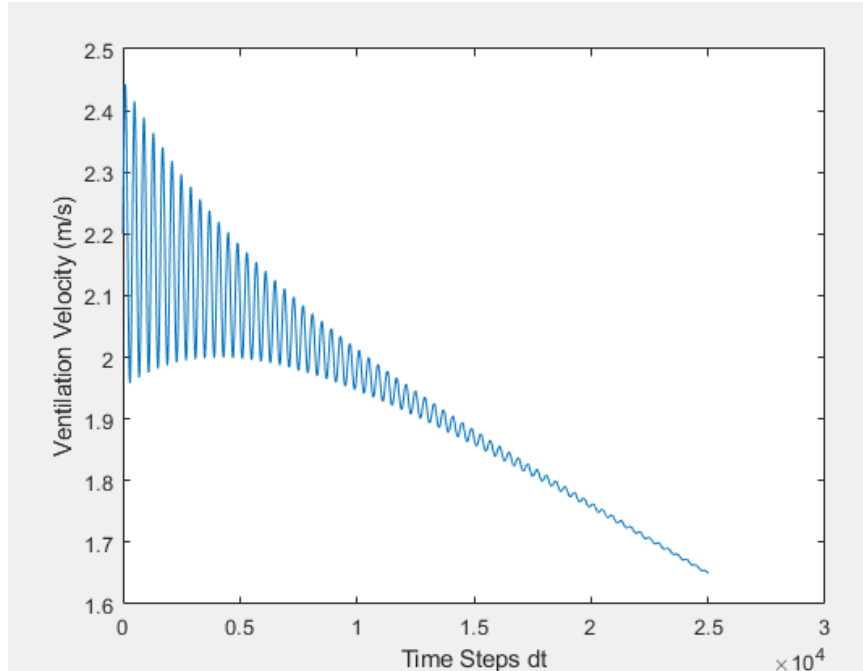


Figure 3.6.1: Example of Oscillating and Decaying Ventilation Velocity of Time.

In addition to a fluctuating and decaying ventilation velocity, we utilized a random number applied to an average methane factor of $0.415 \text{ kg/m}^2\text{s}$. At each discretized time step, the methane produced from the newly cut coal of the ranged randomly between 50% and 100% of this value.

Initial Scenarios

The model was exercised over various scenarios to highlight the benefits of a deployed MWS. Nodes were distributed across the longwall at locations of approximately 30, 60, 90, 121, 181, 212, 242, 273, and 300 m from the HG. For each of the scenarios the initial shearer speed was set to 0.12 m/s. The 1 Hz methane concentrations at the nodal locations was monitored. If any of the nodal concentrations reached a specified threshold (0.9%), the shearer speed was reduced to 90% of the initial value. We utilized 0.9% for methane concentration to avoid any shutdown conditions where possible. As such we were able to compare the durations of a single HG to TG cut along with the number of dangerous situations that required a reduction in shearer rate, and the location of which node identified this threshold. In the base case, of continuous operation with no methane speed reductions, a full cut would take 41.67 minutes.

Figure 3.6.2 presents an example of a baseline scenario where the methane concentration towards the tailgate builds over time. The decrease in ventilation velocity matched exactly the example of Figure 3.6.1. In this scenario, two dangerous situations arose where MWS nodes reported values at or exceeding 0.9%. The first instance occurred at Node 8 where the concentration reached a concentration of 0.9049%. The location of the shearer was within 0.4 m of this node. The shearer velocity was reduced by 10% to 0.108 m/s and proceeded to cut coal. The next instance was a concentration of 0.9046% at Node 9. The shearer was located just ahead of Node 9 by about 1.2 m. It was originally thought, that such a demonstration would not be seen as a beneficial over systems that could utilize the concentration measured at the shearer location. However, the model does not account for the overall length of the shearer or location of the current shearer sensor – instead the shearer is a point source of methane emissions. Literature has

suggested that concentrations should be monitoring at the tips instead of at the midpoint of the shearer. Since the response times of the MWS system meets or exceeds conventional sensor response times, the MWS would in fact be beneficial and notify operations at least 3 seconds sooner than the shearer mounted sensor ($\sim 0.4 \text{ m} / 0.12 \text{ m/s}$ or $1.2 \text{ m} / 0.108 \text{ m/s}$). The final shearer speed was 0.0972 m/s . The total length of time for the cut increased to 43.02 minutes. Since the space domain was discretized in units of 0.8 m , there were 376 locations across the face that could be analyzed (approximately the number of shields). With this control logic the maximum concentration of methane at any discretized location was only 1.0176%.

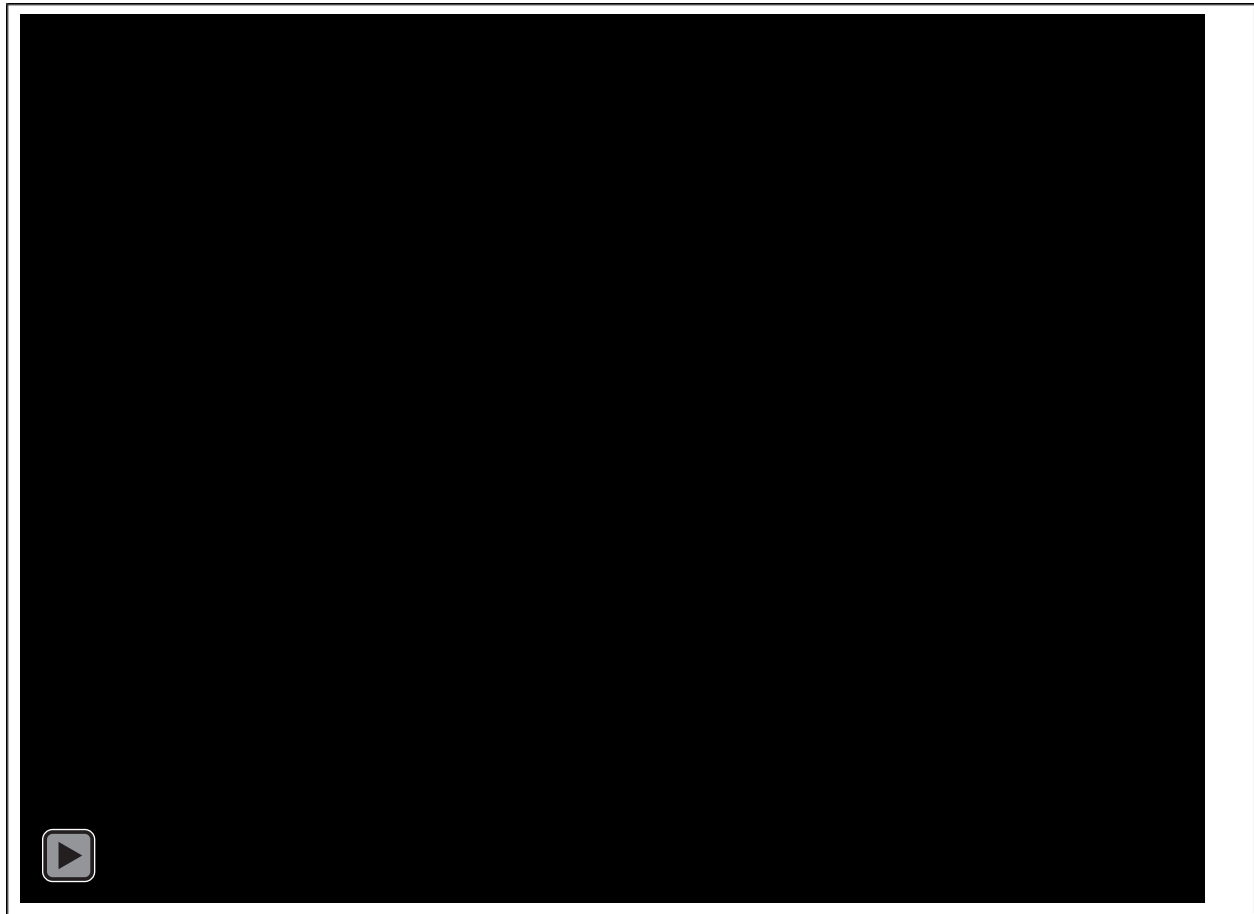


Figure 3.6.2: Results of Baseline MWS Implementation where Nodes 8 and 9 Detected Dangerous Methane Concentration to Inform a Slow Down of Shearer. Animation available here:

https://drive.google.com/file/d/1_ghSVgNENdGEDi3GFD5KoUoVJfoOVq3Z/view?usp=sharing
are link

The next three scenarios were similar to that of Figure 3.6.2, but methane releases occurred at randomly selected locations across the face. These occurred and model node locations of 111, 246, and 306 or about 89, 196, and 244 m from the HG. These locations correspond to Figures 3.6.3, 3.6.4, and 3.6.5, respectively.

Figure 3.6.3 shows three cases where a dangerous condition existed. The first case occurred when the shearer was located about 48.5 m into the cut. At this condition, Node 10 registered a concentration of 0.9000%. At this point, the shearer velocity was reduced to 0.108 m/s and continued cutting until the next dangerous condition which was registered by Node 9 with a concentration of 0.9128% when the shearer was located about 271.8 m into the cut (just 1 m ahead of Node 9). Note that the duration required to reduce the shearer speed is not known and the model assumes it occurs at the next calculation step. The third occurrence occurred when the shearer had only advanced to a location of about 272.5 m (just 0.3 m ahead of Node 9 location). In the first instance, it is clear to see the benefit of monitoring methane at the TG and using that data to modify the shearer speed. One may suggest that a simpler system only monitoring methane at the TG would suffice. But if such a system were deployed, it would not have identified the subsequent dangerous cases that occurred at Node 9. The total duration of the cut was 46.41 minutes. The maximum concentration in across the longwall was limited to 1.0162%.



Figure 3.6.3: Results of MWS Implementation with Methane Release Occurring Approximately 89 m from the HG. Animation available here:
https://drive.google.com/file/d/1_95w6kp2LAnjBz1xYMnBf4kjZ7DgSuna/view?usp=share_link

Figure 3.6.4 presents a similar scenario but where the additional methane injection occurred at a location of 196 m into the cut. In this scenario the MWS identified 7 dangerous scenarios. In this instance all dangerous conditions were detected at Node 10 and occurred when the shearer was located at a position of about 156.5 m into the cut. This was again due to the lack of knowledge on the time required to reduce the shearer speed which may be instantaneous or may take longer than ($0.2 \times 7 = 1.4$ seconds). As such, the shearer speed ended up being reduced to 0.0574 m/s or just less than half the initial speed of 0.12 m/s. The resulting duration of the cut was 63.28 minutes. The maximum concentration at any point along the face (not monitored by Nodes) was only 0.9009%.



Figure 3.6.4: Results of MWS Implementation with Methane Injection Occurring Approximately 196 m from the HG. Animation available here:
https://drive.google.com/file/d/1iGq8Xpb441nWNvEFU3A6aBPoa28vXJP/view?usp=share_link

Figure 3.6.5 presents a similar scenario but where the additional methane injection occurred at a location of 244 m into the cut. In this scenario the MWS again identified 7 dangerous scenarios. In this instance all dangerous conditions were detected at Node 10 and occurred when the shearer was located at a position of about 218.4 m into the cut. This was again due to the lack of knowledge on the time required to reduce the shearer speed which may be instantaneous or may take longer than ($0.2 \times 7 = 1.4$ seconds). As such, the shearer speed ended up being reduced to 0.0574 m/s or just less than half the initial speed of 0.12 m/s. Since the methane injection occurred at a location nearer the TG, the resulting duration of the cut was less than the prior scenario at about 53.9 minutes. The maximum concentration at any point along the face (not monitored by Nodes) was only 0.9154%.



Figure 3.6.5: Results of MWS Implementation with Methane Injection Occurring Approximately 244 m from the HG. Animation available here:
[https://drive.google.com/file/d/1OowWTJJOCDRItBcJ38xBM1taU2MeKBk9/view?usp=sh](https://drive.google.com/file/d/1OowWTJJOCDRItBcJ38xBM1taU2MeKBk9/view?usp=sharing)
are link

Additional Scenarios

The following four scenarios examined impacts of impulses of methane during operations or methane emissions that increased in a non-linear fashion with mining – increasing gassiness as the shearer progresses towards the face. To focus on these other phenomena, the ventilation losses were reduced as shown in Figure 3.6.6.

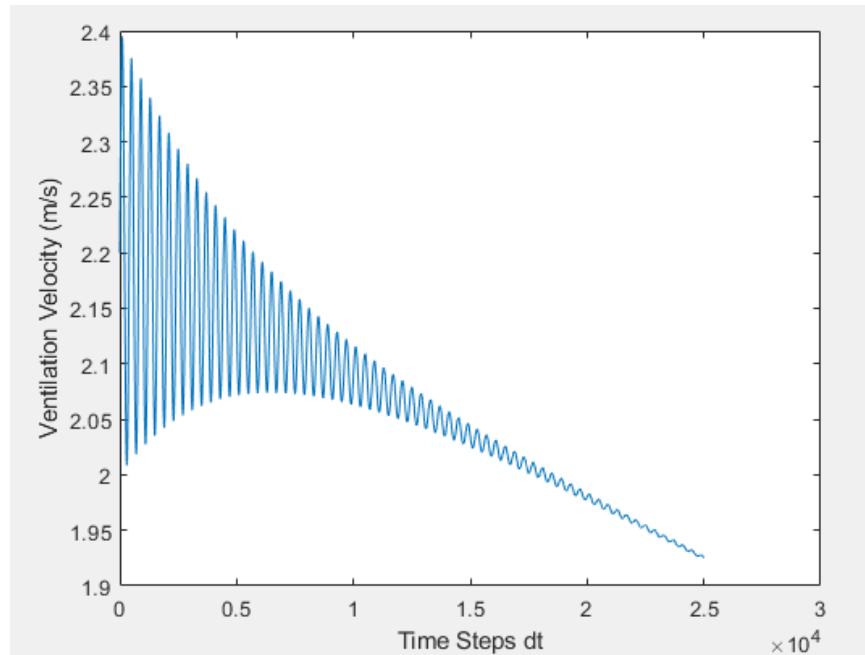


Figure 3.6.6: Example of Oscillating and Decaying Ventilation Velocity of Time with a Reduction in Losses Compared to Earlier Scenarios.

Figure 3.6.7 presents an example of rerunning the baseline scenario with the reduction in ventilation losses (a function of time and distance). Since impulses or non-linear increases in methane were not yet implemented, there were no dangerous scenarios detected by any of the nodes. As such, the total duration of the cut was 41.67 minutes as calculated from a constant shearer speed of 0.12 m/s for a length of 300 m. While no MWS nodes detect concentrations at the threshold of 0.9%, further inspection of the continuous data revealed that higher instantaneous methane emissions did occur. The global maximum concentration was 1.0227%. Instantaneous emissions above 0.9% occurred between Nodes 8 and 9 and Nodes 9 and 10. This may suggest that for general longwall faces, the MWS nodes should not be evenly distributed along the face but weighted to heavily focus node locations nearer the HG section.



Figure 3.6.7: New Baseline Methane Concentrations with a Reduction in Ventilation Losses. No MWS Node Detection of Dangerous Conditions. Animation available here:
[https://drive.google.com/file/d/1yrNdbUHenjkwyU4KIY7JsgccHY_gp4u-/view?usp=share link](https://drive.google.com/file/d/1yrNdbUHenjkwyU4KIY7JsgccHY_gp4u-/view?usp=share_link)

Figure 3.6.8 presents a scenario where the coal seam is not uniform in the methane it releases, i.e., non-linear variable gassiness (logarithm with length). In this particular case, the extra gassy coal was nearer the HG. The MWS detected three dangerous instances. For the first instance, the shearer was located about 9.6 m into the cut when Node 5 detected a concentration of 0.9001%. At this point, the speed was reduced to 0.108 m/s and mining continued until the second and third instances. These were both identified by Node 9 when the shearer was within 0.4 m of this location. In these cases, Node 9 detect concentrations of 0.9201 and 0.9110%. As such, the final shearer speed was 0.0972 m/s, and the total duration was 47.1 minutes. The maximum non-nodal concentration was 1.0028%. Again, the vast majority of non-nodal concentrations exceeding 0.9% were located in the last 1/3rd of the cut suggesting that nodal placement should be weight towards the TG.



Figure 3.6.8: Results of MWS Implementation with Non-Linear Gassiness. Animation available here: https://drive.google.com/file/d/1ptQ8ek-wOYVN0EkVHL5BUuxG5YnqMWe9/view?usp=share_link

Figure 3.6.9 presents a scenario where resulting methane emissions were high up to a location of about 150 m. At about 17 minutes into the cut an impulse of outgas occurs just downwind at around the 200 m mark. This outgassing lasted for a duration of 1 minute (consistent added concentration of 0.8%). When this occurred four dangerous instances were recorded by the MWS. All four cases were identified at Node 7 when the shearer had just past Node 2, about 60.4 to 60.5 m into the cut. This yielded a final shearer rate of 0.0787 m/s for the remainder of the cut, yielding a total duration of 59.1 minutes. While we did not examine the case of increasing the shearer speed, it can be seen that maximum methane concentrations primarily remained in the range of 0.45 to 0.6%. As such, the shearer could have increased its cutting speed to reduce overall cut time, but such safety versus productivity decisions should be made with caution as the shearer still had to cut through about 100 m of the higher methane region.



Figure 3.6.9: Results of MWS Implementation with High Gas Region up to 150 to 200 m with an Impulse Outgassing Lasting about 1 Minute in the 200 m Location. Animation available here: https://drive.google.com/file/d/1Z6h_ur5Hv-c94_GTJX9kmuVX55WQHYP7/view?usp=share_link

Figure 3.6.10 presents a scenario where overall methane emissions from cutting were reduced by about 15% ($0.3609 \text{ kg/m}^2\text{s}$). However, at about 17 minutes into the cut an impulse of outgas occurs just downwind at around the 242 m mark (just ahead of Node 8). This outgassing lasted for a duration of only 1 second but was a peak concentration of about 1.1%. When this occurred three dangerous instances were recorded by the MWS. All three cases were identified at Node 8 when the shearer about 1 m ahead of Node 4, about 120 m into the cut. This yielded a final shearer rate of 0.0875 m/s for the remainder of the cut, yielding a total duration of 51 minutes.



Figure 3.6.10: Results of MWS Implementation with Lower Methane Release from Coal but a Larger Short Impulse of Methane (1.1% for 1 second). Animation available here: https://drive.google.com/file/d/1n5lFNjhfYUIasjBSBdF80jxVGSQXhLQq/view?usp=share_link

Modeling and Demonstration of Capabilities Summary

To demonstrate the capabilities of the system, we utilized a 1-D model with geometries similar to those found in literature. In general, the model focused on methane plumes predominantly created from the active mining of the shearer and the general loss of ventilation air across the longwall face. However, it also enabled examination of variable coal gassiness profiles and outgassing impulses at various locations across the face. While many suggest ventilation on demand (VOD) as a strategy to reduce methane, we realize that such an approach would require more time than simply adjusting the shearer rate.

Some scenarios identified that the end node at the TG identified dangerous gas levels. We note that some industry has already installed a methane sensor near the TG and our modeling suggests this will improve safety. However, in other scenarios the MWS detected high methane emissions at nodes near the shearer or other nodes between the shearer and TG. A single sensor system applied at the TG would not have identified these dangerous cases. We demonstrated that deployment of the MWS coupled with its use to adjust shearer speed will reduce cases of excessive methane. We utilized a threshold of 0.9% but this could be further reduced to ensure that concentrations between nodes remained at or below the regulation of 1.0% methane. This method of control increased production times for a complete HG to TG cut but only increased duration by up to 33% in the scenarios presented. By knowing the methane emissions at multiple locations across the face, operators can take action ahead of entering dangerous locations to improve safety. Finally, we do not that for HG to TG passes, dangerous methane concentrations tended to occur in the last 1/3rd of the face due to the common issue of ventilation losses. In many cases, methane emissions between these last few MWS nodes did exceed 0.9 to 1% methane. This suggests that a non-linear distribution of the MWS nodes that is more heavily weighted towards the TG may be beneficial over a uniform spacing across the face.

4.0 Summary of Accomplishments

4.1 Key Design Findings

For this section, we list the key design findings and accomplishments completed in this research by research task.

1.) Ejector Improvements

- CFD modeling was used to design a multi-nozzle ejector with the aims of improving performance
- Multi-nozzle ejector was 3-D printed and tested experimentally
- Multi-nozzle results were used to modify and scale results for a final ejector design
- The final ejector design was capable of meeting a required gas sample flow rate of 2 SLPM with only 1 SLPM of water flow (reduction in water consumption of 33-50%)
- The final design obtained a peak flow rate ratio of 2.61 (62.5% improvement)
- Such a design is less impacted by pressure and would not require high pressures as previously hypothesized
- Deployment of a 10 node MWS would only increase water consumption of shield spray systems by 1-5%.

2.) Methane Sensor Improvements

- Gasmitter (NDIR) sensors were obtained for evaluation against previous MOS and IRS sensors
- The NDIR had increased capital costs (~\$800 per unit for purchase of 10)
 - Prices are reduced for bulk orders
- The NDIR retained the best attributes of both sensors
 - Good rise and decay times
 - Good low concentration accuracy
 - Excellent high concentration accuracy
 - Less impacted by temperature and pressure (internally compensated)
 - Baseline response time of 17 seconds within MWS (meets or exceeds currently used sensors)
 - Can be internally tuned for faster response in some cases
 - Easily zeroed and spanned (calibrated) in the deployed MWS configuration

3.) Signal Processing Improvements

- Transport time cannot be eliminated but is small in comparison to response time – 4 seconds for given lengths
- MWS node exposed to time varying concentrations determined from models
- Without signal processing (sharpening) the node failed to detect multiple 1% events from tests
- With a time constant of 20 and decay constant of 12, a first order reconstruction technique could improve signal processing
 - Sharpened signal detected all 1% events to which it was exposed

- Average error reduced from 19 to 4% - a reduction in error of 79%
- Sharpening method can be combined with logic analysis to more appropriately report on sharp rises or falls (dc/dt).

4.) Mine Environment Evaluations

- The 2nd generation MWS was deployed at the WVU Mine Training Academy
- Ventilation velocity was measured at three locations
- Ventilation fan speed was modulated to produce average ventilation velocities from ~1 to 2 m/s.
- Mobile and stationary tests were completed with varying injection concentrations supplied to a bluff body via a custom FFS system
- Nodes were sampled at the target flow rate of 2 SLPM to yield a 4 second transport delay
- Methane could be detected and reported across the “face” to the remote CPH located ahead of the entrance (HG region).
- Valves were tested and controlled from the remote CPH location to sample from the “face” and “gob”. Due to high dilution, “gob” sampling locations only yielded measurable concentrations when the injections were direct towards them, as opposed to the “face” (focus of only Test 22).
- The Gasmitter NDIRs were less impacted by temperature and humidity and were easily calibrated with the nodes installed on the “roof” location.
- Nodes could detect methane far below the thresholds of 1 and 1.5% but could also detect cases where those levels were exceeded.
- The MWS was able to detect higher than expected concentrations at Nodes 9 and 10 (compared to upwind nodes). These concentrations were due to the primary flow exiting after Node 8 creating decreased ventilation and increased recirculation in the area of Node 9 and 10. This phenomenon has been highlighted in literature and shows the capability of a single MWS to monitor these areas along with primary nodes across the face.
- The MWS nodal concentrations tended to match well with the location of the bluff body injection cart (mock shearer). In some cases, Node 8 experienced intermittent communication and Node 2 yielded lower concentrations due to its placement in front of an offset.
- The response of the nodes depended on the direction of the moving injection (i.e., with or against the bulk ventilation flow direction). Such response characteristics could be compared with baseline system responses in the laboratory to determine the direction of plumes along the face.
- The rapid decay in downwind concentrations was verified with reduced order 2-D modeling of the mock mine facility. This suggests that the evaluation results of the MWS were likely correct and due to the limited injection rate capabilities due to safety.

5.) System Integration for Deployment

- Discussions occurred with various industry and MSHA members
- MSHA could not comment directly on the design

- Identified additional regulations that should be examined (7 major, 10 total)
 - All required documents for submission and approval for these regulations were developed
- Key design change would be to transition from sealed prototype enclosures to pre-approved explosion proof enclosures
 - XP 5 provided slightly larger volume to enable fitment of all key components and wiring while maintaining a detachable face plate
 - Custom ports/grommets available from MCI on the XP 5
- Additional external hardware identified
 - Pre-approved power supplies, ethernet cables, cable connectors and relays
- Recent modeling confirmed our suggested locations are valuable
 - Peak concentrations occur at the hard to reach shield tip locations
- As is the system could include 3 methane sensors for redundancy
 - Sensors could be replaced to enable active monitoring of other gases of concern – e.g., CO

6.) Modeling and Demonstration of Capabilities

- 1-D model was created with similar geometry to real mines and those used in recent studies – 3 x 6 x 300 m
- Model included key features:
 - Oscillatory and decaying ventilation velocity
 - Variable coal gassiness across the face
 - Randomization of released methane and randomized locations of events
 - Impulse events from 1 second to 1 minute
- Results on 8 example scenarios presented to demonstrate capabilities
- Model MWS nodes were distributed evenly across the face
 - Results match with literature and may suggest that non-linear distributions should be used – e.g., more nodes towards the TG
- Model focused on shearer driven emissions – as such shearer speed was adjusted based on feedback from monitoring of 10 nodes across the face
- The MWS could not only detect elevated emissions at the TG
 - Detected dangerous scenarios at Nodes 5, 7, 8, 9, 10
 - Dangerous scenarios detected at TG and just head of shearer, but also far downstream where sampling does not currently occur
 - Detected dangerous concentrations at multiple nodes within a given scenario – key attribute as opposed to TG monitoring alone
- If coupled to shearer speed control, dangerous scenarios (1 to 1.5%) methane could be avoided along with costly shutdowns
 - Enables continuous mining with only modest increases in total cut duration

5.0 Dissemination Efforts and Highlights

5.1 Intellectual Property

It continues to be our belief that the MWS represents intellectual property. We previously reported an invention disclosure as part of the initial research project. In this project, we have moved forward with the filing of a provisional application and a complete application as noted by the following.

Provisional Patent Application

Johnson, D., Clark, N., Barr, A., and Cappellini, B. Methane Watchdog System, A Cost Effective Approach to Longwall Methane Monitoring and Control. *Application No.: 63/020,817*, Filing Date: May 6, 2020. Washington, DC: U.S. Patent and Trademark Office.

Utility Patent Application

Johnson, D., Clark, N., Barr, A., and Cappellini, B. Methane Watchdog System, A Cost Effective Approach to Longwall Methane Monitoring and Control. *Application No.: 17/308,341*, Filing Date: May 5, 2021. Washington, DC: U.S. Patent and Trademark Office.

5.2 Theses

Barr, Amber. Design and Development of a Multi-Nodal Methane Detection System for Longwall Coal Mining. Thesis, 2020. West Virginia University: Morgantown, WV, USA.

Cappellini, Brian. Improving Real-time Methane Monitoring in Longwall Coal Mines Through System Response Characterization of a Multi-Nodal Methane Detection Network, Thesis, 2021. West Virginia University: Morgantown, WV, USA.

5.3 Public Dissemination

*Peer Reviewed Publication (*Student, Underline – Presenter)*

Cappellini, B.*, Johnson, D., Clark, N., and Barr, A.*, “Improving Real-Time Methane Monitoring in Longwall Coal Mines Through System Response Characterization of a Multi-Nodal Methane Detection Network,” *Proceedings of the ASME International Mechanical Engineering Congress and Exposition*, IMECE2021-69709, 2022. DOI: 10.1115/IMECE2021-69709.

Presentations and Panels

Barr, A.*, Cappellini, B.*, Johnson, D., and Clark, N., “Design and Development of a Multi-Nodal Methane Monitoring System for Improved Mine Safety,” Annual International Pittsburgh Coal Conference, 2020, Pittsburgh, PA, 2020, Virtual Oral Presentation.

Cappellini, B.*, Barr, A.*, Johnson, D., and Clark, N., “Evaluating CFD and Modeling Techniques for a Multi-Nodal Sensor Network Designed for the Detection and Control of Methane in Longwall Coal Mines,” 37th Annual International Pittsburgh Coal Conference, Pittsburgh, PA, 2020, Virtual Oral Presentation.

Cappellini, B.*, Johnson, D., Clark, N., and Barr, A.*, “Improving Real-Time Methane Monitoring in Longwall Coal Mines Through System Response Characterization of a Multi-Nodal Methane Detection Network,” IMECE2021-69709, ASME International Mechanical Engineering Congress and Exposition, Virtual Conference, November 2021. Virtual Oral Presentation.

Johnson, D., ARPA-E Remedy Kick-Off Meeting, Invited Participant – Panelist on - Natural Gas Engines Panel and on Methane Mitigation from Mines Panel. Chicago, IL, June 2022. Panelist.

6.0 Conclusions and Impact Assessment

Under this program, research was conducted, and refinement completed on a second generation prototype Methane Watchdog System (MWS). The MWS is aimed at improving mine health and safety. As a reminder, the MWS is a multi-nodal methane monitoring system that utilizes active sampling to enable gas sampling from difficult locations on shields – at the shield tip and the rear of the shield near the gob region. The second generation system included 10 nodes as the first, which enable sampling at 20 different locations. Research was previously completed on the first generation system and we found six key areas where further research should be conducted. Those six key area were the focus of this project and included: research to improve the water powered ejector for active gas sampling, examination of an alternative infrared based methane sensor (Gasmitter – NDIR), developing a signal sharpening technique to improve the real time accuracy of monitoring continuously varying methane concentrations, deployment and demonstration of the second generation system at the WVU Mine Training academy, examination of remaining design barriers or issues that should be addressed prior to seeking approval from MSHA, and conducting additional modeling to highlight the capabilities of the MWS as a tool to improve mine safety. Based on our review of results and assessment of the findings, we present below the most important conclusions for each of the key areas.

Key Conclusions:

- 1.) Ejector Improvements – Multi-nozzle ejectors were able to meet or exceed the sampling targets of 2 SLPM while reducing water consumption by maximizing peak flow rate ratios.
- 2.) Methane Sensor Improvements – The Gasmitter (NDIR) sensor were higher initial cost but were found to be superior to the other sensors because they retained a balance of the key benefits identified in the other sensors.
- 3.) Signal Processing Improvements – A basic first order reconstruction technique along with basic logic control can significantly reduce the error between real time methane concentration and those reported by the MWS and its active sampling approach.
- 4.) Mine Environment Evaluations – Evaluations at the Mine Training Academy showed that the MWS was capable of detecting methane from moving sources along the face, detecting elevated methane concentrations in areas that had reduced ventilation (i.e., increase recirculation at the tailgate), and demonstrated behavior matched well with predicted methane profiles from 2-D CFD models.
- 5.) System Integration for Deployment – Based on discussions with industry and MSHA, the key modification of the system would be to utilize an MSHA approved explosion proof enclosure to house all MWS nodal components that are not MSHA approved and utilize already approved cables, connectors, and power supplies to integrate the system within shields.
- 6.) Modeling and Demonstration of Capabilities – 1-D modeling showed the monitoring capabilities of the MWS when applied to various scenarios on a 300 m longwall scale. The MWS would provide capabilities of detecting dangerous methane concentrations along the face that would not be readily monitored by a shearer and TG mounted sensor along.

Ultimately, to improve mine health and safety and provide real beneficial impacts, the MWS must be deployed in active longwall mines. Based on the findings of our two programs, we feel

that nearly all laboratory and field research necessary to develop, refine, and demonstrate the MWS has been completed. The results highlight the capabilities of the MWS through real world data and through modeling efforts. We presented eight different scenarios where the MWS would be capable of detecting dangerous methane concentrations. We also demonstrate that the MWS methane signals could be used to adjust shearer production rates (methane concentrations) to enable continuous mining while avoiding costly shutdowns. Our modeling results that such capabilities would reduce average methane concentrations across the long wall face while only modestly increasing the duration of a single pass. In addition, we note that shearers and some TGs already deploy methane sensors, the MWS would enable monitoring nearer to the shield tips – a key area identified in internal and external modeling efforts. Based on our research and assessment, we feel that the second generation MWS system would improve mine safety over current practices.

7.0 Recommendations for Future Work

Based on the findings of this and the prior program, we recommend that future work focus on seeking preliminary approval to at least deploy a MWS as a research system in an active longwall mine. Most other studies and our own rely on limited data sets and various 1, 2, and 3-D models to recreate conditions that may occur in mines. This leads to added uncertainty on the overall accuracy of models and makes true comparisons difficult. While the goal of the MWS is to improve mine safety, its value as a data collection system is likely just as important. Real deployment in a mining environment would enable long term analysis on its operation and any unforeseen issues. Further, data collected from a research deployment would be invaluable not only for further MWS research but also for the broader mine safety and modeling community. Upon submission of the this final report, the WVU researchers will forward the final report to the Office of Technology Transfer (OTT) and request a status update on the patent application and possible transfer of the technology to a commercial entity that has the funds and access necessary to deploy a 3rd generation within a real mining environment. Lessons learned from the deployment should be used to transition the MWS to a commercial system. In the interim, data collected from a mine deployment would enable research in the following areas:

- Analysis of system monitoring and response time and the time required to modify shearer velocity or ventilation
- Use collected data to better verify or modify 1, 2, and 3-D modeling scenarios to create a database of realistic methane profiles for TG to HG and HG to TG passes over multiple cuts of a seam
- Examine the benefits of a weighted distribution of the MWS nodes - focused on decreasing inter-nodal distances from the HG to TG
- Use operating data – pressures and flowrates to examine if filter or filter housing modifications are required
- Combine MWS collected data with activity logs from mining operations to assess if shearer speed control presents as a key measure to control methane emissions
 - This could include the MWS output as a control variable not only to slow the shearer but also to increase its speed where possible (after controlled speed reductions)
- Examine the possible use of batteries in parallel with shield power to enable continued methane monitoring during periods where main power is turned off
- Collaborate with the industry operator to develop a white paper highlighting the benefits and downfalls from deployment in a mine
- Examine the benefits of integrating other key gas sensors such as hydrogen or carbon monoxide sensors within the MWS

8.0 References

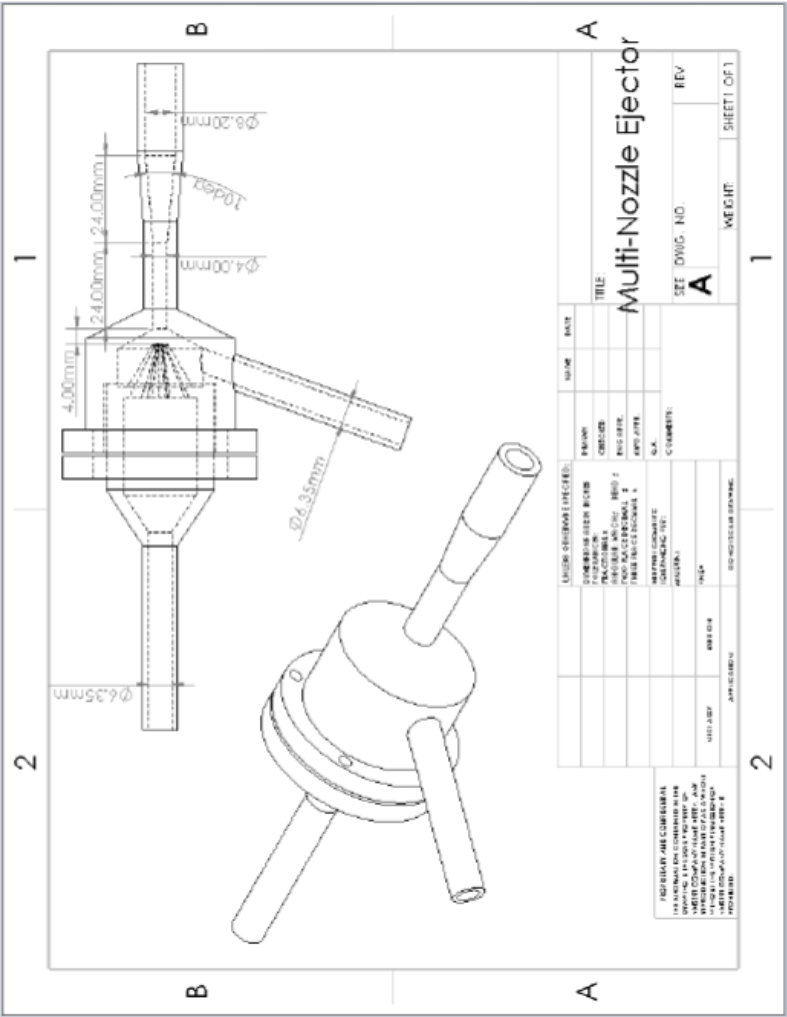
- [1] International Energy Agency. Coal 2022: Analysis and Forecast to 2025. Available Online: <https://www.iea.org/reports/coal-2022>.
- [2] Demirkan, D.C.; Duzgun, H.S.; Juganda, A.; Brune, J.; and Bogin, G. Real-Time Methane Prediction in Underground Longwall Coal Mining Using AI. *Energies*. **2022**, DOI: 10.3390/en15176486.
- [3] Sidorenko, A.A.; Dmitriev, P.N.; Sirenko, Y.G. Predicting Methane Emissions from Multiple Gas-Bearing Coal Seams to Longwall Goafs at Russian Mines. *ARPJ. Eng. Appl. Sci.* **2021**, 16, 851–857.
- [4] Demirkan, D.C.; Duzgun, S.; Juganda, A.; Brune, J.; Bogin, G. Evaluation of Time Series Artificial Intelligence Models for Real-Time/near-Real-Time Methane Prediction in Coal Mines. *CIM J.* **2022**, 1, 1–10.
- [5] Juganda, A. Evaluation of Point-Based Methane Monitoring and Proximity of Detection for Methane Explosive Zones in Longwall Faces of Underground Coal Mines. Thesis, **2020**. Colorado School of Mines: Golden, CO, USA.
- [6] C. Dirix and K. van der Wiele, "Mass Transfer in Jet Loop Reactors," *Chemical Engineering Science*, vol. 45, no. 8, pp. 2333-2340, **1990**.
- [7] T. Otake, S. Tone, R. Kuboi, Y. Takahashi and K. Nakao, "Dispersion of Gas by a Liquid-Jet Ejector," *KAGAKU KOGAKU RONBUNSHU*, vol. 5, no. 4, pp. 366-373, **1979**. DOI: 10.1252/kakoronbunshu.5.366.
- [8] R. G. Cunningham and R. J. Dopkin, "Jet Breakup and Mixing Throat Lengths for the Liquid Jet Gas Pump," *Fluids Engineering*, vol. 96, no. 3, pp. 216-226, **1974**. DOI: 10.1115/1.3447144.
- [9] KOMATSU, PRS Water Spray Summary.
- [10] Murray Energy, Murray Energy Water Supply [Microsoft Excel spreadsheet], **2020**.
- [11] Sensors Europe GmbH, "Operating Manual Gasmitter," Sensors, Erkrath, 2018.
- [12] M. R. Madireddy and N. N. Clark, "Sequential inversion technique and differential coefficient approach for accurate instantaneous emissions measurement," Morgantown, **2006**.
- [13] M. R. Madireddy and N. N. Clark, "Attempts to Enhance the 'Differential Coefficients Method' for Reconstruction of Transient Emissions from Heavy-Duty Vehicles," Morgantown.
- [14] D. Ajtay and M. Weilenmann, "Compensation of the Exhaust Gas Transport Dynamics for

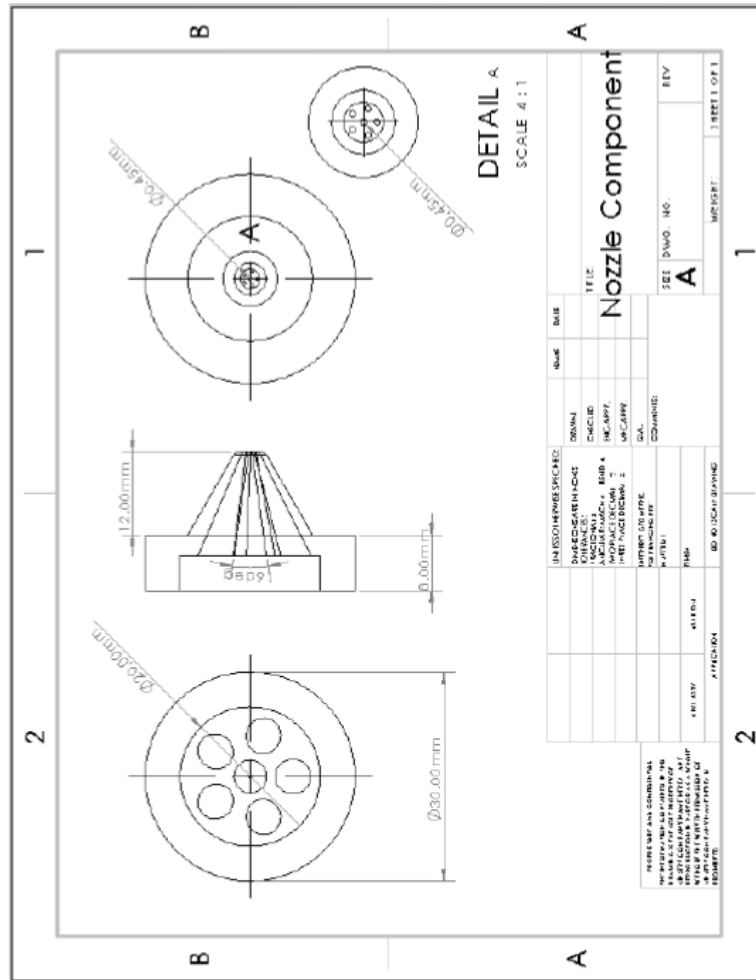
Accurate Instantaneous Emission Measurements," Environmental Science & Technology, **2004**.

- [15] J. M. Cimbala, "Dynamic System Response," Penn State University, **2014**.
- [16] K. Raean, "A Study of The Gibbs Phenomenon in Fourier Series and Wavelets," The University of New Mexico, Albuquerque, **2008**.
- [17] <https://cdn.sparkfun.com/datasheets/Sensors/Biometric/MQ-7%20Ver1.3%20-%20Manual.pdf>
- [18] <https://cdn.sparkfun.com/datasheets/Sensors/Biometric/MQ-8%20Ver1.3%20-%20Manual.pdf>
- [19] https://www.industrialsafetyproducts.com/msa-10106725-sensor-xcell-co-h2s-for-altair-4x-4xr-5x/?gclid=CjwKCAiA0cyfBhBREiwAAAtStHECRwII1Gb2JJIEjyUM_m3ygfESZndtuRPN7zNLOTB1jR2LtTMWmEhoCVSUQAvD_BwE

9.0 Appendices

9.1 Appendix A: Final Ejector Drawings





9.2 Appendix B: Additional Test Details

- Test 1
 - Box File Name: XB0000-000-666
 - FFS File Name: 0000-010-47
 - Data Quality: Okay – low concentrations
 - Fan Speed: 1,000 RPM
 - Time: 900 sec
 - Description:
 - Cart moving up and down with methane starting 300 sec into test
- Test 2
 - Box File Name: XB0000-000-667
 - FFS File Name: 0000-010-48
 - Data Quality: Okay – low concentrations
 - Fan Speed: 1,000 RPM
 - Time: 900 sec
 - Description:
 - Cart moving up and down with methane starting 300 sec into test
- Test 3
 - Box File Name: XB0000-000-668
 - FFS File Name: 0000-010-49
 - Data Quality: Okay
 - Fan Speed: 1,000 RPM
 - Time: 900 sec
 - Description:
 - Cart moving up and down with methane starting 300 sec into test
- Test 4
 - Box File Name: XB0000-000-670
 - FFS File Name: 0000-010-52
 - Data Quality: Okay
 - Fan Speed: 1,000 RPM
 - Time: 710 sec
 - Methane on: 20 sec
 - Cart moving: 40 sec
 - Cart turn around: 380 sec
 - Cart return: 710 sec
 - Description:
 - Cart moving up and down tunnel with methane being released at a steady rate
 - Second gasmitter in series did not observe methane on either pass
- Test 5
 - Box File Name: XB0000-000-671
 - FFS File Name: 0000-010-53
 - Data Quality: Okay
 - Fan Speed: 1,000 RPM
 - Time: 843 sec
 - Methane on: 20 sec
 - Cart moving: 40 sec
 - Cart turn around: 360 sec
 - Cart return: 645 sec
 - Description:

- Cart moving up and down tunnel with methane being released at a steady rate
 - Second gasmitter in series did not observe methane on return pass
- Test 6
 - Box File Name: XB0000-000-672
 - FFS File Name: 0000-010-54
 - Data Quality: Okay
 - Fan Speed: 1,000 RPM
 - Time: 753 sec
 - Methane on: 20 sec
 - Cart moving: 40 sec
 - Cart turn around: 360 sec
 - Cart return: 630 sec
 - Description:
 - Cart moving up and down tunnel with methane being released at a steady rate
 - Second gasmitter in series did not observe methane on return pass
- Test 7
 - Box File Name: XB0000-000-673
 - FFS File Name: 0000-010-55
 - Data Quality: Good
 - Fan Speed: 1,000 RPM
 - Time: 868 sec
 - Methane on: 20 sec
 - Cart moving: 100 sec
 - Cart turn around: 390 sec
 - Cart return: 700 sec
 - Description:
 - Cart moving up and down tunnel with methane being released at a steady rate
 - Second gasmitter in series did not observe methane on return pass
- Test 8
 - Box File Name: XB0000-000-674
 - FFS File Name: 0000-010-56
 - Data Quality: Okay
 - Fan Speed: 1,000 RPM
 - Time: 721 sec
 - Methane on: 20 sec
 - Cart moving: 40 sec
 - Cart turn around: 340 sec
 - Cart return: 640 sec
 - Description:
 - Cart moving up and down tunnel with methane being released at a steady rate
 - Second gasmitter in series did not observe methane on either pass
- Test 9
 - Box File Name: XB0000-000-675
 - FFS File Name: 0000-010-57
 - Data Quality: Okay
 - Fan Speed: 1,500 RPM
 - Time: 753 sec
 - Methane on: 20 sec
 - Cart moving: 40 sec
 - Cart turn around: 360 sec
 - Cart return: 630 sec
 - Description:

- Cart moving up and down tunnel with methane being released at a steady rate
 - Second gasmitter in series did not observe methane on return pass
- Test 10
 - Box File Name: XB0000-000-676
 - FFS File Name: 0000-010-58
 - Data Quality: Okay
 - Fan Speed: 1,500 RPM
 - Time: 736 sec
 - Methane on: 20 sec
 - Cart moving: 45 sec
 - Cart turn around: 310 sec
 - Cart return: 640 sec
 - Description:
 - Cart moving up and down tunnel with methane being released at a steady rate
 - Second gasmitter in series did not observe methane on either pass
- Test 11
 - Box File Name: XB0000-000-677
 - FFS File Name: 0000-010-59
 - Data Quality: Good
 - Fan Speed: 1,500 RPM
 - Time: 814 sec
 - Methane on: 20 sec
 - Cart moving: 100 sec
 - Cart turn around: 390 sec
 - Cart return: 700 sec
 - Description:
 - Cart moving up and down tunnel with methane being released at a steady rate
 - Starting to see methane build up in TG
 - Hose break at 300 sec, fixed at 360 sec
- Test 12
 - Box File Name: XB0000-000-678
 - FFS File Name: 0000-010-60
 - Data Quality: Good
 - Fan Speed: 1,500 RPM
 - Time: 621 sec
 - Methane on: 20 sec
 - Methane off: 495 sec
 - Position: 3
 - 1 CFM: 20-90
 - 2 CFM: 90-205
 - 3 CFM: 205-320
 - 4 CFM: 320-495
 - 0 CFM: 495-621
 - Description:
 - Stationary test
- Test 13
 - Box File Name: XB0000-000-679
 - FFS File Name: 0000-010-61
 - Data Quality: Okay
 - Fan Speed: 1,000 RPM
 - Time: 693 sec
 - Methane on: 20 sec

- Methane off: 530 sec
 - Position: 3
 - 1 CFM: 20-115 4,5
 - 2 CFM: 115-215 4,5,6
 - 3 CFM: 215-342 4,5,6,7,9,10
 - 4 CFM: 342-530 4,5,6,7,9,10
 - 0 CFM: 530-693
 - Description:
 - Stationary test
- Test 14
 - Box File Name: XB0000-000-680
 - FFS File Name: 0000-010-62
 - Data Quality: Okay
 - Fan Speed: 1,000 RPM
 - Time: 623 sec
 - Methane on: 20 sec
 - Methane off: 480 sec
 - Position: 6
 - 1 CFM: 20-175 7,9,10
 - 2 CFM: 175-285 7,8,9,10
 - 3 CFM: 285-390 7,8,9,10
 - 4 CFM: 390-480 7,8,9,10
 - 0 CFM: 480-623
 - Description:
 - Stationary test
- Test 15
 - Box File Name: XB0000-000-681
 - FFS File Name: 0000-010-63
 - Data Quality: Okay
 - Fan Speed: 1,000 RPM
 - Time: 501 sec
 - Methane on: 20 sec
 - Methane off: 350 sec
 - Position: 6
 - 1 CFM: 20-115 7,9,10
 - 2 CFM: 115-215 7,8,9,10
 - 3 CFM: 215-305 7,8,9,10
 - 4 CFM: 305-350 7,8,9,10
 - 0 CFM: 350-501
 - Description:
 - Stationary test
- Test 16
 - Box File Name: XB0000-000-683
 - FFS File Name: 0000-010-64
 - Data Quality: Good
 - Fan Speed: 1,000 RPM
 - Time: 612 sec
 - Methane on: 20 sec
 - Methane off: 420 sec
 - Position: 3
 - 1 CFM: 20-150 4,6,9
 - 2 CFM: 150-235 4,6,9,10

- 3 CFM: 235-340 4,5,6,7,8,9,10
 - 4 CFM: 340-420 4,5,6,7,8,9,10
 - 0 CFM: 420-612
 - Description:
 - Ceiling sampling, stationary test
- Test 17
 - Box File Name: XB0000-000-684
 - FFS File Name: 0000-010-65
 - Data Quality: Good
 - Fan Speed: 1,000 RPM
 - Time: 813 sec
 - Methane on: 20 sec
 - Methane off: 640 sec
 - Position: 3
 - 1 CFM: 20-155 4,6,9
 - 2 CFM: 155-280 4,6,9
 - 3 CFM: 280-445 4,5,6,9,10
 - 4 CFM: 445-585 4,5,6,7,8,9,10
 - 5 CFM: 585-640 4,5,6,7,8,9,10
 - 0 CFM: 640-813
 - Description:
 - Ceiling sampling, methane 45 degrees
- Test 18
 - Box File Name: XB0000-000-685
 - FFS File Name: 000-010-66
 - Data Quality: Okay
 - Fan Speed: 1,500 RPM
 - Time: 607 sec
 - Methane on: 20 sec
 - Methane off: 510 sec
 - Position: 3
 - 1 CFM: 20-155 4
 - 2 CFM: 165-280 4,9
 - 3 CFM: 280-425 4,5,9
 - 4 CFM: 425-510 4,5,6,9
 - 0CFM: 510-607
 - Description:
 - Ceiling sampling, methane 45 degrees
 -
- Test 19
 - Box File Name: XB0000-000-686
 - FFS File Name: 0000-010-67
 - Data Quality: Okay
 - Fan Speed: 1,500 RPM
 - Time: 721 sec
 - Methane on: 25 sec
 - Methane off: 600 sec
 - Position: 3
 - 1 CFM: 25-140 4
 - 2 CFM: 140-260 4
 - 3 CFM: 260-420 4,5,6,9
 - 4 CFM: 420-600 4,5,6,9

- 0 CFM: 600-721
- Description:
 - Ceiling sampling, methane 45 degrees
- Test 20
 - Box File Name: XB0000-000-687
 - FFS File Name: 0000-010-68
 - Data Quality: Okay
 - Fan Speed: 1,000 RPM
 - Time: 652 sec
 - Methane on: 20 sec
 - Methane off: 520 sec
 - Position: 3
 - 1 CFM: 20-180 4
 - 2 CFM: 180-280 4
 - 3 CFM: 280-400 4,6
 - 4 CFM: 400-520 4,6,9
 - 0 CFM: 520-652
 - Description:
 - Ceiling sampling, methane 45 degrees
- Test 21
 - Box File Name: XB0000-000-688
 - FFS File Name: 0000-010-69
 - Data Quality: Okay
 - Fan Speed: 1,000 RPM
 - Time: 588 sec
 - Methane on: 20 sec
 - Methane off: 500 sec
 - Position: 3
 - 1 CFM: 20-120 4
 - 2 CFM: 120-220 4
 - 3 CFM: 220-370 4,6,9
 - 4 CFM: 370-500 4,5,6,9
 - 0 CFM: 500-588
 - Description:
 - Stationary test, methane along ceiling
- Test 22
 - Box File Name: XB0000-000-689
 - FFS File Name: 0000-010-70
 - Data Quality: Okay
 - Fan Speed: 1,000 RPM
 - Time: 534 sec
 - Methane on: 30 sec
 - Methane off: 445 sec
 - Position: Entrance
 - 1 CFM: 30-100 Nothing
 - 2 CFM: 100-170 Nothing
 - 3 CFM: 170-240 4
 - 4 CFM: 240-335 2,4,5
 - 5 CFM: 335-445 2,3,4,5,9
 - 0 CFM: 445-534
 - Description:
 - Stationary test, valves open to gob sample location, straight down from front

9.3 Appendix C: Additional Information for MWS Certification

ASAP 2008: Application Procedures for Evaluation of Mine-Wide Monitoring Systems, Barrier Classifications, and Sensor Classifications

- 5.2.4: Create block diagram of system

Figure C1 is a flow chart depicting which sensors and parts of the multi-nodal Methane Watchdog System (MWS) and the general flow direction of the sample.

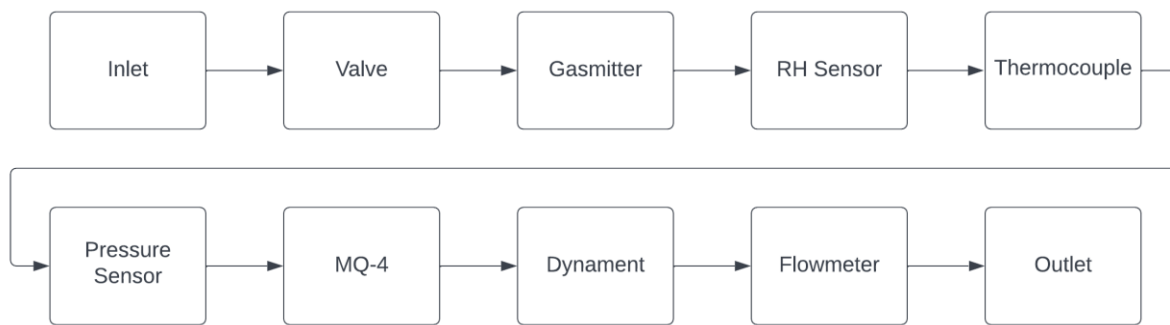


Figure C1: Flow Chart of MWS Components.

- 5.2.5: Manual for Installation and Maintenance

1.0 Purpose

To provide a standard operating procedure for installation and maintenance of the multi-nodal system. This document also specifies the necessary equipment for such practices.

2.0 Scope

This manual relates to the proper installation and maintenance of the multi-nodal system.

3.0 References

3.1. ASAP 2008: “Application Procedures for Evaluation of Mine-Wide Monitoring Systems, Barrier Classifications, and Sensor Classifications”

4.0 Definitions

4.1. MWS-Methane Watchdog System, a multi-nodal methane monitoring system to improve longwall safety.

4.2. CPH-Central processing hub, a computer used to control the MWS and to compile data collected from it. The CPH will also serve to send a de-energizing signal to the shearer and communicate with the operator current levels of methane. Depending on the

DAQ software in use, the CPH could serve to regulate shearer speed as well, but this determination is left up to the operator.

4.3. DAQ-Data acquisition, software, and hardware necessary to process analog and digital signals.

4.4. AI-Analog input, low voltage direct current signals from sensors to the DAQ system for monitoring and recording by the CPH.

4.5. LED-Light emitting diode, flashing blue LEDs are visible within each node showing that the Gasmitter is operational and a flashing green LED on the ICP Con are visible when properly powered and communicating.

4.6 PSIG-Pounds per square inch of gauge pressure, unit of pressure.

5.0 Procedure: Installation

5.1. Install box(es) to shield:

5.1.1. Box(es) should be installed on the underside of shields with power connections made to the shield such that the shield will power the boxes. The system must use a certified power supply capable of meeting the power consumption of each system node as defined in Table C1.

Table C1: Power Consumption by Component of Nodes.

Component	Supply Voltage	Operating Current	Power Usage
	V	mA	W
ICP Con	24	208	5
MQ-4	5	188	0.94
Dynamant	5	35	0.175
RH Sensor	5	13	0.065
MAP Sensor	5	20	0.1
RTD Thermocouple Transmitter	24	20.3	0.487
Valve	24	700	20
Converter	24	130	3.12
Gasmitter	24	24	0.576
Totals		1339	30.46

5.2. Box(es) should be connected together via ethernet cables and connected to the CPH;

5.2.1. Box(es) may also be individually connected to the CPH if deemed desirable.

5.3. Once power and communication cables are installed, integrate the box(es)'s sensors into the CPH system, refer to Table C2 for the analog channels used in each node.

Table C2: Sensor AI Channels

Channel	Sensor
ai 0	Temperature Transmitter
ai 1	Dynament
ai 2	RH
ai 3	MQ-4
ai 4	Pressure
ai 5	Relay
ai 6	Flow Sensor
ai 7	Gasmitter

5.4. Once sensors are integrated into DAQ equipment, ensure all sensors are reading correctly, and calibrate as needed following instructions found in the response to ASAP 2016 5.11.

5.5 Connect the ejector gas inlet to the sample exhaust port of the node. Connect the water inlet port of the ejector to a water supply line. Ensure the water supply is regulated to around 100 PSIG and capable of lowing one liter per minute. Adjust the water pressure or flow rate where applicable to achieve a target gas flow rate of two liters per minute.

6.0 Procedure: Maintenance

6.1. Refer to the response to ASAP 2016 5.11 for equipment needed for maintenance and general guidelines regarding it.

6.2. Ensure all cable connections are secured and no fraying of the wires has occurred.

6.3. Ensure the box(es)'s connection to the shields is strong and not compromised.

6.4. Ensure ethernet cables are not beginning to loosen and detach.

6.5. Verify all nodes are communicating with the CPH and that all signals within each node are available within the CPH;

6.5.1 If a node is not recognized by the CPH, recheck the ethernet cable.

6.5.2 Each node includes a fuse to protect over current, if internal LEDs are not flashing, check and replace the fuse and reconnect to certified power supply.

6.6 Verify that gas sample flow rates are within specifications – target one standard liter per minute \pm 0.5 standard liters per minute. If adjustments in ejector pressure and flowrate are not capable of producing adequate gas sample flow, check sampling pressure;

6.6.1 Within the CPH channels for the node in question, examine the pressure within the sampling system. If the pressure is trending negative (less than 13 PSIG) examine, clean, and replace node filters.

6.7. Check on a monthly basis, the condition of each node's filters. If the sample pressure is low, visually inspect may the internal filter element and replace if visually caked with coal dust particles.

6.8. Periodically perform bump-tests as with other methane sensors. Zero drift must be adjusted when each node is sampling ultra-zero air (<1 part per million of hydrocarbons). Period span checks should be conducted using either 1.0 or 1.5% methane in air bottled gas.

End of Basic Manual.

ASAP 2016: Standard Application Procedures for Approval or Evaluation of Intrinsically Safe Apparatus and Associated Apparatus per 30 CFR Part 18

5.2: Description of electrical circuits

Specific voltage and current requirements as well as ranges are provided in the supplemental documents, see the manuals included in the submission. Additionally, a table breakdown of the current, voltage and power requirements is provided in ASTP 2232. Figure C2 presents an overall wiring diagram of the MWS nodes.

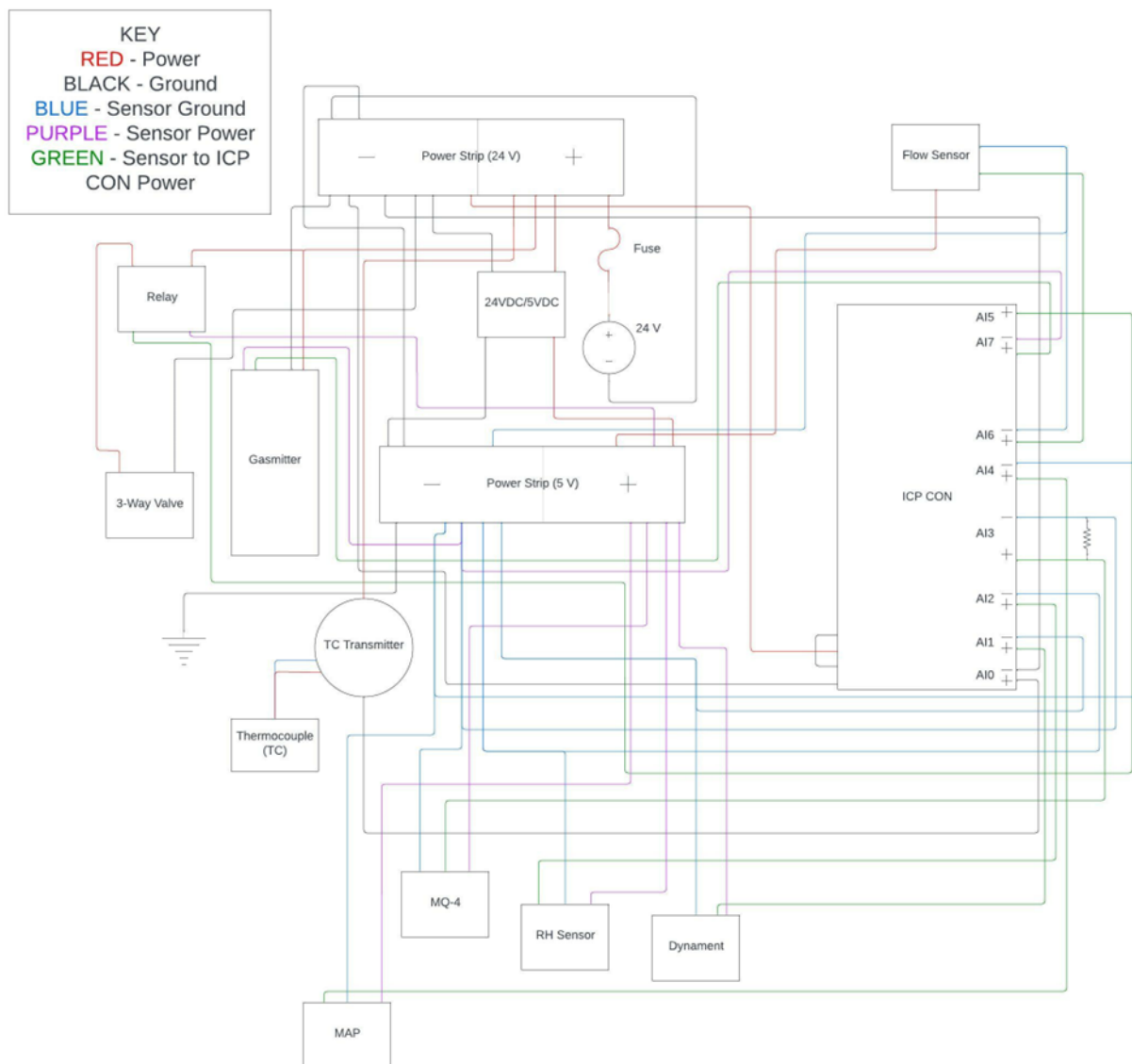


Figure C2: Internal Wiring Diagram of Each Node. Note the experimental system uses 24 volts, a production system would utilize 12 volts as discussed later.

5.6: Drawing list adequate to describe all equipment

See the appendix for basic drawings of the components, additional detailed drawings and specifications of each internal component would be required in the full application pursuant to APOL 2048.

Figure C3 provides an overview drawing of each node of the MWS. Each component labeled along with gas sample flow path.

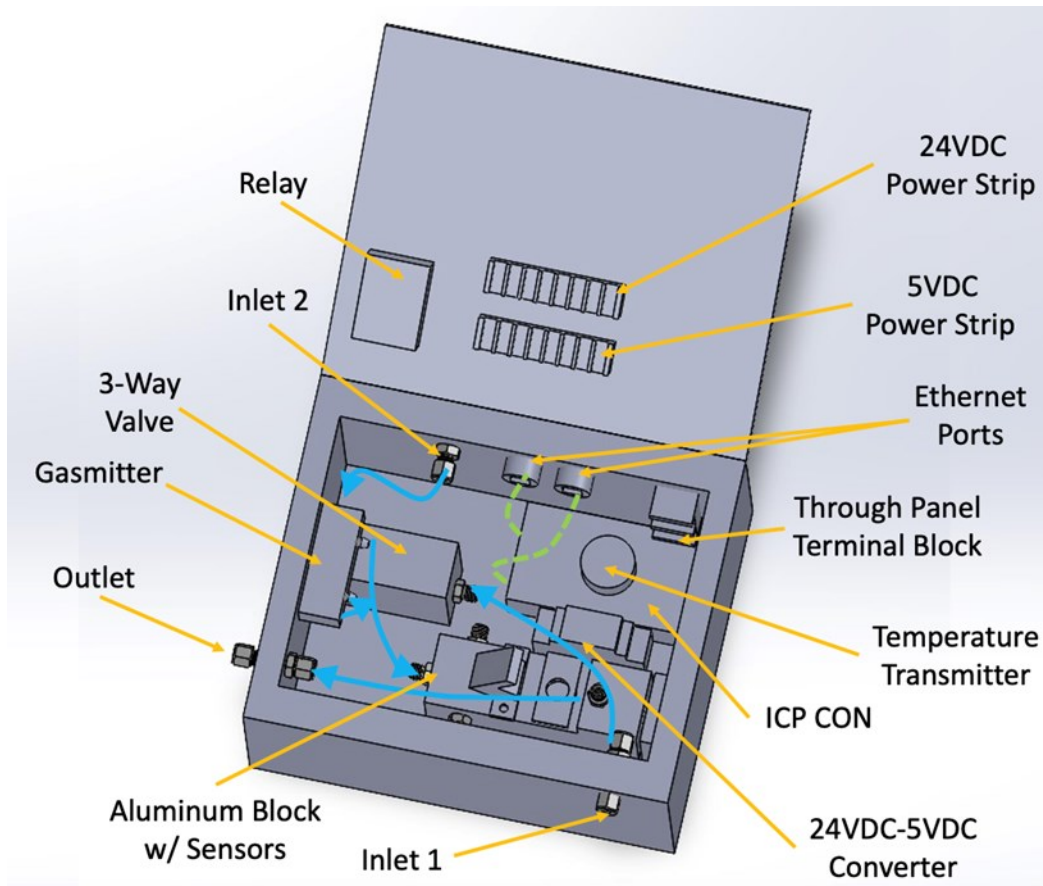


Figure C3: CAD Drawing of Current Box with Labeled Components.

5.9: Bill of materials

Table C3 presents a bill of materials for internal components, their name, quantity, and a brief description. In addition to key components, each of the required wires from Figure C2 are detailed in Table C4. Table C5 includes a bill of materials for specific sensors within each node.

Table C3: Bill of Materials of Content of Boxes.

Item	Quantity	Description
Sensor Block	1	Contains a collection of sensors including: MQ-4, Dynament, Pressure Sensor, RH Sensor, & Thermocouple
Relay	1	Used
3-Way Valve	1	Determines where sampled flow enters
24 VDC-5 VDC Converter	1	Converts DC power to be safe for sensors
24 VDC & 5 VDC Terminal Block	1	Holds different wires in place to power box
ICP Con	1	Analog to digital converter and digital/analog out for relay and communication
Temperature Transmitter	1	Converts thermocouple signal to function with ICP Con
Ethernet Ports	2	Used to daisy-chain the individual ethernet cords of the boxes together and provide communication pathway to the central processing hub
Assorted Wires	50	Power box components
Ethernet Cords 2"	2	Enables pick up of nodal signal and communicates to other boxes as well as the central processing hub
Vinyl Tubing 3/16" ID, 5/16" OD	24"	Carry sampled air to sensors
5 Amp Fuse	1	Provides protection against over-current surges
Fuse Holder	1	Holds fuse
5/8" Bolt	6	Acts to keep compression tube fittings in place
Barbed Tube Fittings	2	Connects sampling tubing to various sensors and the sensor block
12 VDC-24 VDC Converter	1	As shields typically run 12 VDC, this component will move the voltage to what is the operating voltage of the boxes
Compression Tube Fittings	6	Acts to keep sampling tubing in place

Table C4: Assorted Wires and Their Specifications.

Component	Gauge	Length (in)	Max Voltage (V)	Max Current (mA)	Expected Current (mA)	Quantity
Grounding Wire	12	6	24	2943.9	0	1
Fuse Holding Wire	16	12	12	2943.9	1339	1
Valve	18	6	24	1666.7	700	2
Gasmitter	18	12	24	48	24	3
ICP Con	22	12	24	416.7	208	2
Pressure Sensor	24	12	5	40.0	20	3
Voltage Converter	24	12	24	536.0	268	4
Relay	24	12	5	24	12	6
Flow Sensor	24	12	5	60	30	3
MQ-4	24	12	5	376	188	4
Dynament	24	12	5	70	35	3
RH Sensor	24	12	5	26	13	3
Thermocouple Transmitter	24	12	24	40.6	20.3	4
Relay	24	18	5	24	12	4

Table C5: Sensors Bill of Materials.

Item	Quantity	Sensor Type	Manufacturer	Make	Model	Operating Voltage	Manufacturer Contact Information
MQ-4	1	Methane Monitor	Winsen	Winsen	MQ-4	24	0086-371-67169097/ sales@winsensor.com
IR	1	Methane Monitor	Dynament	MSH2ia	LS/HC/5/V/P/F	5	44-1623-663636
Gasmitter	1	Methane Monitor	Sensors-Inc	Sensors-Inc	Gasmitter-0-2	5-12	49-0-2104-141880
RH Sensor	1	Humidity	Honeywell	HH-4602	HH-4602-L-CP	4-5.8	1-877-841-2840
Thermocouple	1	Temperature	Omega	TMQSS	062U-2	N/A	1-800-766-6342
Thermocouple Transmitter	1	Temperature	Hicomponent	Intelligent RTD	PT100	12-35	86-153-38828617
Pressure Map Sensor	1	Pressure	Borg Warner	BorgWarner	EC7034	5	662-473-3100
Flow Sensor	1	Air Speed	Reenas	FS2012	1100-NG	5	408-284-8200

5.11: Equipment required to test and inspect devices

Equipment that is required to test and inspect devices is summarized in Table C6.

Table C6: Items Needed to Test and Inspect Boxes.

Item	Description
Ultra-Zero Air	Gas cylinder filled with ultra-zero air – compressed dry air free of hydrocarbons for zeroing gas sensors.
Calibration or Span Gas	A known methane concentration should be mixed with supply air for sampling with the boxes – 1 or 1.5% methane in air by volume.
Gas Divider	Used to mix the methane and air and to "step" the supplied mixture up in the boxes, this can be done before installation and periodically when maintenance which requires the removal of the box is deemed necessary.
Pump	Provides force behind the movement of air through boxes, used when calibrations are completed outside of the mine, otherwise ejectors would be used.
DAQ Software	Determines what level of methane is being detected by boxes, installed on CPH.
Ventilation Equipment	Used to safely dispose of methane-air mixture.
Voltmeter	Used to determine if power supply is sufficient.
Gasmitter Calibration Program	Program used to calibrate the analog output of Gasmitter sensors.
Flow Controller	Controls the speed and volume at which the pump moves the flow.
Tubing	Connects the box to the pump and methane-air mixture.

ASTP 2232: Spark Ignition Test

7.2.2.1: Pursuant to this section, the maximum currents must be provided. Table 1 presented the currents of the current system. Assuming the system is connected to shield power via an approved power supply, the voltage would be limited to 12 volts. This would double the operating current. Table C7 presents this additional data for each component and the total node.

Table C7: Operating Current with Reduction to 12 V Operation. Note only 24 V Components Would Be Reduced to 12 V as highlighted.

Component	Supply Voltage	24 V Operating Current	12 V Operating Current	Power Usage
	V	mA	mA	W
Relay	5	12	24.0	0.06
Flow Sensor	5	30	60.0	0.15
ICP Con	24	208	416.7	5
MQ-4	5	188	376.0	0.94
Dynamment	5	35	70.0	0.175
RH Sensor	5	13	26.0	0.065
MAP Sensor	5	20	40.0	0.1
RTD Thermocouple Transmitter	24	20.3	40.6	0.487
Valve	24	700	1666.7	20
Converter	24	130	260.0	3.12
Gasmittter	24	24	48.0	0.576
Totals		1380.3	3027.9	30.46

ASTP 2228: Methane Monitor Moisture Test

5.3: Assembly must function in environments of relative humidity greater than 85%.

To validate this, the acceptable relative humidity ranges for each component was determined based on manufacturer's specifications. Table 8 presents the acceptable ranges for each device.

Table 8: Valid Relative Humidity Ranges of Sensors

Sensor	Relative Humidity Range (%)	Sources
Valve	0-100	Manual
RH	0-100	Manual
MQ-4	0-95	Manual
Thermocouple	0-98	Manual
TC Transmitter	0-100	Manual
Gasmittter	0-95	Manual
Flow Sensor	0-100	Manual
Dynamment	0-95	Manual

7.6: Methane mixture tested at 2.1% and readings recorded

Pursuant to this section, methane sensors are required to be exposed to a concentration of at least 2.1% and accurately report methane. To assess this, 3% bottled methane was supplied to a node and the data were recorded over time, see Figure C4. As noted, the error of the MQ-4 is higher for higher concentration gases. Its best characteristics were fast response and sensitivity to lower concentrations on the order of 1000 parts per million. Table C9 presents the error for the three sensors, and we note the primary sensor, the Gasmitter, was accurate at this level.

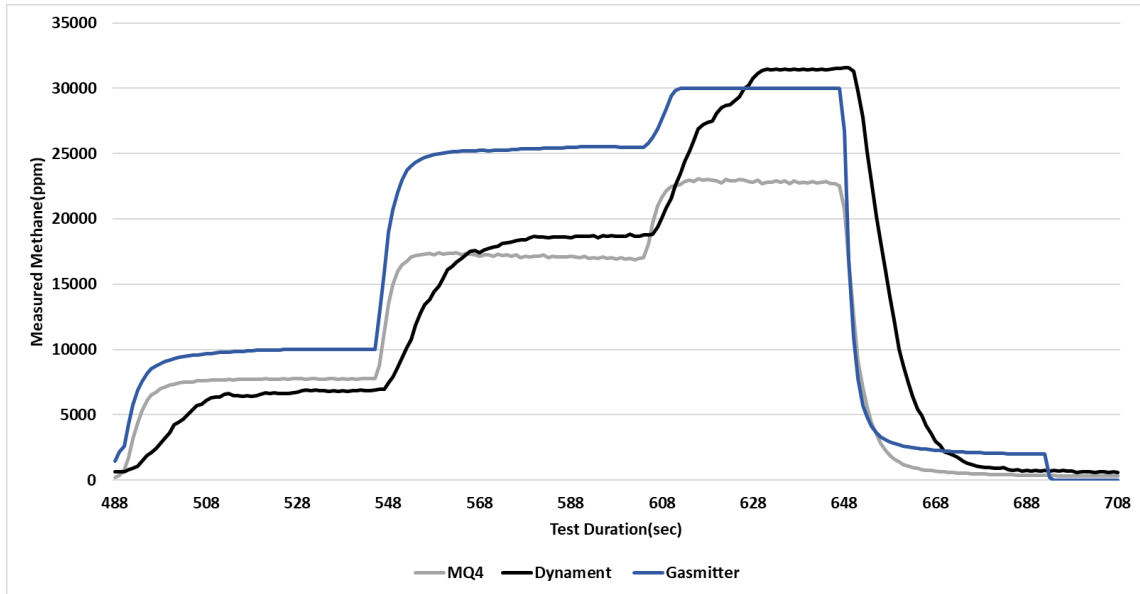


Figure C4: Recorded Methane Concentration During a Ramp Test To 3% Methane by Volume.

Table C9: Relative Error of Sensors.

Sensor	Relative Error (%)
MQ-4	25.0
Dynament	8.3
Gasmitter	0.0

ASTP 2219: Impact Test of Encapsulated Electrical Assemblies

Pursuant to this and other standards and through communication with MSHA, CSE, and others, an X/P enclosure must replace the current enclosure. To meet the space requirements to enable all components to be mounted internally, we have selected the MCI 7015-35223-4 X/P 5. The specifications are found in Appendix A. Table C10 presents a comparison of the dimensions of the sealed research box and the X/P 5 enclosure. Through contact with MCI, they can modify the hole locations for the required pass throughs without sacrificing MSHA compliance. To verify internal volume requirements, the components were again modeled in CAD to ensure adequate space as shown in Figure C5.

Table C10: Current and Replacement Enclosure Dimensions.

Dimension	Current Box	XP Enclosure 5
Length (in)	11.75	14
Height (in)	6	6.5
Width (in)	9.875	9.875

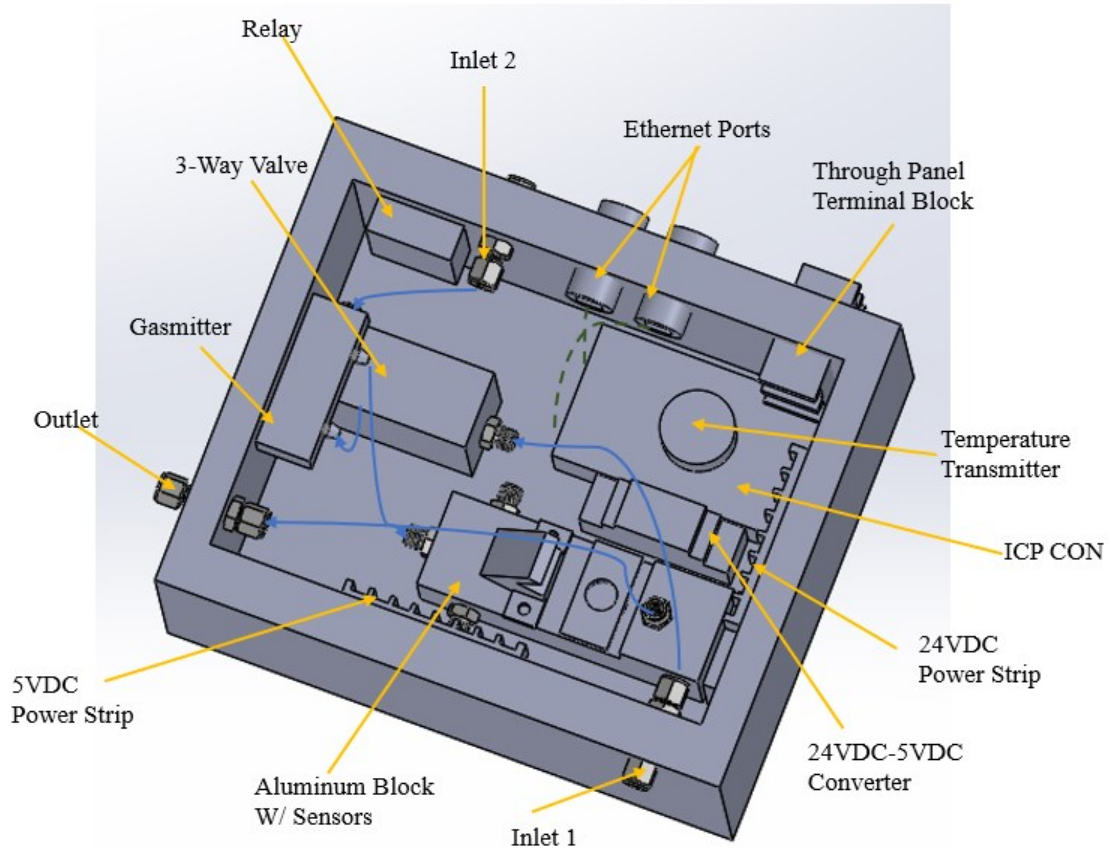


Figure C5: MWS Node Redesign with X/P 5 Enclosure.

To meet MSHA certifications, connections, and wires outside of the box were selected from approved components. The following items are MSHA approved.

- Power Supply
 - Austdac Pty Ltd AC 36W Intrinsically Safe Power Supply
 - <https://www.hubbell.com/austdac/en/Products/Electrical-Electronic/Mining-Products/Power-Supply/AC36W/p/10224587>
- Ethernet Cable
 - Belden 7929A CAT 5e, 4 Pair, Stranded with Foil Shield

- <https://www.industrialnetworking.com/pdf/Belden-79XXA-Bulk-Cable.pdf>
- Power Cable Connector
 - 400 X/P-TLB 2-pole plug – Model X/P-3309-2
 - https://www.andersonindustrialandmining.com/Mining/xp_tlb400.html
- Ethernet Connector
 - Solexy BXF Explosion-Proof/Intrinsically Safe Ethernet Coupler
 - <https://www.solexy.net/products/explosion-proof-is-ethernet-barrier-coupler-fitting/>

In addition, our system uses relays within boxes and at the CPH. These relays enable the ability to control external mining equipment upon reaching the alarm thresholds. The solid state relays could be replaced with intrinsically safe Start and Stop Relays from BeckerSMC which are already approved by MSHA.

- Stop Relay – C4325-001 (Base C4325-002)
- Start Relay – C4325-005 (Base C4325-006)
- <https://beckersmcusa.com/product/intrinsically-safe-relays>

W.V. Code 36-54-3: Methane Monitors

3.5: Pursuant to this requirement, the MWS must give a warning signal at methane concentration 1% in such a manner that the operator will recognize it. We previously discussed the ability of the CPH to control relays for audible and visual alarms. Figure C6 provides another user interface warning showing the methane content above 1% to the operator.

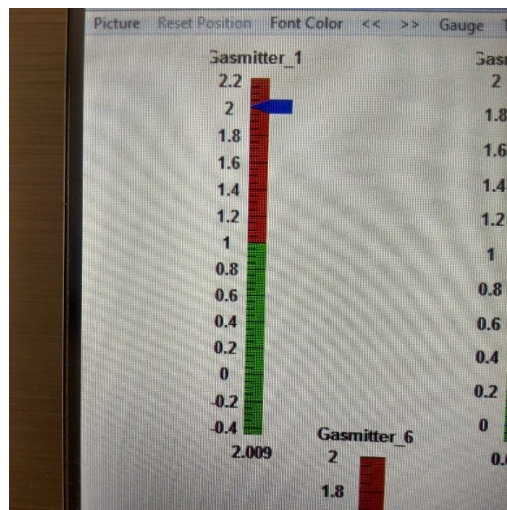


Figure C6: CPH Display Alerting Methane Concentration Above 1% on Node 1.

W.V. Code 36-54-4: Actions for Excessive Methane

4.2.1: Methane levels at or above 1% (in working area) shall cause de-energization of equipment in the immediate area except for atmospheric monitoring systems and changes will be made to the ventilation.

Pursuant to this requirement the system must be capable of controlling a relay that could deenergize equipment. Figure C7 shows an example of the digital control signal for a valve test where a valve is controlled to be on and off repeatedly over the course of about two minutes.

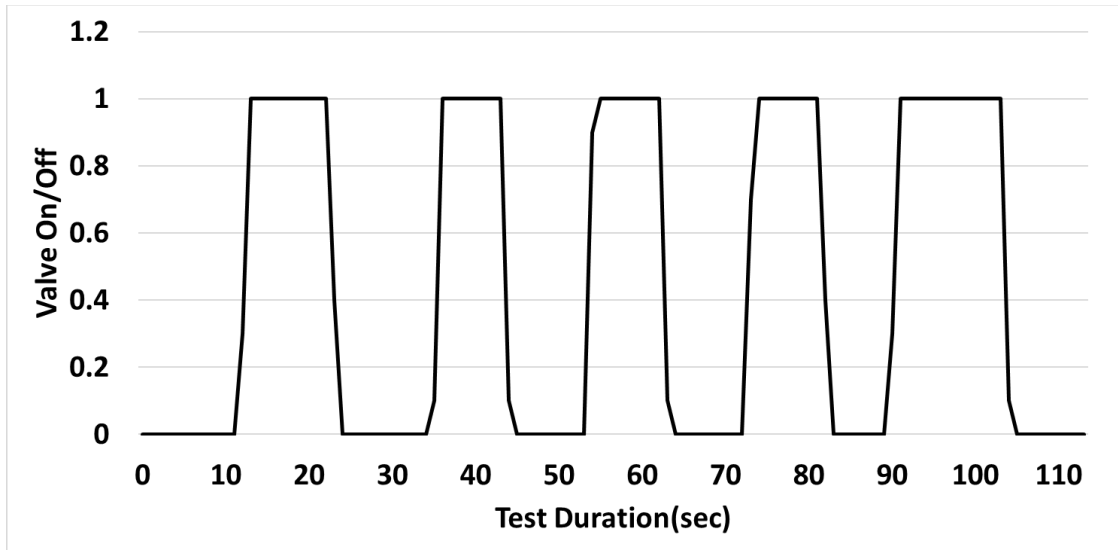
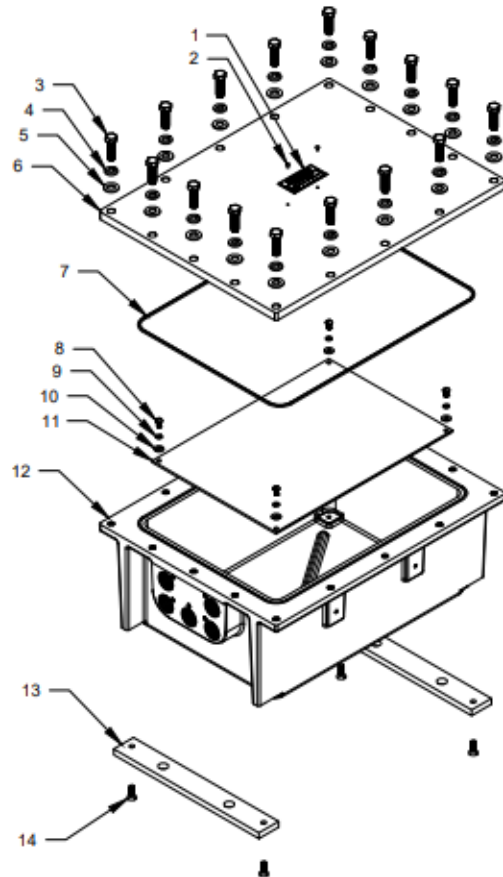


Figure C7: Demonstration of Required Control Capability of the MWS.

COMPONENTS: Explosion Proof Box



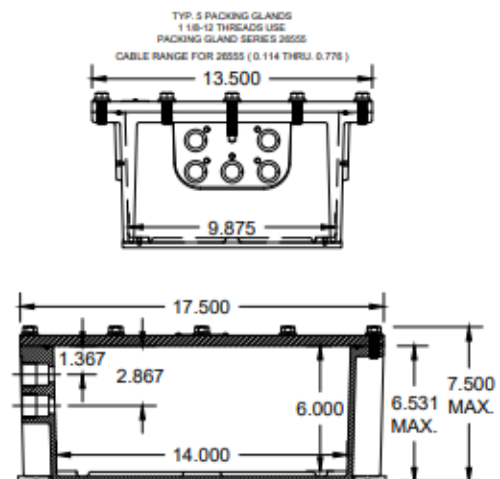
Mining Controls Inc.
P.O. Box 1141
Beckley, WV 25802
304-252-6243



7015-35223-4

XP Enclosure 5 Glands

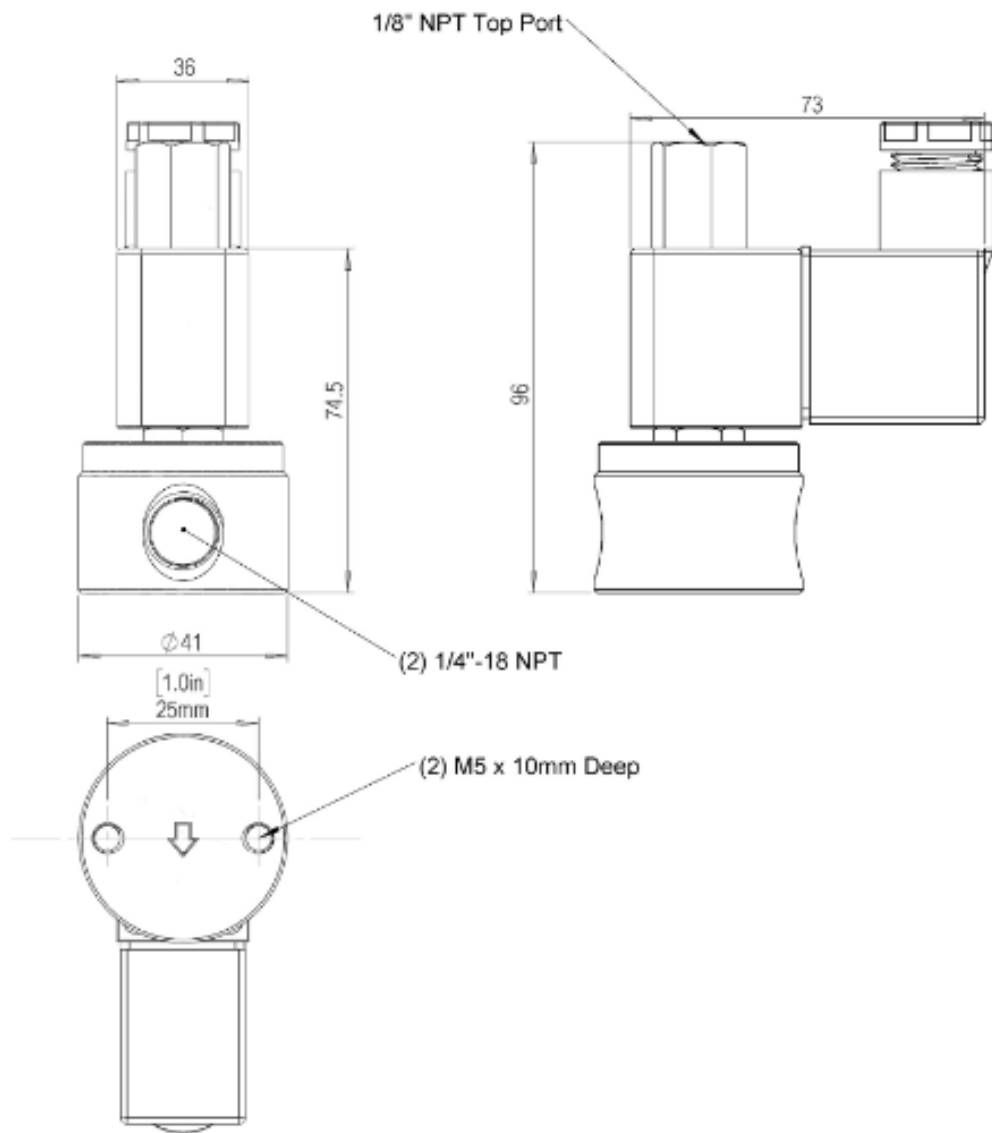
Item	Qty.	Part Number	Description
1	1	1044-20011	CERTIFICATION TAG
2	2	1041-50005	# 4 X 3/16 DRIVE SCREW
3	16	1041-50006-4	BOLT 3/8-16 X 1 1/4 HEX
4	16	1041-50008	LOCK WASHER 3/8
5	16	1041-50007	FLAT WASHER 3/8
6	1	2010-35244	ALUM. BLANK COVER
7	60	1033-34890	3/32 DIA. O-RING MATERIAL
8	4	1041-50000-1	SCREW #10-24 X 1/2 ROUND HEAD
9	4	1041-50001	WASHER #10 LOCK
10	4	1041-50130	WASHER #10 FLAT
11	1	2022-35223-3	INTERNAL MOUNTING PLATE
12	1	2010-35223-2	HOUSING MACHINING
13	2	7014-35341	MOUNTING FOOT
14	4	1041-50238-1	SCREW 1/4-20 X 3/4 FLAT HEAD



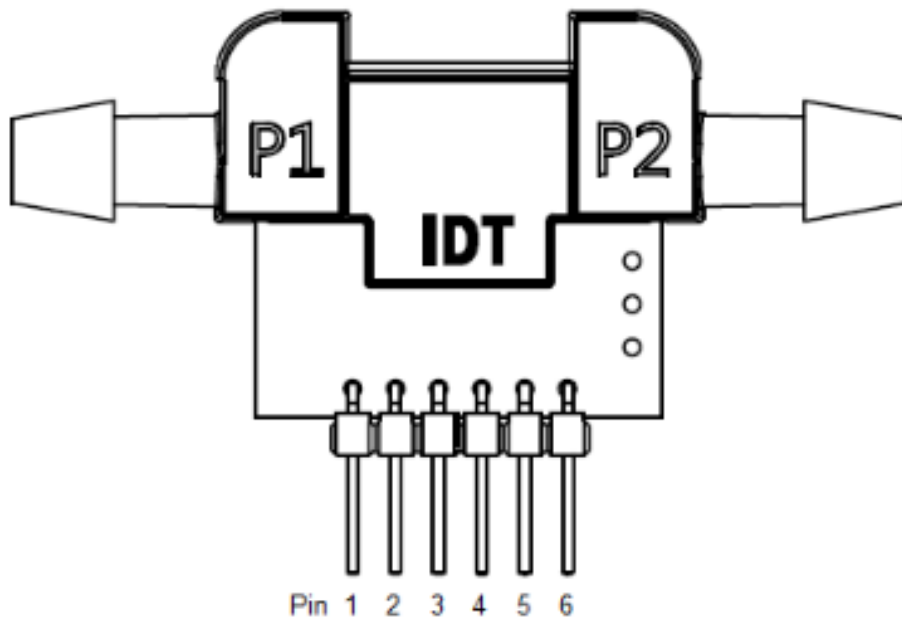
Mining Controls Inc. 304-252-6243

TDS-7015-35223-4 REV-A 11-18-09

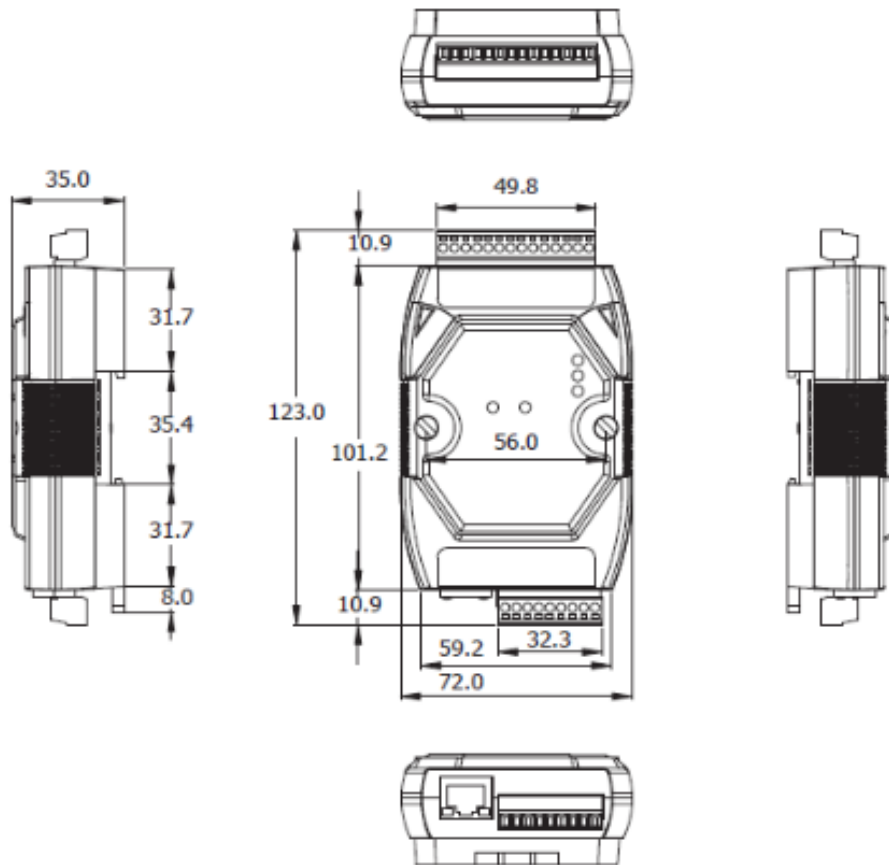
3-Way Valve



Flow Meter



ICP Con



MQ-4

Model			MQ-4
Sensor Type			Semiconductor
Standard Encapsulation			Bakelite, Metal cap
Target Gas			Methane
Detection range			300~10000ppm(CH ₄)
Standard Circuit Conditions	Loop Voltage	V _L	≤24V DC
	Heater Voltage	V _H	5.0V±0.1V AC or DC
	Load Resistance	R _L	Adjustable
Sensor character under standard test conditions	Heater Resistance	R _H	26Ω±3Ω(room tem.)
	Heater consumption	P _H	≤950mW
	Sensitivity	S	R _s (in air)/R _s (in 5000ppmCH ₄)≥5
	Output Voltage	V _s	2.5V~4.0V (in 5000ppm CH ₄)
	Concentration Slope	α	≤0.6(R _{5000ppm} /R _{1000ppm} CH ₄)
Standard test conditions	Tem. Humidity	20℃±2℃; 55%±5%RH	
	Standard test circuit	V _L :5.0V±0.1V; V _H :5.0V±0.1V	
	Preheat time	Over 48 hours	

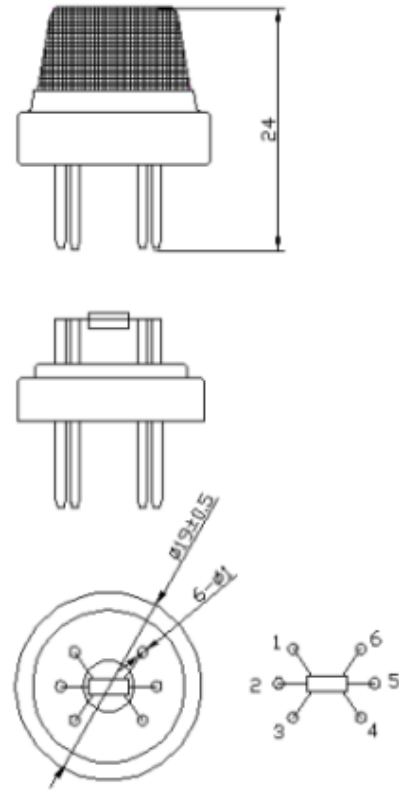
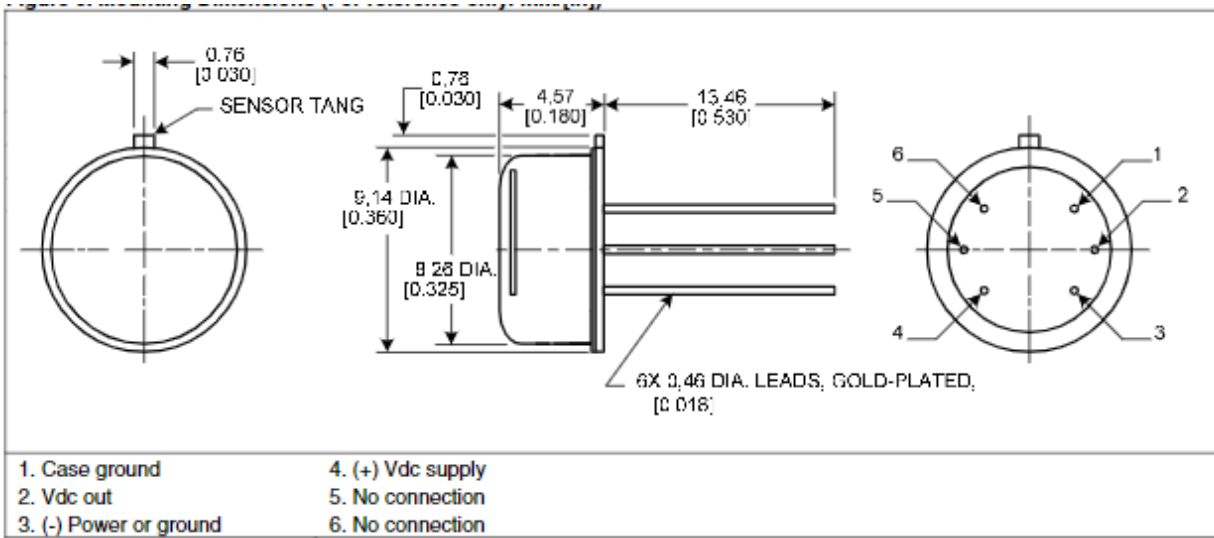


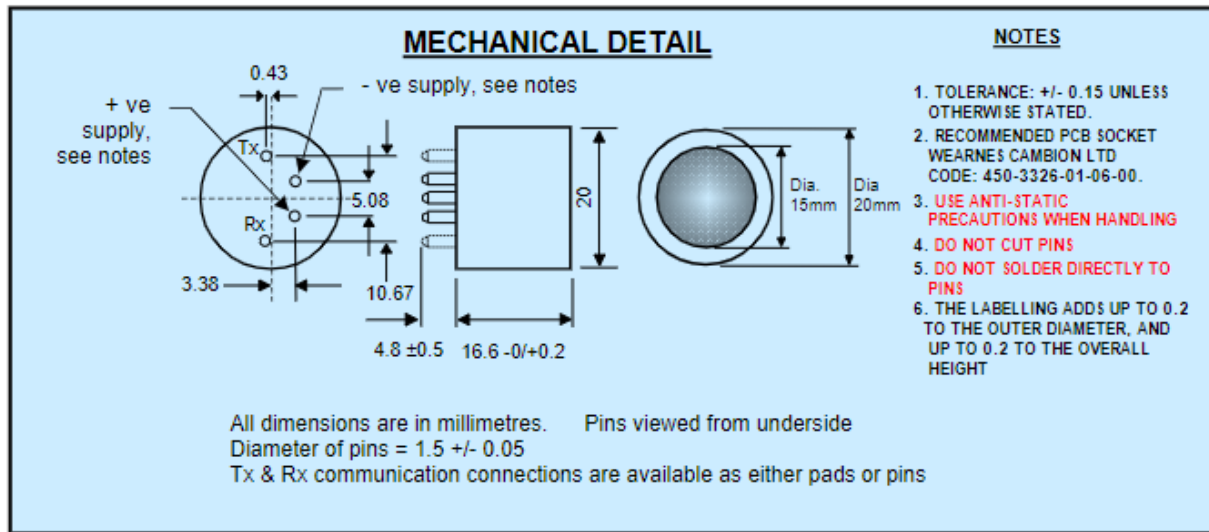
Fig1. Sensor Structure

Unit: mm

Relative Humidity Sensor



Dynamant

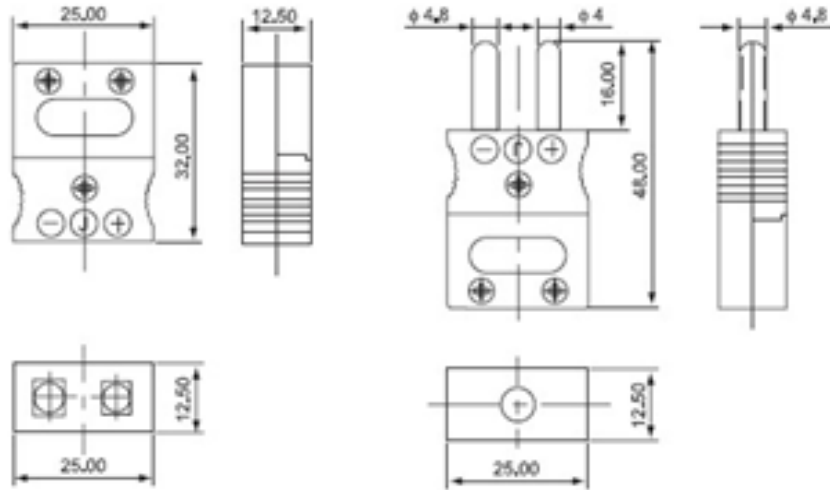


Gasmitter

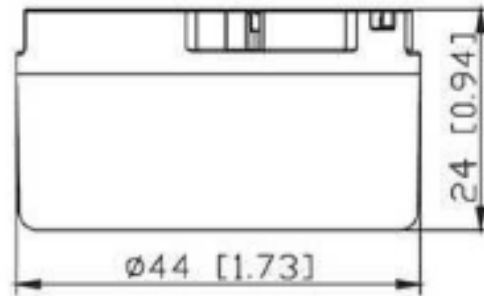
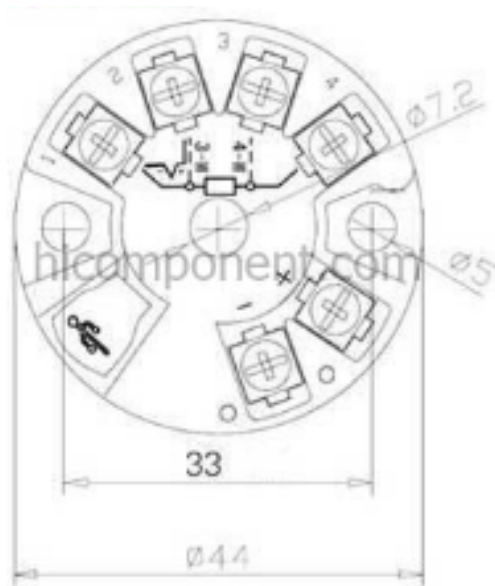


General	
Measuring principle	Non dispersive infrared sensor (NDIR) dual wavelength
Measuring Response ¹	
Linearity Error	$\leq \pm 1\% \text{ FS}^*$
Lower detection limit	$< 0,5\% \text{ FS}^*$
Repeatability at zero	$\pm 0,2\% \text{ FS}^*$
Repeatability at span	$\pm 1\% \text{ FS}^*$
Long term stability	$\pm 2\% \text{ FS}^*$ (12 months under laboratory conditions)
Influencing Variables ¹	
Temperature dependence at zero	$\pm 0,5\% \text{ FS}^*$ per 10K
Temperature dependence at span	$\pm 1\% \text{ FS}^*$ per 10K
Pressure dependence at zero	0%
Pressure dependence at span	
Time Response	
Warm up	within 10s operational, less than 30 minutes to reach specification
Response time (T_{90})	3...45s (depending on used sensor element, flow, tube length, digital attenuation)
Gas Inlet Conditions	
Ambient temperature	0...50°C in process / -20...60°C in storage
Gas pressure	800...1200mbar
Ambient humidity	< 95% RH (non condensing)
Flow range (gas)	0,1...0,75 l/min (constant)
Calibration	
Zero- / Spanpoint calibration	Zero point and span point adjustable with software command / Zero point via button on the PCB
Electric Properties	
Operating voltage	12VDC (10...42VDC)
Power consumption	Max. 3W
Status/Failure visualization	Status and failure LED on the PCB
Analog output (linearized)	0...20mA, 4...20mA; Max. 50Ω load at current output
Digital output	RS232-Interface,
Dimensions	
PCB dimension	160 x 50mm; Height : 45mm (connectors and tubes)
Weight	max. 800g
Tube connector	3mm (outside diameter); Hose inside diameter < 3mm
*FS= full scale	
¹ = Referred to 1013 mbar sample gas pressure, 25°C ambient temperature and 0,75 l/min constant gas flow	
Disclaimer: Specifications are subject to change without notice. While due caution has been exercised in the production of this document, possible errors and omissions are unintentional.	

Thermocouple



Temperature Transmitter



Unit: mm (in)

Pressure Sensor



9.4 Appendix D: 1-D Modeling Code

```
clc, clear
% Objective 6 - 1D advection model for case studies
% Upwind method (FTCS)
% Full scale version

% Model Parameters
A=0.25;
f=10000;
n=100;
bigT=1/f;
tt=[0:bigT/100:2.5*n*bigT];
c=A*exp(-tt*200).*sin(.5*pi*f*tt)+2.2-22.*tt;
L = 300; % Length of Longwall [m]
dx = 0.8; % Space discretized step [m]
dt = 0.2; % Time discretized step [s]
%c_data = xlsread('Baseline_emission_practice_data', 'Vent Data', 'M1:M800');
% Ventilation data
%c = repelem(c_data,40); % Ventilation data sampled/reduced [m/s]
%c = 2; % Velocity [m/s] the (t) needs to be removed from 'm_air' and 'c'
below
T = 25000; % Amount of time steps [#]
sample_rate = 1/dt; % Number of time steps per second [Hz]
x = [0:dx:L]; % Node locations [m]
CFL = c*(dt/dx); % Courant-Friedrichs-Lewy stability criterion (<= 1)

% Checks for stability based on chosen discretized step parameters
for i = 1:length(c)
    if c(i) >= dx/dt
        error = dx/dt;
        fprintf('Check for stability, c must be less than error =')
        disp(error)
        return
    else
        end
end

% Flow domain parameters
h = 3;
w = 6;
area_vent = w*h; % [m^2]
density_air = 1.229; % [kg/m^3]
m_methane = 0.83/2; % mass rate methane released from cutting [kg/m^2*s]
m_air = density_air*c*area_vent; % [kg/s]

% Ventilation loss
meth_add = logspace(0,1,376);
meth_add=(meth_add-1)/9;

% Initial Condition
fx = zeros(T,length(x));
fx(1,:) = linspace(0.01,0.1,length(x)); % baseline concentration profile or
zeros for initial condition.
```

```

% Shearer Data
shearer_rate = 0.12; % m/s
k=2;
fxnew = fx;
leaknode=155
for t = 2:T

    % Amount of coal cut to derive methane released
    coal_cut(t) = shearer_rate*dt;
    lim=0.9;

    % Stopping production if methane exceeds a threshold
    % danger1 = find(fx(t-1,:) > 0.9); % defines methane concentration
    threshold to slow down shearer [% CH4]
    if (fxnew(t-1,38)>lim) || (fxnew(t-1,76)>lim) || (fxnew(t-
1,114)>lim) || (fxnew(t-1,152)>lim) || (fxnew(t-1,190)>lim) || (fxnew(t-
1,228)>lim) || (fxnew(t-1,266)>lim) || (fxnew(t-1,304)>lim) || (fxnew(t-
1,342)>lim) || (fxnew(t-1,376)>lim) % Number of instances where value is above
threshold [# of timesteps] before executing a reduced shearer rate
        shearer_rate = 0.9*shearer_rate; % reduction factor (new shearer
rate) if threshold is reached
        leaknode=0;
        coal_cut(t) = shearer_rate*dt;
        danger(1,:) = ([38,76,114,152,190,228,266,304,342,376,0] ./ 376*300);
        danger(k,:) = [fxnew(t-1,38), fxnew(t-1,76), fxnew(t-1,114), fxnew(t-
1,152), fxnew(t-1,190), fxnew(t-1,228), fxnew(t-1,266), fxnew(t-1,304), fxnew(t-
1,342), fxnew(t-1,376), shearer_position(t-1)];
        k=k+1;

    end

    shearer(t) = shearer_rate;
    r(t) = (0.5 + ((1.0-0.5).*rand));
    methane(t) = m_methane.*r(t);
    methane_released(t) = (coal_cut(t)*h*methane(t));
    methane_conc(t) = ((methane_released(t)/(methane_released(t) +
m_air(t)*dt))*100*(28.97/16);

    % Tracking shearer location based on cutting rate
    if coal_cut(t) == 0
        shearer_position(1) = shearer_rate*dt;
        shearer_position(t) = shearer_position(t-1);
    else
        shearer_position(1) = shearer_rate*dt;
        shearer_position(t) = shearer_position(1) + shearer_position(t-1);
    end

    % Finding closest node to current shearer location
    n_shearer = round(shearer_position(t)/dx);

    for n = 2:length(x)

```

```

        meth_corrected = methane_conc(t) + (methane_conc(t)*1*meth_add(n)); %
added to mimic vent loss across longwall
        if n < n_shearer
            fxnew(t,n-1) = fx(1,n-1);
        elseif n == n_shearer % & fx(t-1,n) < 0.6 % second condition defines
threshold to stop shearer
            fxnew(t,n) = meth_corrected + fx(t,n-1); % this should be the
function of methane released from shearer
        elseif n > n_shearer & n < leaknode
            fxnew(t,n) = fx(t-1,n) - 1*c(t)*(dt/dx)*(fx(t-1,n)-fx(t-1,n-1));
        else
            fxnew(t,n) = fx(t-1,n) - c(t)*(dt/dx)*(fx(t-1,n)-fx(t-1,n-1));
        end
    end

    fx(t,:) = fxnew(t,:);
    %     for n=1:length(x)
    %         fx(t,n) = fxnew(t,n)+fx(1,n);
    %     end

    node_1(t) = fx(t,38);
    node_2(t) = fx(t,76);
    node_3(t) = fx(t,114);
    node_4(t) = fx(t,151);
    node_5(t) = fx(t,189);
    node_6(t) = fx(t,226);
    node_7(t) = fx(t,264);
    node_8(t) = fx(t,301);
    node_9(t) = fx(t,339);
    node_10(t) = fx(t,376);

    nodal_data(t,:) = [node_1(t), node_2(t), node_3(t), node_4(t), node_5(t),
node_6(t), node_7(t), node_8(t), node_9(t), node_10(t)];

    if shearer_position(t) >= L;
        break
    end

end

% Plotting and video creation
% myVideo = VideoWriter('node246');
% myVideo.FrameRate = 5;
% open(myVideo);

for k = 1:50:length(shearer)
    plot(x,fx(k,:))
    %     hold on
    %     plot(x,fx(1,:))

    xlabel('Location Along Longwall [m]')
    ylabel('Methane Concentration [%]')
    axis([0,L,0,1.2])

```

```

%     title(['Methane profile at t =', num2str(round((k*dt)/60)), 'min'])
%     title(['Max methane conc. = ', num2str(max(fx(k,:))), '%', 'Shearer rate
= ', num2str(shearer(k)), 'm/s'])
%     pause(0.01)
%     frame = getframe(gcf);
%     writeVideo(myVideo, frame)
end
% close(myVideo)

% Post processing results - downsampling to 1 Hz
% node_1_down = downsample(node_1,round(sample_rate));
% node_2_down = downsample(node_2,round(sample_rate));
% node_3_down = downsample(node_3,round(sample_rate));
% node_4_down = downsample(node_4,round(sample_rate));
% node_5_down = downsample(node_5,round(sample_rate));
% node_6_down = downsample(node_6,round(sample_rate));
% node_7_down = downsample(node_7,round(sample_rate));
% node_8_down = downsample(node_8,round(sample_rate));
% node_9_down = downsample(node_9,round(sample_rate));
% node_10_down = downsample(node_10,round(sample_rate));
%
% nodal_data_down =
[node_1_down,node_2_down,node_3_down,node_4_down,node_5_down,node_6_down,node
_7_down,node_8_down,node_9_down,node_10_down];

% Total coal cut [m]
total_coal_cut = sum(coal_cut);

% Time required for the shearer to make a single pass
duration = t*dt/60 % [min]

% Maximum methane concentration reported at each node of the MWS
nodal_max_concentration = max(nodal_data_down)

% plot(nodal_data_down(:,5),'linewidth',1)
% xlabel('Time [s]')
% ylabel('Methane Concentration at Node 5 [%]')
% axis([0,length(nodal_data_down),0,2.5])

node_data = timeseries(node_10_down);

```